R-08-124

Ductile and brittle structural evolution of the Laxemar-Simpevarp area: an independent analysis based on local and regional constraints

Giulio Viola, Geological Survey of Norway

October 2008

SKB

Ductile and brittle structural evolution of the Laxemar-Simpevarp area: an independent analysis based on local and regional constraints

Giulio Viola, Geological Survey of Norway

October 2008

Abstract

This report discusses the main aspects of the ductile and brittle deformational evolution of the Laxemar-Simpevarp area. Based on the interpretation of existing potential field geophysical data, it is suggested that the structural ductile grain of the region is controlled by large, c. EW trending shear zones with an overall sinistral strike-slip kinematics. The Oskarshamn Shear Zone (OSZ) and the Mederhult lineament are two examples of these shear zones and it is proposed that the ductile lineaments mapped in Laxemar-Simpevarp are genetically linked to shearing accommodated by these shear zones. The structural interpretation of the geophysical imagery of the Laxemar-Simpevarp regional model area and the available meso-scale structural information indicate that the Laxemar-Simpevarp study area can be interpreted as the analogue of a large-scale S/C' structural pattern. In detail, the Äspö shear zone and other similarly oriented ductile shears represent C' shear bands that deform sinistrally the intervening EW lineaments (the S surfaces), which locally are significantly crenulated/folded in response to their asymptotic bending into the C' shears. This geometric and kinematic interpretation implies that, in contrast to existing reconstructions and models, EW- and not NE-trending shear zones become the main structural ductile feature of the region. Shear forces acting parallel to these main zones can successfully explain all the ductile structures described and reported from the area. The greatest compressive stress at the time of ductile shearing would trend NE-SW.

The brittle deformation history of the region is complex and results from the multiple reactivation of fracture- and fault sets caused by the many orogenic episodes that affected the area during 1.5 Gyr of geological brittle evolution. Fault-slip data from outcrops and oriented drill cores were used to compute paleo-stress states. In the general absence of time markers that help constrain the relative timing of the multiple faulting events, the metamorphic grade of mineralizations coating the striated planes was of help in distinguishing earlier and "higher-grade" from later and "colder" structures. Faulted Ordovician limestones on the island of Öland, however, provided a useful marker to distinguish pre- from post-Ordovician paleo-stress tensors.

Two compressional, c. NNW-SSE and NNE-SSW oriented shortening episodes generated sets of conjugate, steep strike-slip fractures coated by epidote and quartz. These sets (referred to as "set I" and "set II", respectively) formed during the late stages of the Svecokarelian and possibly also of the Gothian Orogeny, soon after the region entered the brittle deformation domain c. 1.5 Ga ago. Although it is natural to expect extensional periods affecting the region at the end of these major orogenic episodes, no systematic set of brittle extensional fractures could be identified with confidence. The Mesoproterozoic Sveconorwegian orogeny, which in the area is believed to have caused an overall c. EW shortening, generated fractures and faults that are assigned to "set III", a set of conjugate strike-slip faults, which constrain a c. EW σ_1. Late Sveconorwegian extension/transtension is known to have caused intrusion of 978–946 Ma old and c. NS trending doleritic dykes. The Caledonian shortening, oriented from c. NW-SE to EW, reactivated set III but also formed a new, similarly oriented set of sub-vertical strike-slip fractures in the Ordovician limestones of Öland. Permian transtension was oriented NE-SW and caused a prominent set of moderately-dipping NW-SE trending normal faults in the pre-Cambrian basement of the study area. A second set of normal faults accommodating NW-SE extension is also documented. NE-SW trending clastic dykes filled by remobilised Cambrian sandstones may be the result of this extensional phase. Two other, distinct NE-SW and NNW-SSE oriented shortening events (referred to as "set b" and "set c", respectively) are recorded in the Ordovician limestones and can be tentatively linked to the far-field effects of the Laramide and Alpine orogenies. Each of these deformation processes caused the reactivation of suitably-oriented pre-existing faults and fractures, thus significantly complicating the unravelling of the brittle deformation history.

Sammanfattning

Denna rapport behandlar huvuddragen av den plastiska och spröda deformationsutvecklingen i Laxemar-Simpevarpsområdet. Baserat på tolkning av befintliga geofysiska potentialfältsdata, anses de plastiska strukturella dragen i området vara styrda av stora, ca O-V-liga, skjuvzoner karakteriserade av sinistrala horisontalrörelser. Oskarhamnszonen (OSZ) och Mederhultszonen är två exempel på dessa skjuvzoner, och det antas att de plastiska zoner som dokumenterats i Laxemar-Simpevarpsområdet är genetiskt länkade till dessa större zoner. Den strukturella tolkningen av geofysiska data i det regionala modellområdet och tillgängliga mesoskopiska strukturella data, indikerar att Laxemar-Simpevarpsområdet kan tolkas som en analog till en storskalig S/C' struktur. Sett i detalj kan Äspöskjuvzonen och andra liknande plastiska skjuvzoner med samma riktning antas representera skjuvband (C'-ytor) som sinistralt deformerar de mellan-liggande O-V-liga zonerna (S-ytor). De senare är lokalt deformerade som ett resultat av deras asymptotiska böjning in i C'-zonerna. Denna geometriska och dynamiska tolkning innebär, till skillnad från tidigare rekonstruktioner och modeller, att O-V-liga skjuvriktningar, istället för NO-SV-liga, dominerar den strukturella bilden i regionen. Skjuvkrafter som verkar parallellt med de O-V-liga zonerna kan förklara alla plastiska strukturer som finns rapporterade från det aktuella området. Den största kompressionsspänningen under den plastiska skjuvningen hade därmed en NO-SV-lig orientering.

Den spröda deformationsutvecklingen i regionen är komplex på grund av den flerfasiga reakti-veringen av sprick- och förkastningszonerna som en effekt de orogeneser som påverkat området under 1,5 miljarder år av den geologiska utvecklingen. Observationer av förkastningsrörelser i hällar och orienterade borrkärnor har använts för att beräkna dåtida spänningsförhållanden i berggrunden (paleostress). På grund av generella problem att relativt åldersbestämma de fler-fasiga förkastningsepisoderna har sprickmineraliseringarna på förkastningsplanen använts som ett stöd för att skilja mellan äldre "varmare" och yngre "kallare" strukturer. Förkastnings-strukturer i ordoviciska kalkstensblottningar på Öland har dock använts för att skilja mellan pre- och post-ordoviciska spänningsriktningar.

Två kompressionshändelser, en i ca NNV-SSO-lig och en i NNO-SSV-lig riktning bildade konjugerande spricksystem av branta, epidot- och kvartsfyllda sprickor vilka domineras av horisontalrörelser. Dessa sprickgrupper (kallade "grupp I" och "grupp II") bildades i slutfasen av den svekokarelska, och möjligen också den gotiska orogenesen, efter vilken deformationen i berggrunden definitivt skedde under spröda förhållanden, dvs för ca 1,5 miljarder år sedan. Även om det är naturligt att förvänta sig perioder av extension i slutfasen av eller efter större orogena händelser, har inga systematiska extensionssprickor identifierats. Den mesoproterozoiska svekonorvegiska orogenesen, som i Laxemar-Simpevarpsområdet antas ha lett till en generell ca O-V-lig förkortning, gav upphov till sprickor och förkastningar som hänförs till "grupp III", ett system av konjugerande horisontalförkastningar vilkas orientering överensstämmer med en O-V-lig orienterad σ_1. Extension/transtension under sensvekonorvegisk tid är dokumen-terad inom området genom förekomsten av diabasgångar som är relaterade till ett system av 978–946 miljoner år gamla N-S-liga diabaser. Under den kaledoniska orogenesen drabbades berggrunden inom området av NV-SO/O-V-lig kompression, vilken ledde till reaktivering av sprickorna i grupp III, men också bildning av nya subvertikala sprickor i den ordoviciska kalkstenen på Öland. De senare domineras av horisontalrörelser och har likartad riktning som sprickorna i grupp III. Under permisk tid utsattes berggrunden i området för tensionsrörelser i NO-SV-lig riktning, vilken ledde till bildning av medelbrant stupande NV-SO-liga normal-förkastningar. Ett system av normalförkastningar som är kopplade till extension i NV-SO-lig riktning har också identifierats. Sprickor i NO-SV-lig riktning som är fyllda med remobiliserad kambrisk sandsten är möjligen ett resultat av denna extensionsfas. Två andra distinkta NO-SV- och NNV-SSO-liga kompressionshändelser (kallade "b" respekive "c") är identifierade i den ordoviciska kalkstenen och dessa kan möjligen vara effekten av de avlägsna Laramidiska och Alpina orogeneserna. Var och en av de nämnda deformationshändelserna orsakade reaktivering av lämpligt orienterade redan existerande sprickzone, vilket därmed avsevärt försvårar rekon-struktioner av den spröda deformationshistorien.

Contents

1 Regional geological setting, structure and aim of the study

The Laxemar-Simpevarp area is located along the eastern coast of Sweden approximately 230 km south of Stockholm (Figure 1-1). The investigation area is situated in the western part of the Fennoscandian Shield /Koistinen et al. 2001/. The rocks of the study area consist largely of intrusive rocks belonging to the Transscandinavian Igneous Belt (1.86–1.65 Ga), an enormous batholith with a NW trend intruded along the tectonic grain of the Svecokarelian (or Svecofennian) orogen (1.95–1.75 Ga) to the northeast. The two dominant lithologies in the study area are the 1,800 ± 4 Ma Ävrö granites, which are generally heterogeneous in composition ranging from quartz-monzodiorites to granites, and equigranular quartz-monzodiorites dated at 1,802 ± 4 (U-Pb on zircon /Wahlgren et al. 2004/). Fine-grained diorites also make up a significant part of the Simpevarp peninsula. Diorites are locally intruded by small intrusions of gabbro, granite as well as dykes and pegmatites. Hallandian granites (Götemar and Uthammar plutons, dated at 1,452 +11/–9 Ma and 1,441 +5/–3 Ma, respectively /Åhäll 2001/) occur in the area together with well-preserved N-S trending dolerite dykes of likely late Sveconorwegian age (978–946 Ma Blekinge-Dalarna dolerites /Söderlund et al. 2005/). For a more extensive overview and description of the local geology, the reader is referred to the comprehensive summary contained in /Söderbäck 2008/.

This study is subdivided into two main sections, sections 2 and 3, respectively.

Section 2 provides an overview of the ductile evolution of the study area, based on the analysis of existing geophysical, structural and geochronological data. It also proposes a linkage between the local structural grain and the larger tectonic picture.

Section 3 focuses instead on the brittle evolution of the Laxemar-Simpevarp area. It uses the results of the field structural analysis and structural logging of numerous deformation zones reported by /Viola and Venvik Ganerød 2007ab, 2008/ to elaborate and propose an evolutionary scheme for the locally-accommodated brittle deformation. Paleo-stress states are computed by inverting homogeneous sets of fault-slip data and these are used to assign the observed brittle deformational features to the numerous tectonic episodes that affected this part of Scandinavia from c. 1.5 Ga ago, the estimated time at which the Laxemar-Simpevarp area entered the brittle deformation realm.
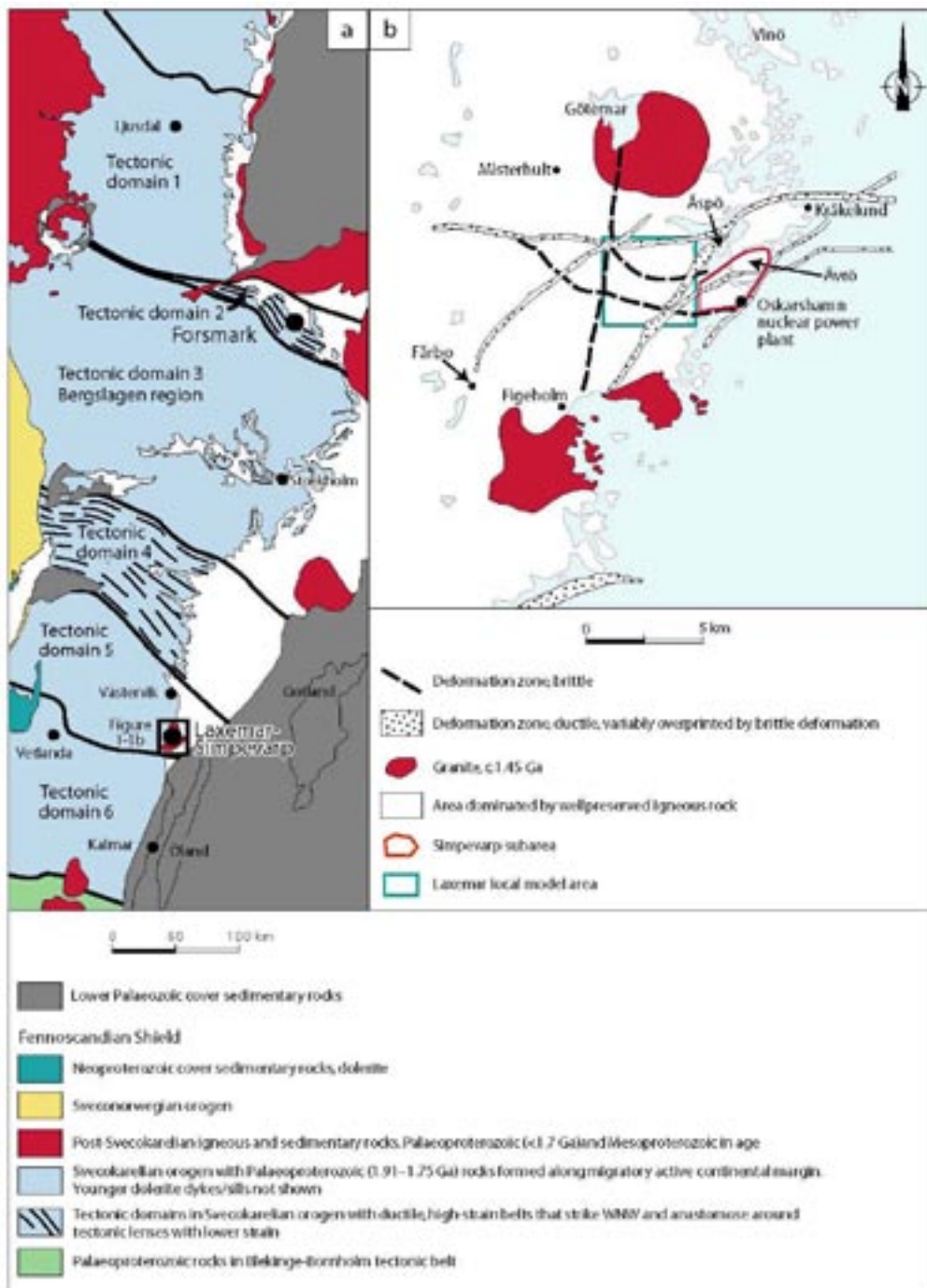
Figure 1-1. *(a) Svecokarelian tectonic domains and post-Svecokarelian rock units in the south-western part of the Fennoscandian Shield, southeastern Sweden (taken from /Söderbäck 2008/ and modified after /Koistinen et al. 2001/). (b) Simplified view of the bedrock geology in the Laxemar-Simpevarp area and surroundings. Note the c. 1.45 Ga Hallandian granites.*

2 Ductile evolution

2.1 The existing model

/Wahlgren et al. 2008/ propose a well-defined ductile framework in their site descriptive model study, summarised in Figure 2-1. The most significant ductile shear zones within the local model area are deformation zones ZSMNE004A and ZSMNE005A, which are generally interpreted as being two distinct branches of what has traditionally been called the Äspö shear zone. These belts are rather heterogeneous and are characterized by irregular, anastomosing networks of mylonitic horizons. Shearing occurred under upper greenschist facies metamorphic conditions, at temperatures between 400 and 450°C /Lundberg and Sjöström 2006/.

Only one attempt at directly dating the ductile deformation event was made. /Drake et al. 2007/ report an $^{40}Ar/^{39}Ar$ age of c. 1.4 Ga from a muscovite grain from the mylonitic foliation in the Äspö shear zone. The interpretation of this age is not straightforward because the dated sample was collected from a drill core that intersects a complex deformation zone characterized by highly fractured and partially altered mylonites. The validity of this unexpectedly young age is therefore questioned by /Drake et al. 2007/, in that the mylonites in the area are commonly believed to be older than the granitic intrusions at Götemar (1.45 Ga, /Åhäll 2001/) and Uthammar (1.44 Ga, /Åhäll 2001/). This young age was thus preferentially interpreted as resulting from heating and resetting of an existing muscovite above its Ar-closing temperature (c. 350°C) in connection with the intrusions of these nearby granites and associated hydrothermal fluid circulation. The general assumption remains therefore that ductile shearing predates c. 1.4 Ga.

According to this view, ductile deformation zones of the Laxemar-Simpevarp area are geneti-cally linked to the late stages of the Svecokarelian orogeny, dominated by c. N-S-oriented bulk crustal shortening. In this dynamic model, the kinematics of E-W trending ductile structures is suggested to be reverse, whereas zones oriented NE-SW and NW-SE are interpreted as sinistral and dextral, respectively (Figure 2-1). The age of ductile deformation is bracketed between 1.81 and 1.76 Ga, therefore only slightly younger than the intrusion and solidification of the TIB rocks in the region.
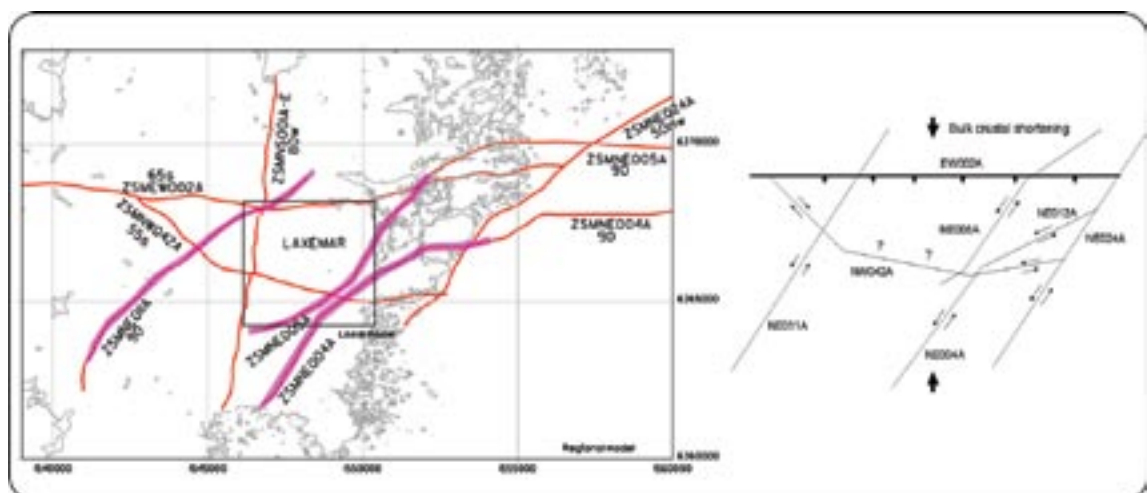
Figure 2-1. *Regional framework of significant deformation zones, three main ductile belts ZSMNE004A, ZSMNE005A and ZSMNE011A and a schematic conceptual kinematic interpretation for the study area. The interpretation and the figure are from /Wahlgren et al. 2008/.*

2.2 An alternative interpretation of the ductile framework

/Viola and Venvik Ganerød 2007ab, 2008/ have dealt only marginally with the details of the ductile evolution of the study area, and limited themselves to the geometric characterization of the ductile deformation zone cores intersected by the inspected cored boreholes. Only one mylonitic outcrop (PSM007634, located in deformation zone ZSMNE004A) was studied and the sense of shear of its low greenschist facies mylonites was established to be sinistral /Viola and Venvik Ganerød 2007a/. This result is in agreement with the observations of a more regional study of ductile structures by /Lundberg and Sjöström 2006/. The study by /Lundberg and Sjöström 2006/, however, focuses exclusively on the kinematics and characteristics of shear zones exposed in the Laxemar-Simpevarp area and does not attempt an integrated analysis of the larger scale, regional ductile history.

It is however believed that, in order to frame the reconstructed brittle evolution described in Section 3 into an internally consistent scheme (the main aim of this report), it is important to also review independently the available information and knowledge of the regional ductile history, which is integral part of the continuous deformational evolution of the area under examination. It is likely that ductile shear zones are of utmost importance in dictating the basic geometric assembly of the bedrock in this segment of the Baltic shield.

The following sections elaborate therefore on an alternative model for the ductile evolution of the Laxemar-Simpevarp area. The model is to a certain extent speculative and more work would be needed to better constrain some of its assumptions and conclusions. Nonetheless, in the opinion of the writer it remains a valid alternative and should be considered in future studies.

### 2.2.1 Main aspects of the regional structural picture

The analysis presented below is based on the study of the spatial relationships among the many lineaments identified with different levels of confidence during several years of investigations of the Laxemar-Simpevarp area and the existing high-resolution airborne magnetic anomaly map of south Sweden by SGU /Kero 2004/. No field work was conducted in order to verify the proposed reconstruction.

The qualitative visual inspection of the geophysical dataset allowed the identification of specific structural relationships and structural patterns and permitted assigning the ductile deformation zones that are exposed in the target areas to a regional kinematic framework. Figure 2-2 shows the airborne magnetic anomaly map for a large portion of SE Sweden /Kero 2004/.

The large, prominent NW-SE trending high magnetic body in the central part of the figure corresponds to part of the Småland-Värmland igneous belt, a sub-domain of the Transscandinavian Igneous Belt (TIB), the bedrock of which is dominated by igneous rocks that formed in the time interval 1.86–1.65 Ga. The study area is located in the SE segment of this magnetic high, immediately north of the town of Oskarshamn (Figure 2-2 and Figure 2-3). A simple visual inspection of this part of the TIB reveals the presence of several, differently oriented "lineaments" (of unverified origin) that crisscross the entire region.

Some of these lineaments have the same orientation of systematic sets of brittle lineaments described in more detail below and are thus assumed to belong to the same class of "late" brittle structural features and as such will be discussed in section 3, which deals with brittle deformation.

The local structural grain, however, is characterized to a large extent by a set of linear features that trend generally NW-SE, although they are locally deflected and reoriented, especially in the southernmost part of the magnetic high, not far from Oskarshamn (white lines in Figure 2-3). The NW-SE-trending "fabric" is characterized by regularly-spaced lineaments that generally are very continuous laterally. On first inspection, it is not clear whether these lineaments correspond to structural or compositional heterogeneities, but are here assumed to be steeply dipping based on their very regular linear trend.
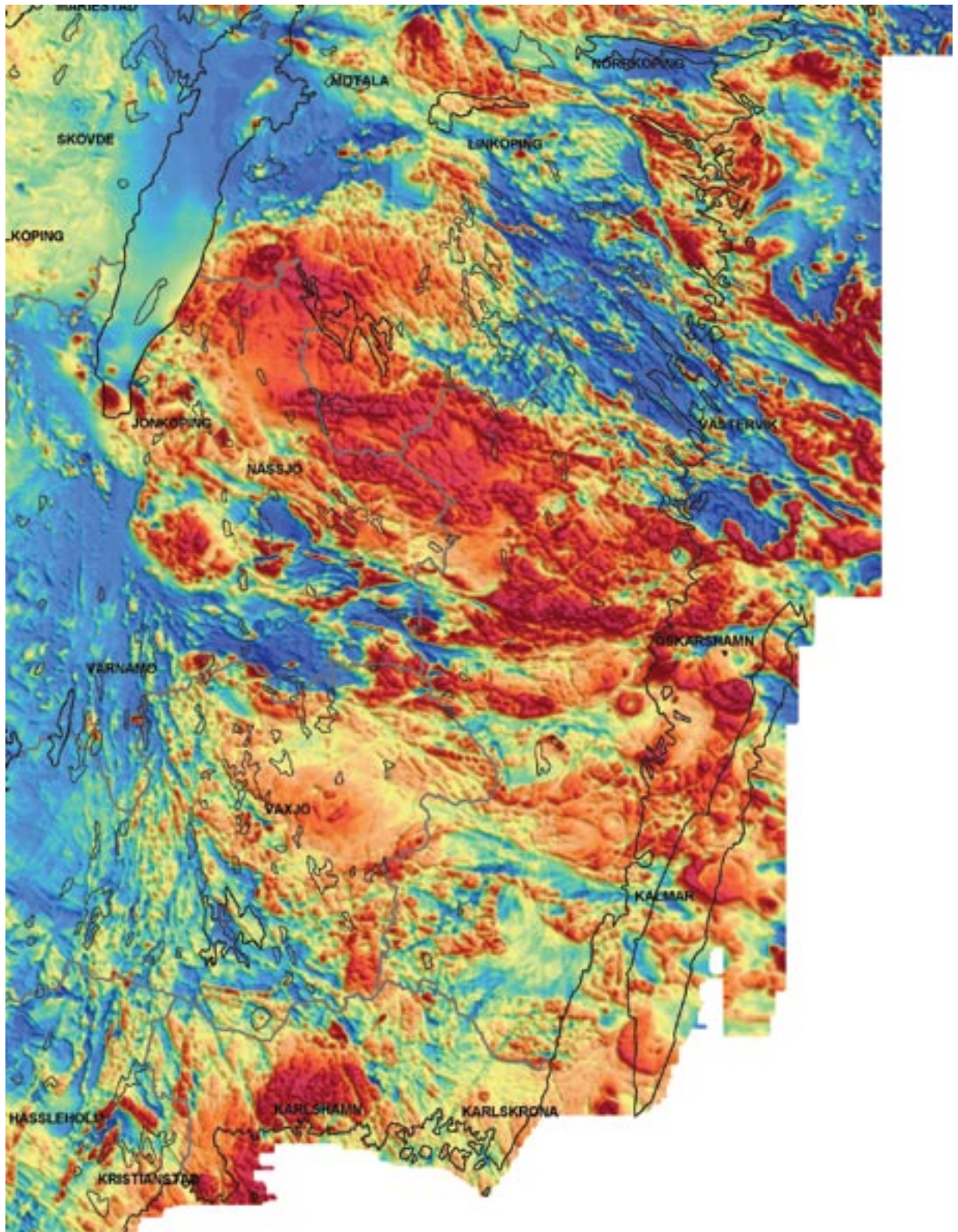
Figure 2-2. *Magnetic anomaly map of southeast Sweden, courtesy of SGU, the Geological Survey of Sweden /Kero 2004/. Data acquired with a 200 m flight line spacing, 40 m sampling interval and 30–60 m ground clearance.*
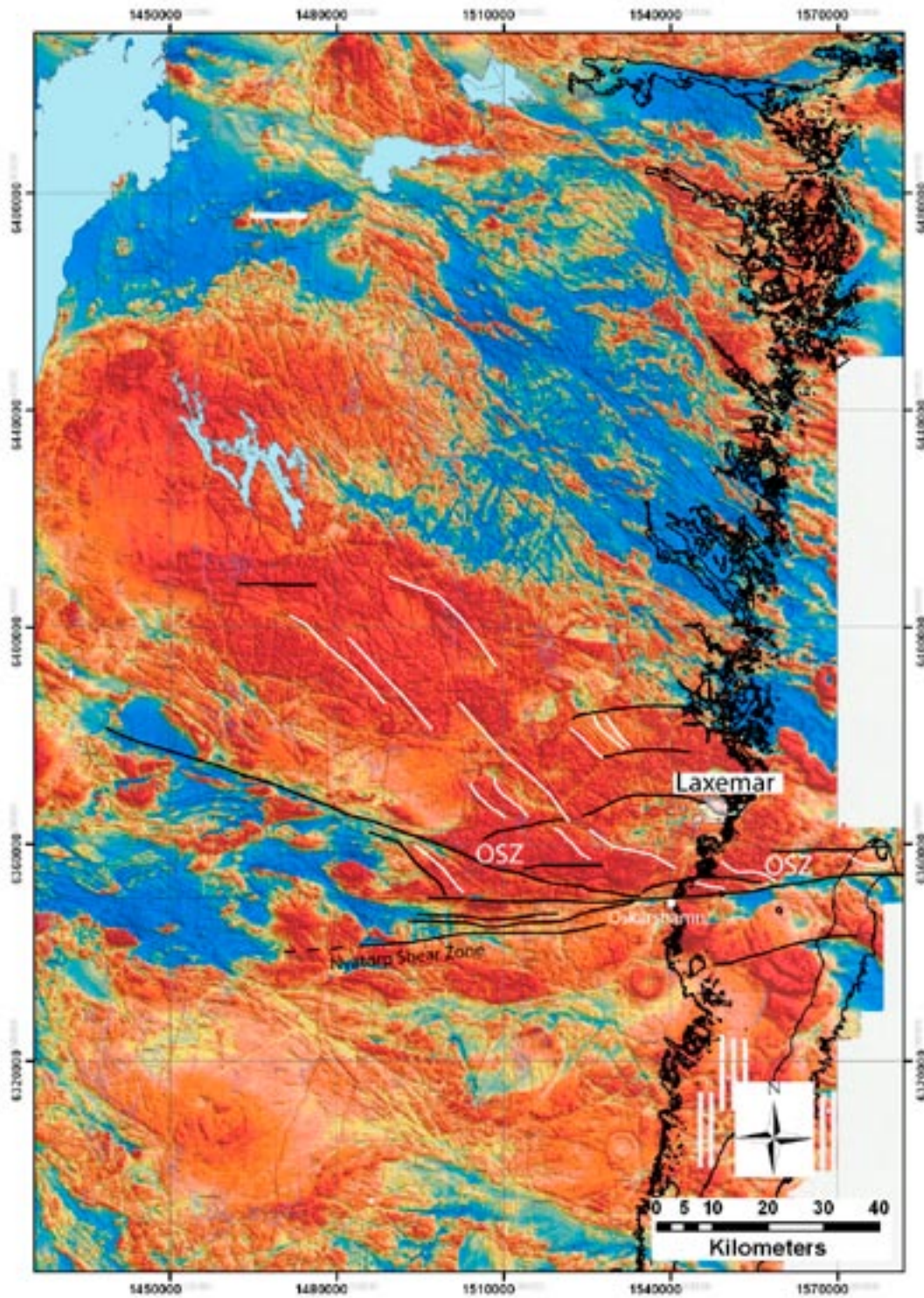
Figure 2-3. *Airborne magnetic anomaly map of southeast Sweden. A complex set of ENE-WSW trending shear zones is identified and referred to as Oskarshamn Shear Zone (OSZ). The Nyatorp Shear Zone is described by /Skjernaa 1992/.*

Detailed analysis of the airborne magnetic anomaly map shows that these lineaments are transacted by discrete, E-W-to ENE-WSW-trending shear zones (black lines in the figure). The most prominent of these features extends, as seen on the geophysical map, for more than 70 km; it strikes ENE-WSW and runs immediately north of the town of Oskarshamn (Figure 2-3). It is here referred to as "Oskarshamn shear zone (OSZ)". The OSZ has a very simple and straight trend in the east, whereas it becomes an irregular composite structure to the west, where its termination is interpreted as being characterized by a series of ESE-WNW-trending horse-tailed shear zones that splay off the main trend and continue towards Jönköping. The OSZ is thus defined by a zone of narrow, anastomosing steep shear zones. This system, the easternmost continuation of which in the Baltic Sea remains unexplored by this study in that no high-resolution geophysical coverage is available to the author, forms apparently a major structural discontinuity that separates regions of slightly different magnetic signatures, with the TIB to the north of it displaying generally higher magnetic values. Moreover, the northern block is also characterized by a more pervasive structural grain than the TIB rocks to the south.

The OSZ seems to be spatially linked to the southernmost limit of the so-called Oskarsrhamn-Jönköping Belt, a c. 150 km long belt of supracrustal and intrusive rocks enveloped by the younger TIB intrusive rocks. The supracrustals within this belt consist of arkoses and conglomerates together with mafic to acid volcanic rocks (see review in /Mansfeld 1996/).

/Skjernaa 1992/ described in detail the Nyatorp Shear Zone (Figure 2-3), possibly part of this system of shear zones. Her field and microstructural investigations invariably showed down-dip normal kinematics along ENE-WSW-trending and NNW steeply-dipping mylonites. Such displacement, however, is suggested to have possibly formed during a later reactivation of the shear zone and its initiation as a strike-slip corridor is considered likely. Moreover, there are other shorter lineaments, predominantly in the northern block, that have similar orientation to the main OSZ, possibly defining a broad, c. E-W-trending shear corridor. As evident from geological and geophysical maps of southeast Sweden, there are several steep deformation zones that often define lithological boundaries and dissect the Proterozoic bedrock with approximate E-W trends.
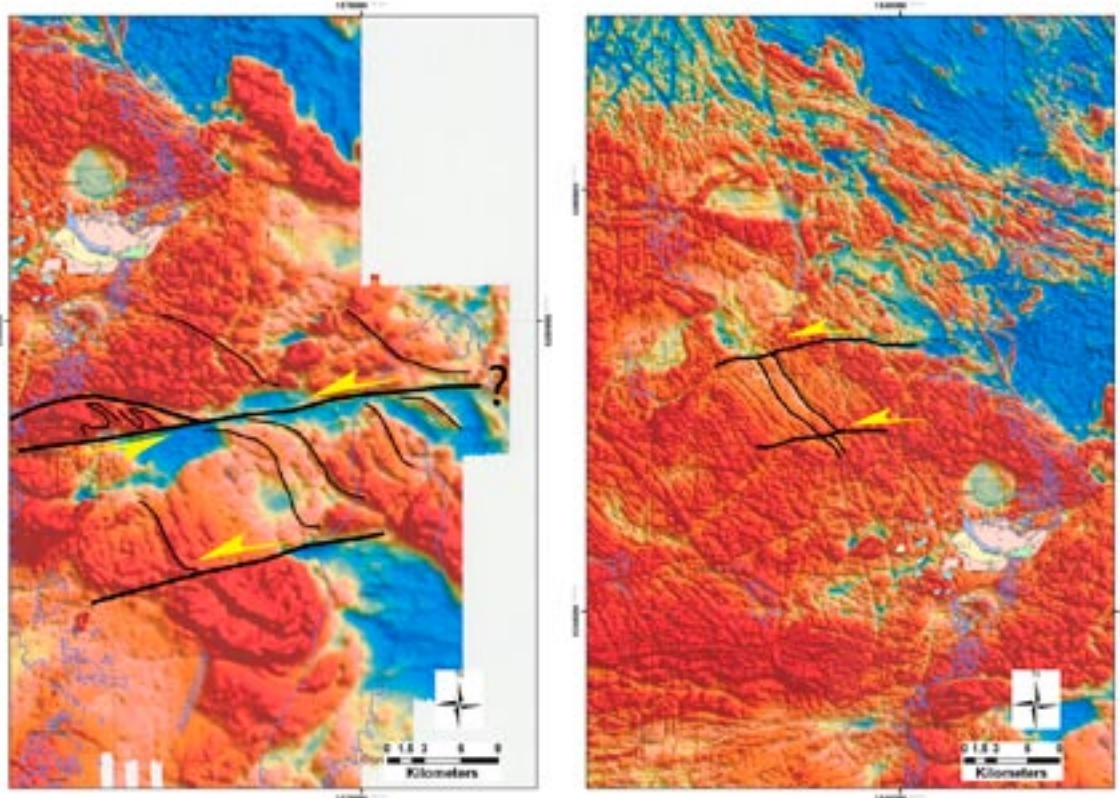
Geometric relationships between the OSZ, the shorter lineaments parallel to it and the pervasive NW-SE lineaments in the TIB help define useful structural criteria to establish at least part of the kinematic evolution of the OSZ, although the lack of information on the orientation of the mean OSZ stretching lineation prevents detailed kinematic reconstructions. Nonetheless, given the clear asymmetries recognizable along the trend of the OSZ, it is reasonable to assume that the OSZ is (or has at least been during part of its evolution) a strike-slip shear corridor, accommodating more or less oblique shear, and that the airborne magnetic anomaly map provides a section close to the XZ plane of maximum 2D strain.

Figure 2-4 shows two of the examples used to infer sinistral kinematics for the OSZ shear corridor, as indicated by S/C geometric relationships and asymmetric sinistral drag folds along the strike of the shear zone. Sinistral kinematics are also suggested by the orientation of the NW-SE linear fabric in the TIB north of the OSZ (white lines of Figure 2-3), which tends to rotate counter clockwise towards the OSZ, thus attaining a more E-W orientation, in line with their asymptotical bending into the shear zone orientation in response to sinistral shearing. The trend of the lithological contacts in the Laxemar-Simpevarp model area is also progressively rotated and, whereas in the western part of the study area contacts strike generally NW-SW, in the east they attain a c. E-W orientation, thus in agreement with the observations made above.

As to the timing of the (multiple?) movement of the OSZ, the only robust constraint is that it postdates the emplacement of the TIB rocks, which it deforms.

An assessment of the implications of the establishment of the OSZ shear zone system and of its inferred sinistral component of movement would require a separate, specific study, which is beyond the scope of this report. It is suggested that a modern kinematic study of these lineaments should be performed so as to constrain their complete (and possibly polyphase) ductile and brittle evolution.

Figure 2-4. Examples of the suggested kinematic interpretation of the OSZ and subsidiary lineaments. Shear sense is inferred on the basis of S/C geometric relationships and asymmetric sinistral drag folds along the shear zone.

### 2.2.2 The local ductile structural framework

After the analysis of the major ductile features affecting the Oskarshamn area presented above, it is necessary to summarize and interpret the local ductile structures of the Laxemar-Simpevarp area in the light of the characteristics of the suggested regional ductile deformational framework. The main goal is to match the lineaments recognised locally to the broader picture, so as to be able to use geometric and kinematic compatibility criteria among ductile features of different order as a validating tool for the final models. Figure 2-5, for example, shows all ductile and brittle deformation zones identified and constrained within the Laxemar-Simpevarp regional model area, whereas Figure 2-6 zooms into the Laxemar local model area and its deformation zones. It is clear that if a consistent kinematic and geometric structural interpretation is to be proposed for the local model area, this has to be done by referring to the broader structural framework.
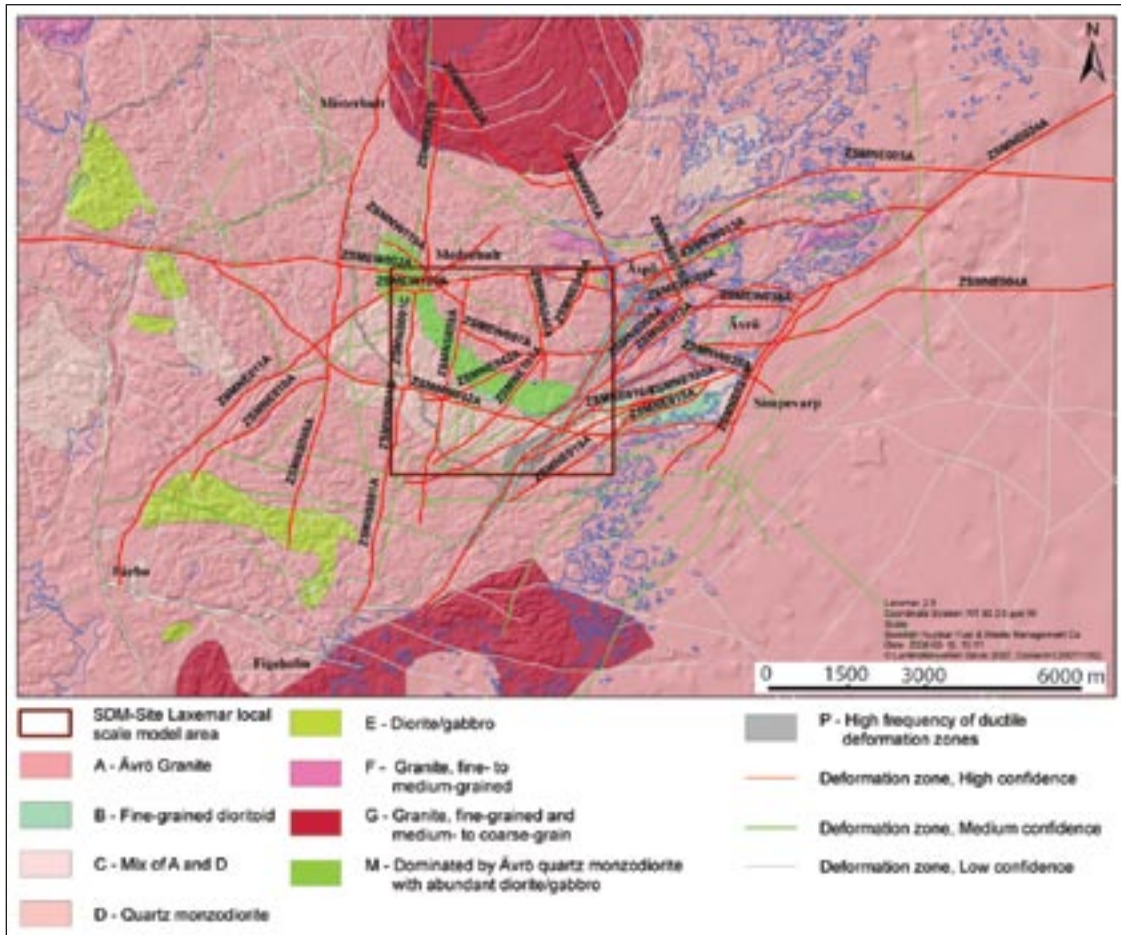
Figure 2-5. *Overview of the deformation zones and rock domains modelled deterministically in the Laxemar-Simpevarp regional model area. The figure is taken from /Wahlgren et al. 2008/.*

The ductile deformation zones exposed in the Laxemar-Simpevarp area and immediate surroundings (Figure 2-5 and Figure 2-6) are low-grade ductile to brittle-ductile shear zones that vary in thickness from millimetres up to tens of meters. Different sets of deformation zones were identified, modelled and assigned with properties. Although commonly overprinted by brittle deformation, the majority of these zones contain ductile precursors, thus demonstrating that the dominant structural framework was formed when the bedrock still responded to applied stresses in a ductile fashion. A comprehensive description and analysis of their characteristics is given in /Wahlgren et al. 2008, Söderbäck 2008/ and the reader is referred to those reports for more detailed information.
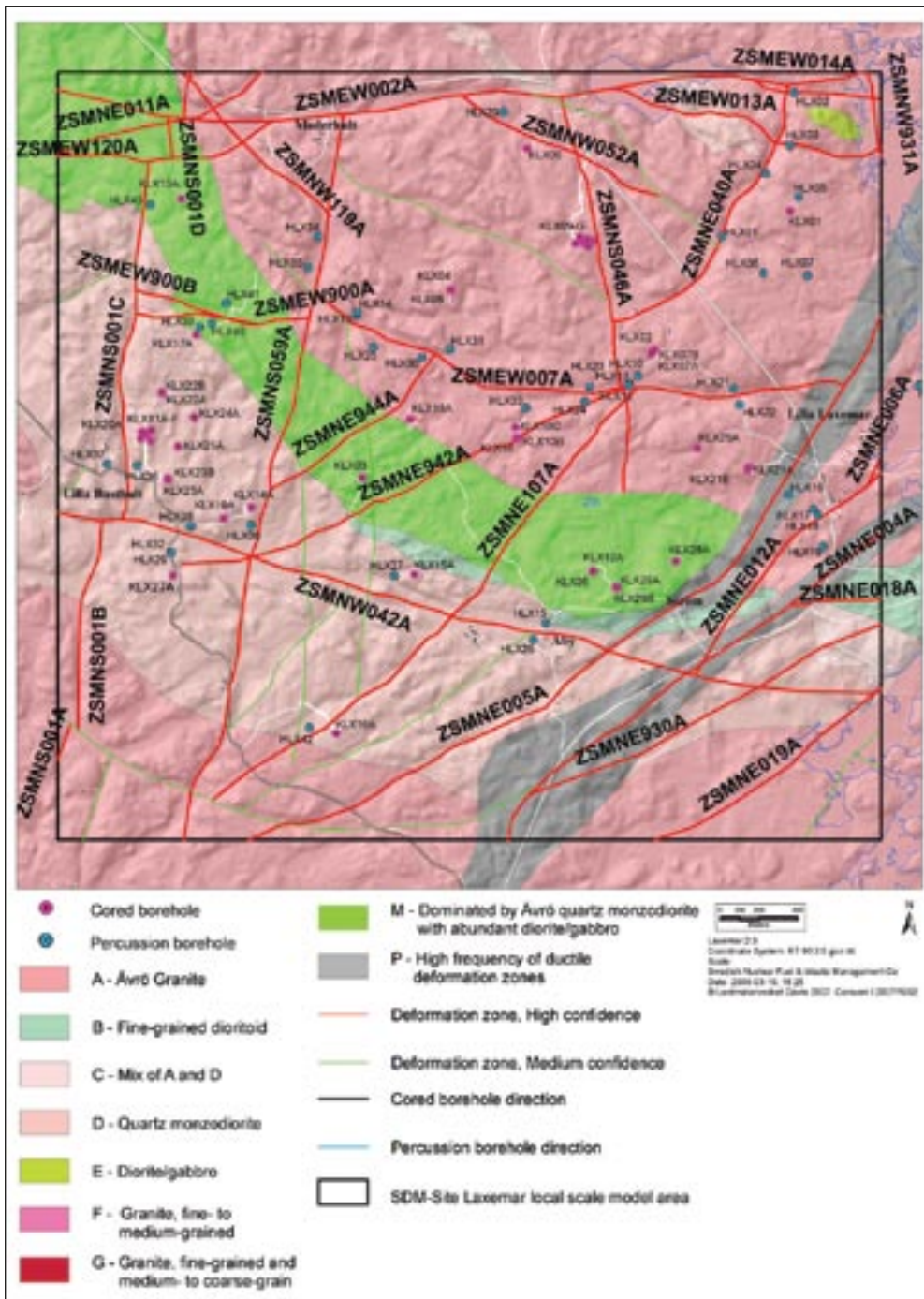
Figure 2-6. *Overview of the deformation zones and rock domains modelled deterministically in the Laxemar local model area. Location of cored and percussion boreholes is also shown. The figure is taken from /Wahlgren et al. 2008/.*

The study of the high-resolution geophysical data of the regional model area is extremely useful for the understanding of the ductile framework exposed in the Laxemar-Simpevarp area. Figure 2-7 shows the available airborne magnetics for the regional model area. The characteristics and main results of each survey carried out during the site investigation study are summarised by /Wahlgren et al. 2008/. In this report, the total magnetic field dataset (Figure 2-7 top) and its two vertical derivatives are used (Figure 2-7 centre and bottom). Much can be learned, particularly from the vertical derivatives of the total magnetic field, which amplify short-wavelength information at the expense of long-wavelength information, thus enhancing the edges of magnetic lineaments and the structural grain in the upper part of the bedrock.

16
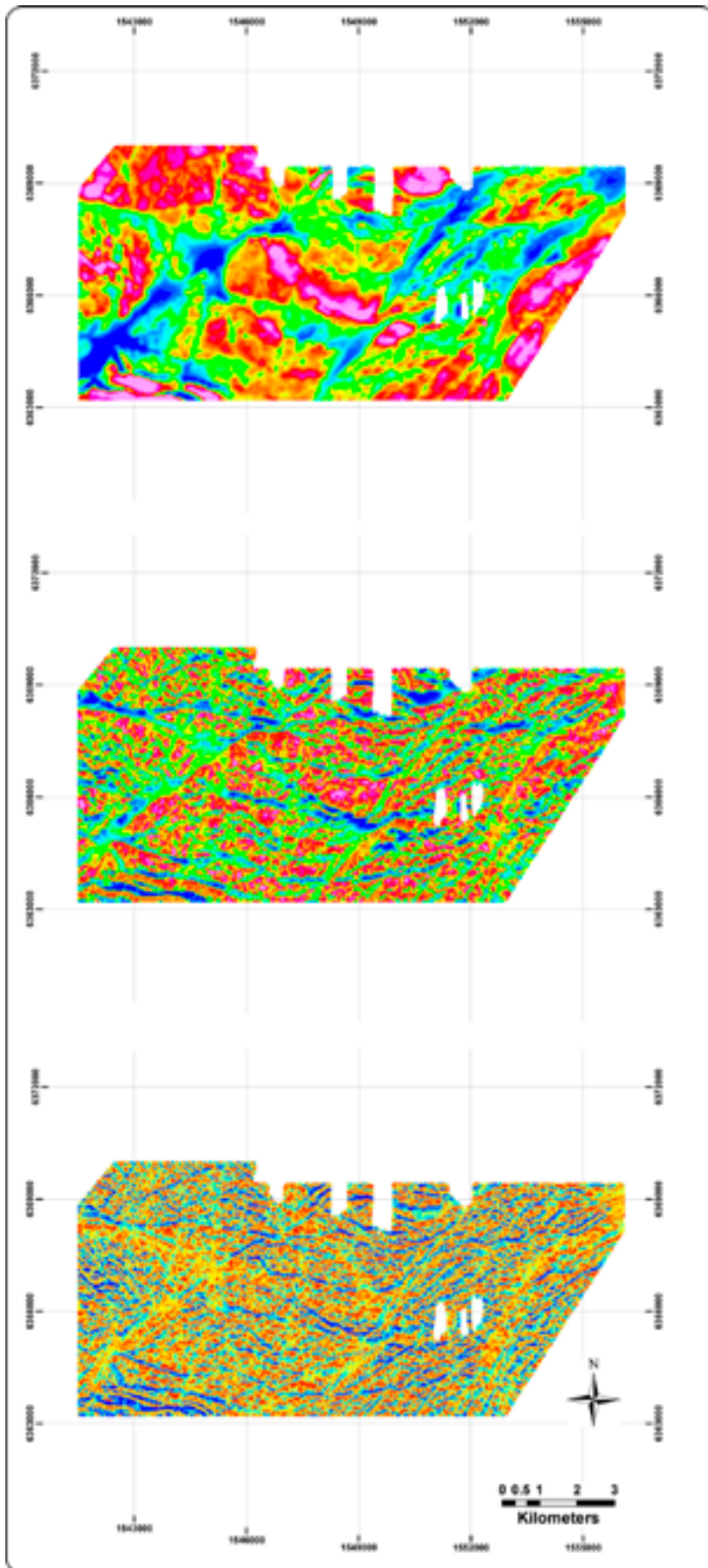
Figure 2-7. *Total magnetic field plus its first and second vertical derivatives of the regional model area (top, centre and bottom images, respectively).*

17

During the different phases of the Oskarshamn site investigation, the degree of resolution of available magnetic total field data has progressively increased and as a result the possibility to identify also narrow and short lineaments has continuously improved. The integrated analysis of the multitude of lineaments recognisable from the airborne magnetic data was included in the site investigation programme. Geophysical lineaments were studied by means of field work, geophysical profile measurements, trenching, drilling activities and single-hole interpretations with the goal of assessing their true geological significance. Figure 2-8, for example, shows what deformation zones correspond to individual magnetic lineaments as seen on the second vertical derivative of the total magnetic field.

The structural interpretation of the first and second vertical derivatives has proved to be particularly informative as to the relationships among the main ductile deformation zones of the regional and especially local model areas. Deformation zones ZSMNE004A, ZSMNE005A, ZSMEW002A, ZSMNS059A and ZSMNE011A (Figure 2-6) display a significant ductile component that corresponds to lineaments identified within the regional model area and their mutual spatial relationships are shown in Figure 2-9, in 2 and 3D respectively.

The structural pattern highlighted by Figure 2-9a suggests a ductile scenario that differs from that proposed by /Wahlgren et al. 2008/. The magnetic lows corresponding to deformation zones ZSMNE011A, ZSMNE004A and ZSMNE005A show a geometry similar to that described as C' structure /Berthé et al. 1979/, shear bands /White et al. 1980/ or ECC /Platt and Vissers 1980/. These shear zones deform sinistrally sets of intervening, c. E-W trending magnetic lineaments, referred to here as S surfaces. Such shear-band structures are generally envisaged as developing late in a shear zone history as the result of instability in the stretching, strongly anisotropic mylonitic foliation (i.e. a form of asymmetric foliation boudinage). A visual comparison to textbook field examples may help illustrate better the similarity between the proposed interpretation of the second derivative map and the more commonly observed outcrop-scale examples (Figure 2-10).
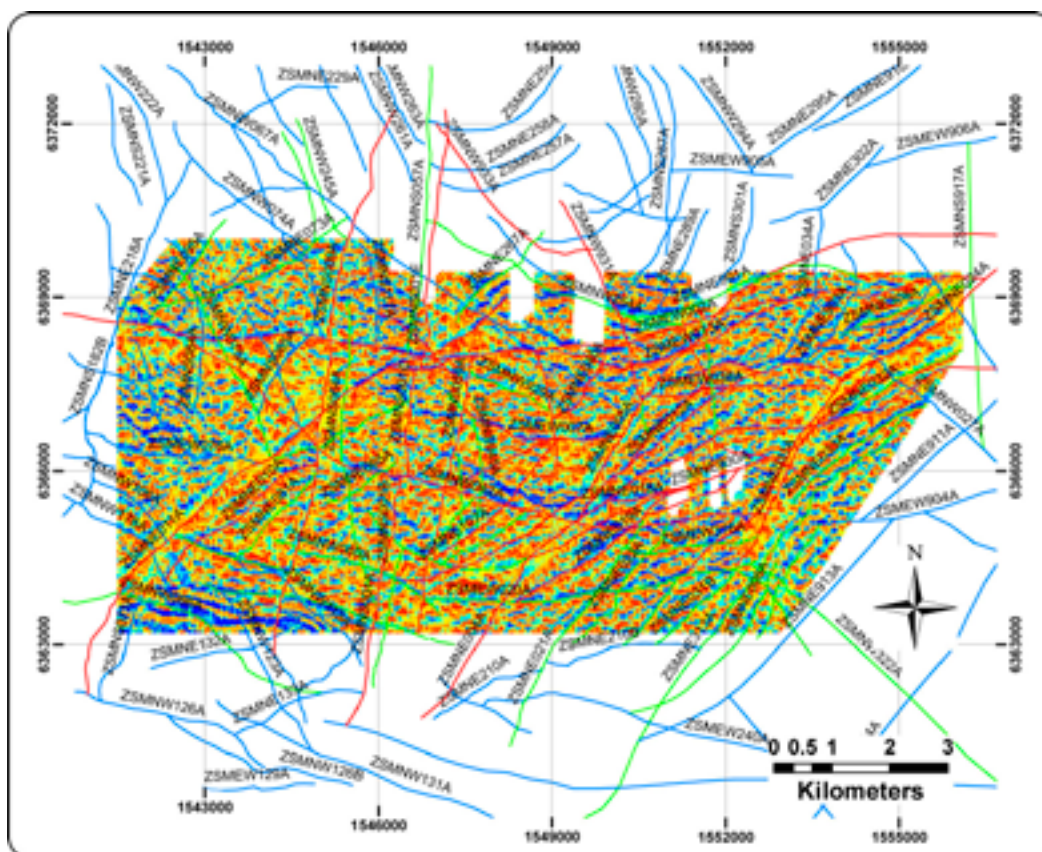
Figure 2-8. *Second vertical derivative of the total magnetic field covering the regional model area overlain by the identified deformation zones (red: high confidence, green: medium confidence and blue: low confidence lineament).*
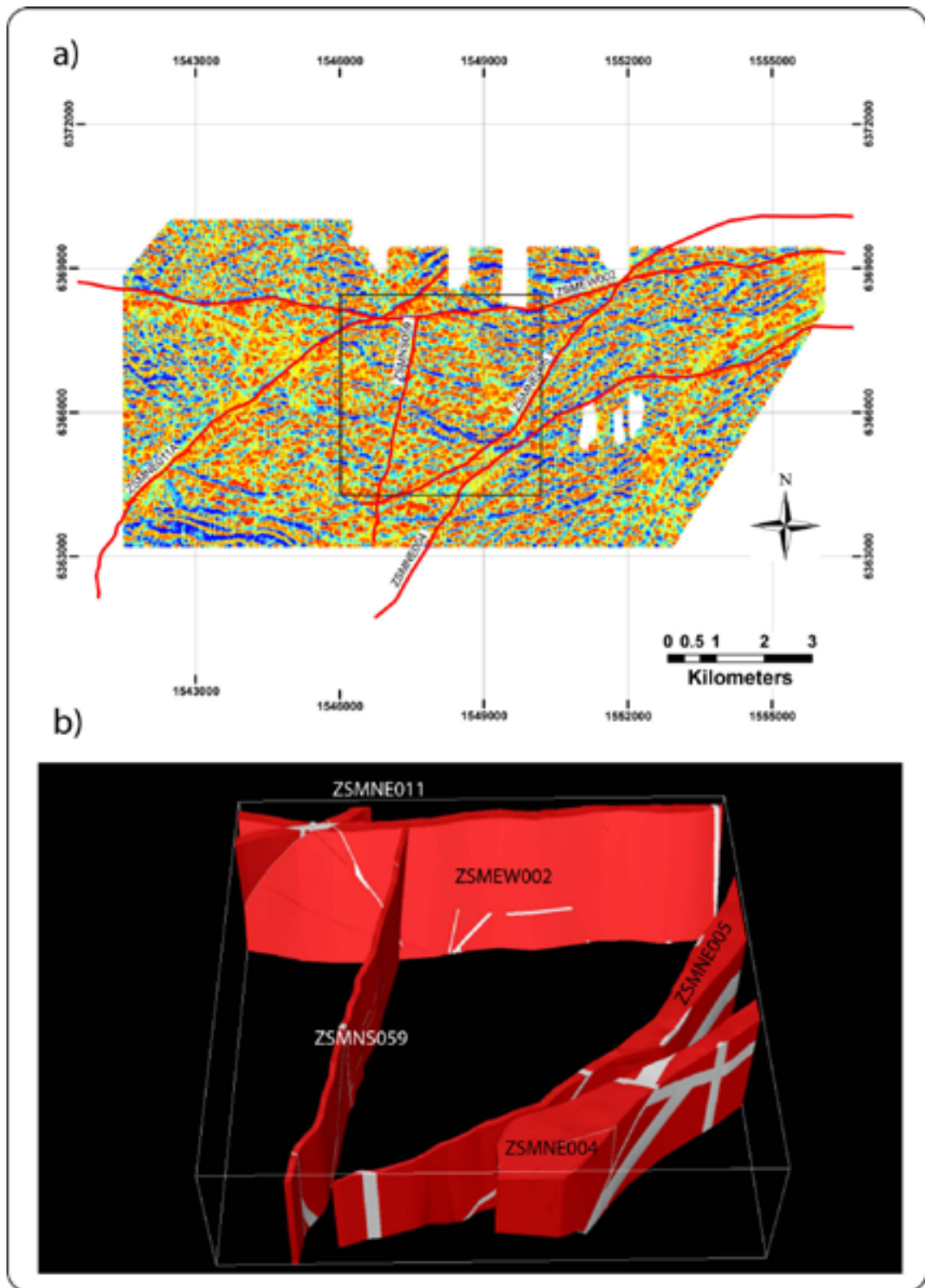
Figure 2-9. *a): Trace of ductile deformation zones drawn on the second vertical derivative of the total magnetic field. The black square locates the local model area. b): Ductile deformation zones modelled in a 3D space representing the local model volume. View to the north.*

19
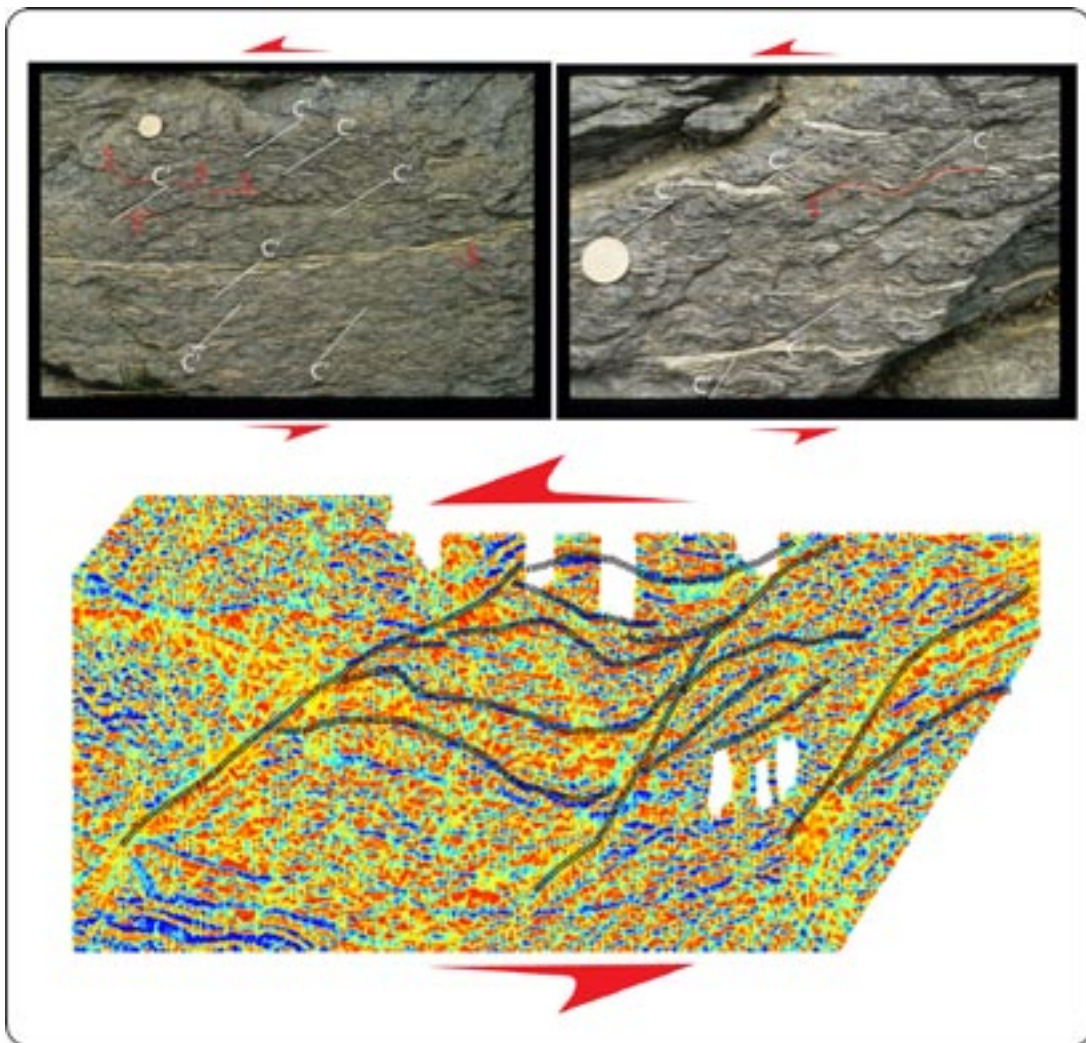
Figure 2-10. *Field examples of S/C' fabrics from the Mortirolo shear zone, Italian Central Alps. S/C' fabrics can be read as a form of asymmetric foliation boudinage. Both photographs are taken looking down onto a sub-horizontal pavement. The geometric relationships between the newly formed shear planes C' and the pre-existing foliation planes S suggest an overall sinistral sense of shear parallel to the foliation planes. The interpreted geophysics for the Laxemar-Simpevarp regional model shows very similar geometric relationships between ZSMNE004A, ZSMNE005A, and ZSMNE011A (C' shears; but also ZSMNE024A and ZSMNE031A, not discussed here in detail), and the c. E-W-trending magnetic lineaments (S planes). The asymmetry of deflection of the S planes into the C' shears indicates sinistral shearing along a c. E-W shear corridor.*

As shown by Figure 2-10, there is indeed a strong similarity between the geometry of the ductile features in the Laxemar-Simpevarp area and classic mesoscale S/C' fabrics. The most striking aspects of this comparison are the presence of sub-parallel ductile shear belts (ZSMNE011A, 024A, 31A, 004A and 005A), the C' shears, which deform sinistrally intervening, E-W trending lineaments, the S planes. These lineaments are significantly crenulated/folded in response to their dragging into the C' shears, a geometric pattern indeed very similar to that shown in the photographs of the field examples. A difference is the fact that C' shears visible in the geophysics seem to be at a slightly higher angle to the S planes than observed in the outcrop-scale cases documented here. This might be due, however, to the existence of planar anisotropies in the TIB rocks at the time of ductile shearing, which determined a slight deviation from the expected pattern.

As mentioned above, C' shears are believed to form relatively late in the shearing sequence and definitively after S surfaces. The asymptotic bending of S planes is itself a strong argument that S planes are prekinematic with respect to shearing along C' shear bands. In this respect it is

useful to study the spatial "connection" between, for example, ZSMEW007A and ZSMEW009A (S surfaces in this model) and ZSMNE005A (a C' shear band). Figure 2-11 shows the details of these geometric relationships circled by two black ellipses. The regional lineaments in the figure are drawn following the latest SKB "deformation zones" version (Laxemar 2.3); their locations reflect long and detailed multidisciplinary investigations, including field analysis, geophysical surveying, trenching, single-hole and DEM interpretation. When possible, they are defined by a median line and envelope, which marks the actual deformation zone width at the surface. The black ellipses of Figure 2-11, however, show two areas where, on the basis of the structural model presented here, the traces of ZSMEW007A and 009 are questioned and should possibly be re-evaluated. ZSMEW007A easternmost and ZSMEW009 westernmost terminations against ZSMNE005A are in fact straight and the lineaments are terminated very sharply. This is at odds to the remaining part of the map, where the lineaments follow exactly two low magnetic belts (Figure 2-11), whereas close to ZSMNE005A their traces abandon such low magnetic corridors, cut them across discordantly and abut against the trace of the NE-trending 005A lineament.
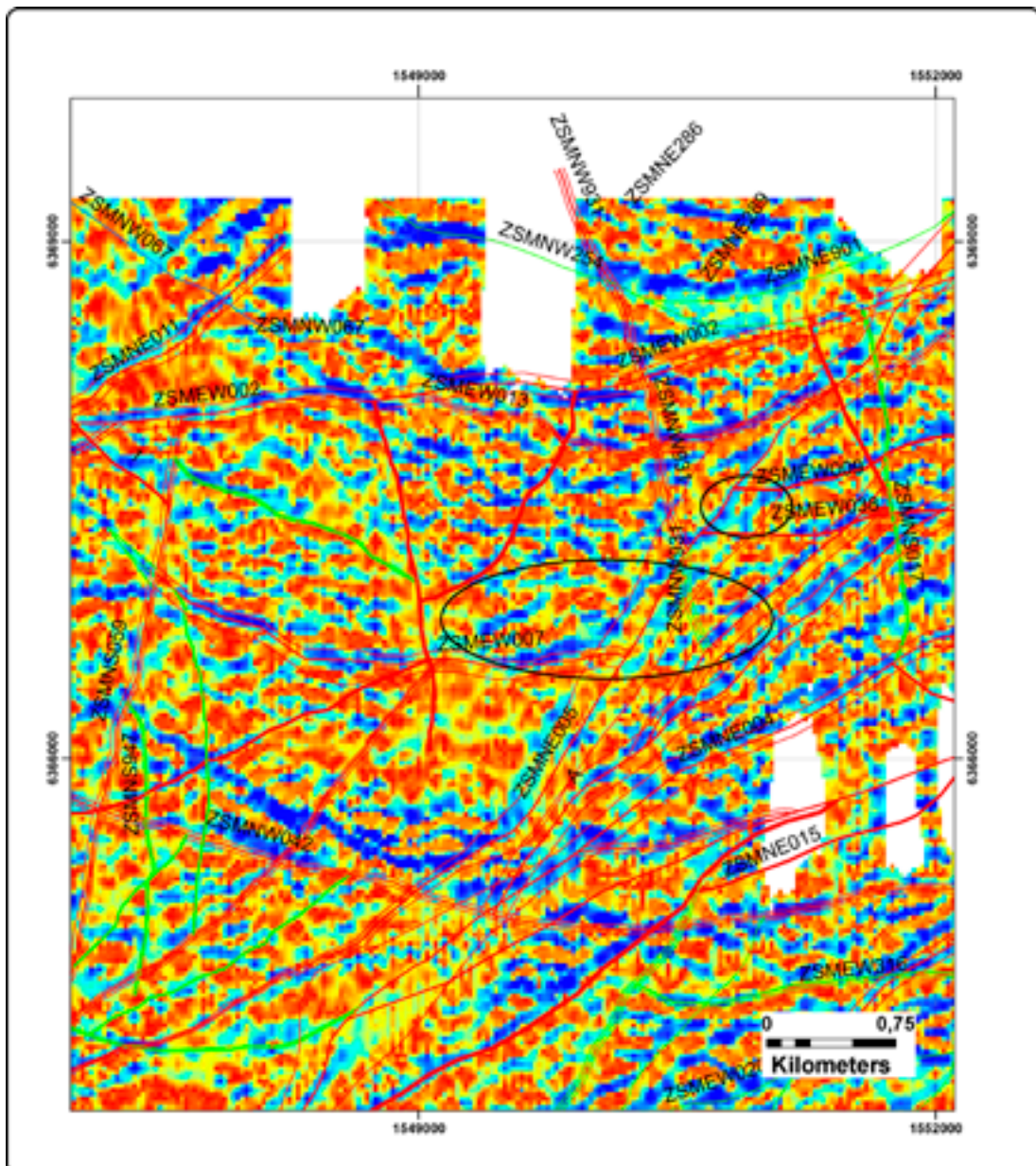

Figure 2-11. *Two black ellipses show the spatial relationships between ZSMNE005A, ZSMEW007A and 009 as seen on the second derivative of the total magnetic field. See Figure 2-12 for the alternative proposed here.*

An alternative to this interpretation is shown in Figure 2-12, where it is suggested that lineaments ZSMEW007A and ZSMEW009 can be connected through sinistral displacement across ZSMNE005A.

The coloured solid circles in the figure represent samples analysed by /Mattsson 2006/ for anisotropy of magnetic susceptibility from rocks collected across the Äspö shear zone, i.e. ZSMNE005A. The main goal of the study was to test how far from the zone boundaries variations in the magnetic properties related to the ductile deformation process can be identified. Green dots plot Ävrö granite samples whose magnetic properties were not affected by the effects of shearing, yellow dots plot the reconstructed transition zone and red dots the actual core of the mylonitic shear zone. It is worth noting that the deflection of ZSMEW007A to the ENE in response to its sinistral dragging is confined to an area to the west of ZSMNE005A, which corresponds to its transition zone, according to the results of /Mattsson 2006/. This observation supports the new proposed trace of ZSMEW007A in Figure 2-12, where the low magnetic belt, which is EW trending in the W, changes progressively its orientation and swings in ZSMNE005A.
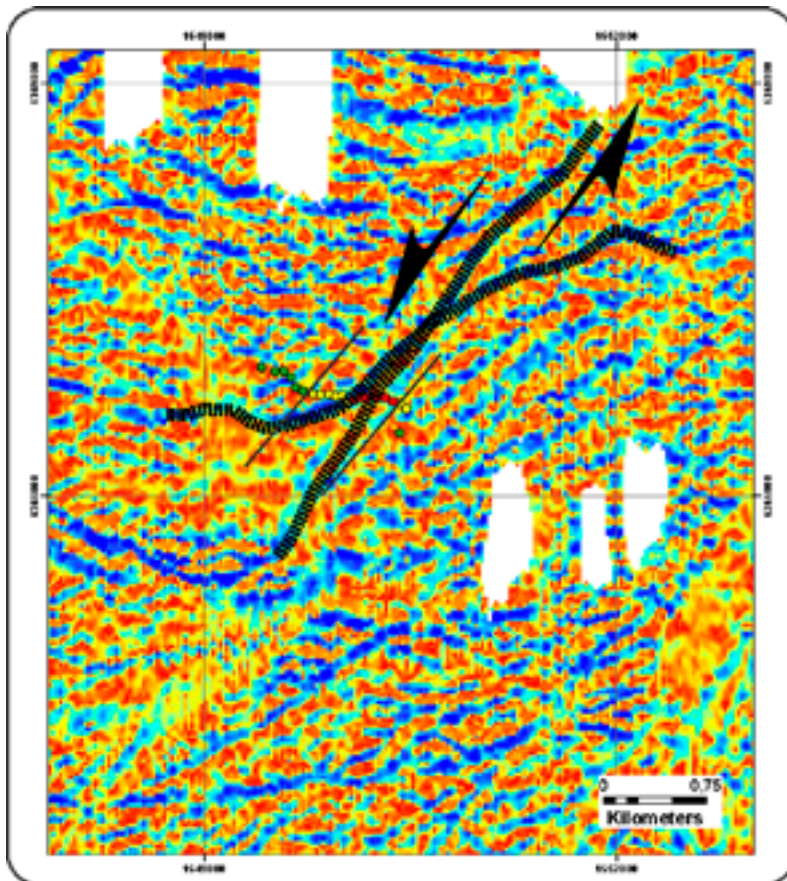

Figure 2-12. *Alternative model proposing a connection between ZSMEW007A and ZSMEW009A. The two lineaments are asymptotically bent and displaced along the sinistral ZSMNE005A. Coloured circles show the location of the samples of the study on magnetic anisotropy of rocks across lineaments ZSMNE004A and 005 by /Mattsson 2006/. See text for more details.*

If true, this model would imply that ZSMEW007A and ZSMEW009A (plus all other features that are dragged in the Äspö shear zone) are syn- to pre- sinistral shearing along the Äspö shear zone. Systematic work carried out on ZSMEW007A, a dominant structure in central Laxemar, has led to the conclusion that the lineament strikes E-W to ESE-WNW, is c. 80 m thick and dips to the north at 35° to 45°. More importantly, the zone is interpreted and modelled as being wholly brittle. This is in general agreement with many observations, including the detailed logging of cores intersecting the lineament (DZ5 of KLX04A and DZ4 in KLX09; /Viola and Venvik Ganerød 2007ab/ and field structural analysis of the lineament as exposed in a surface trench /Viola and Venvik Ganerød 2007a/. However, minor occurrences of brittle-ductile/ductile precursors were observed and interpreted as evidence of foliated cataclasites in a red gouge component sampled from the trench (Figure 2-13; /Viola and Venvik Ganerød 2007a/).

The kinematics of the lineament remains dubious and only suggestions could be made on it being a top-to-the north/north-east normal fault.

ZSMEW009A is reported as striking c. EW and dipping c. 75° to the south /Rhén et al. 1997/. It contains a mylonitic core and a significant central zone of clay-gouge. These characteristics suggest caution when proposing a connection to ZSMEW007A. On the other hand, it is well acknowledged that ductile features are commonly overprinted and locally obliterated in the area by younger brittle events (which would account for the lack of obvious and pervasive ductile precursors along ZSMEW007A) and the change of dip direction could be reflecting spatial adjustments of the fault/shear plane in response to its passive dragging into the Äspö shear zone.
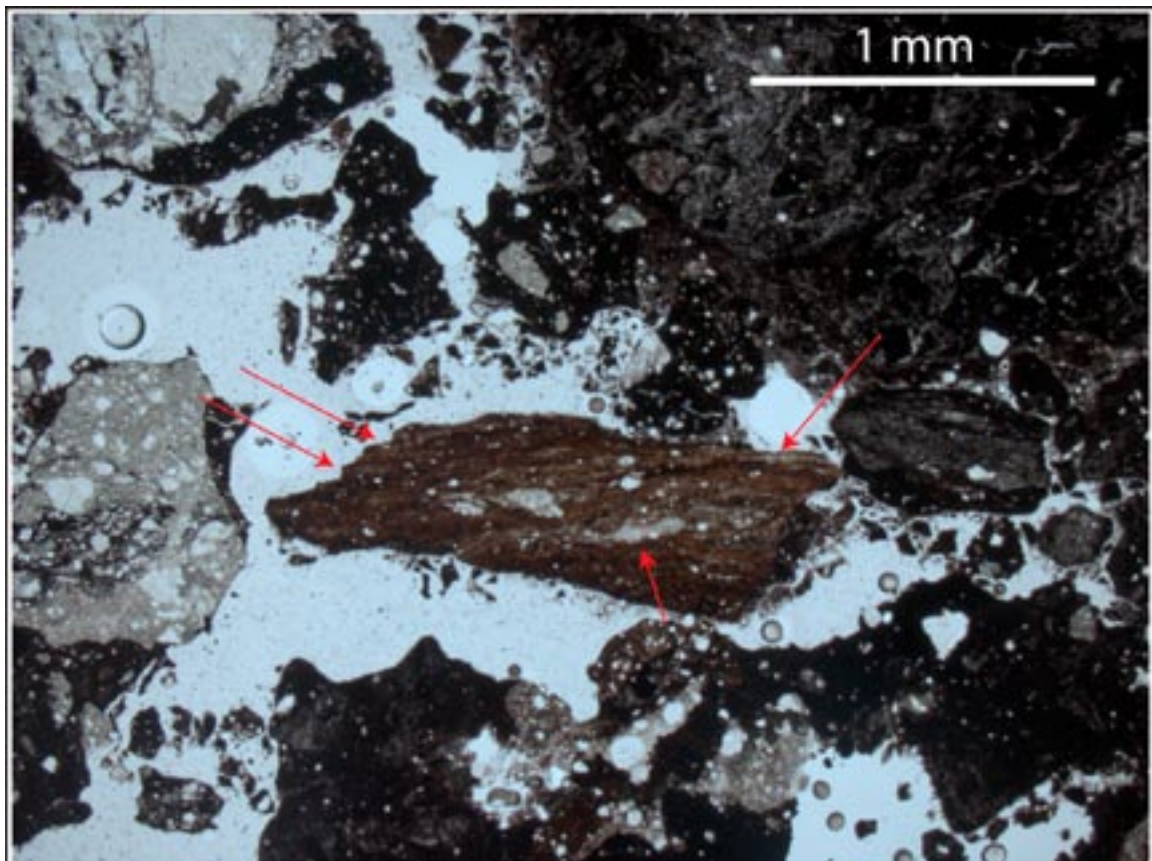
Figure 2-13. *Clast of foliated cataclasite from the trench dug across ZSMEW007A and described by /Viola and Venvik Ganerød 2007a/. Red arrows indicate continuous foliation planes that can be followed within the clast. Plagioclase crystals are locally stretched along the foliation.*

23

2.3 Discussion

The implications of the model presented above are straightforward.

If ZSMEW007A, described as entirely brittle, is deformed by ZSMNE005A and ZSMNE004A, which are instead ductile, it is necessary to consider multiple ductile shearing episodes and also the possibility of the existence of earlier localised brittle precursors to some of the ductile shear zones. The 1.4 Ga age from the Äspö shear zone of /Drake et al. 2007/ can be thus alternatively interpreted as a real crystallization age, reflecting a renewed ductile phase after the intrusion of the Götemar and Uthammar granites at about 1.45 Ga. This ductile phase would postdate earlier ductile shearing. As mentioned above, /Wahlgren et al. 2008/ assign the whole ductile history of the area to the waning stages of the Svecokarelian orogeny, at c. 1.76 Ga, thus slightly later than the TIB crystallization at c. 1.80 Ga.

On the other hand, ZSMEW009A, the possible eastward continuation of ZSMEW007A, has an obvious ductile core overprinted by penetrative brittle deformation. If similar characteristics are considered possible also for ZSMEW007A, then it remains to be established whether dragging and shearing of the latter occurred once its brittle overprint had already been accommodated.

As shown in Figure 2-14, there is convincing evidence that lineament ZSMNS059A cuts across the Uthammar granite and therefore postdates its intrusion. Its corresponding magnetic lineament is one of the clearest lineaments in the local model area. The zone has a clear ductile character, marked by the occurrence of mylonitic outcrops. Available evidence suggests it to be sub-vertical, c. 50 m thick, and detailed mapping of surface outcrops indicates strike-slip sinistral kinematics /Lundberg and Sjöström 2006/. Its sinistral ductile kinematics can be envisaged as being part of the same structural framework of ZSMNE004A, 005A and 011A, whereby it possibly represents a sinistral Riedel shear to the NE-striking ductile shear zones. In this case, its effects on the Uthammar granite would argue for a phase of ductile shearing post Uthammar intrusion, possibly at 1.4 Ga. Significant brittle activity has, however, also been reported for ZSMNS059A, with abundant crush zones and slickensided planes. It cannot be excluded, therefore, that the Uthammar granite is only affected by the brittle deformation linked to the reactivation of ZSMNS059A under brittle conditions.

/Viola and Venvik Ganerød 2007ab, 2008/ have documented a few deformation zones (for example DZ 10 of KLX12 and DZ1 of KSH03A) containing convincing evidence of ductile deformational features exploiting and overprinting pre-existing brittle structures, thus corroborating a model with at least two distinct ductile phases, the latest of which postdates earlier brittle features.

In order to validate this model, still speculative at this stage, accurate and reproducible ages from other mineral phases that are synkinematic to the ductile shearing are necessary.

A major consequence of the proposed model is that, in contrast to the kinematic reconstruction of /Wahlgren et al. 2008/ (Figure 2-1), EW- and not NE-trending lineaments and shear zones become the main structural feature of the region. Shear forces acting parallel to these main shear zones can successfully explain all the ductile features described and reported from the area. The greatest compressive stress would trend NE-SW and not c. N-S as proposed by /Wahlgren et al. 2008/.

The analysis of Figure 2-15 provides important elements in support to this model. ZSMNE004A and ZSMNE005A, which are generally interpreted as components of the Äspö shear zone in the local model area, display a dramatic change of strike once they are traced away from the local model area into the Baltic Sea and to the west. From a NE strike in the Laxemar-Simpevarp area, they are progressively reoriented to an EW orientation. In the light of the results of the regional overview presented at the beginning of this section, it is suggested that their "real" orientation is c. EW, i.e. parallel to the OSZ, and that they are deflected to a NE strike due to their passive bending into the Äspö C' shear zone. As a consequence, it is confusing to equate ZSMNE004A and 005A to the Äspö shear zone, because the label Äspö should only be used to refer to the shear zone that deformed and bent asymptotically these otherwise E-W trending lineaments, i.e. the C' shears.
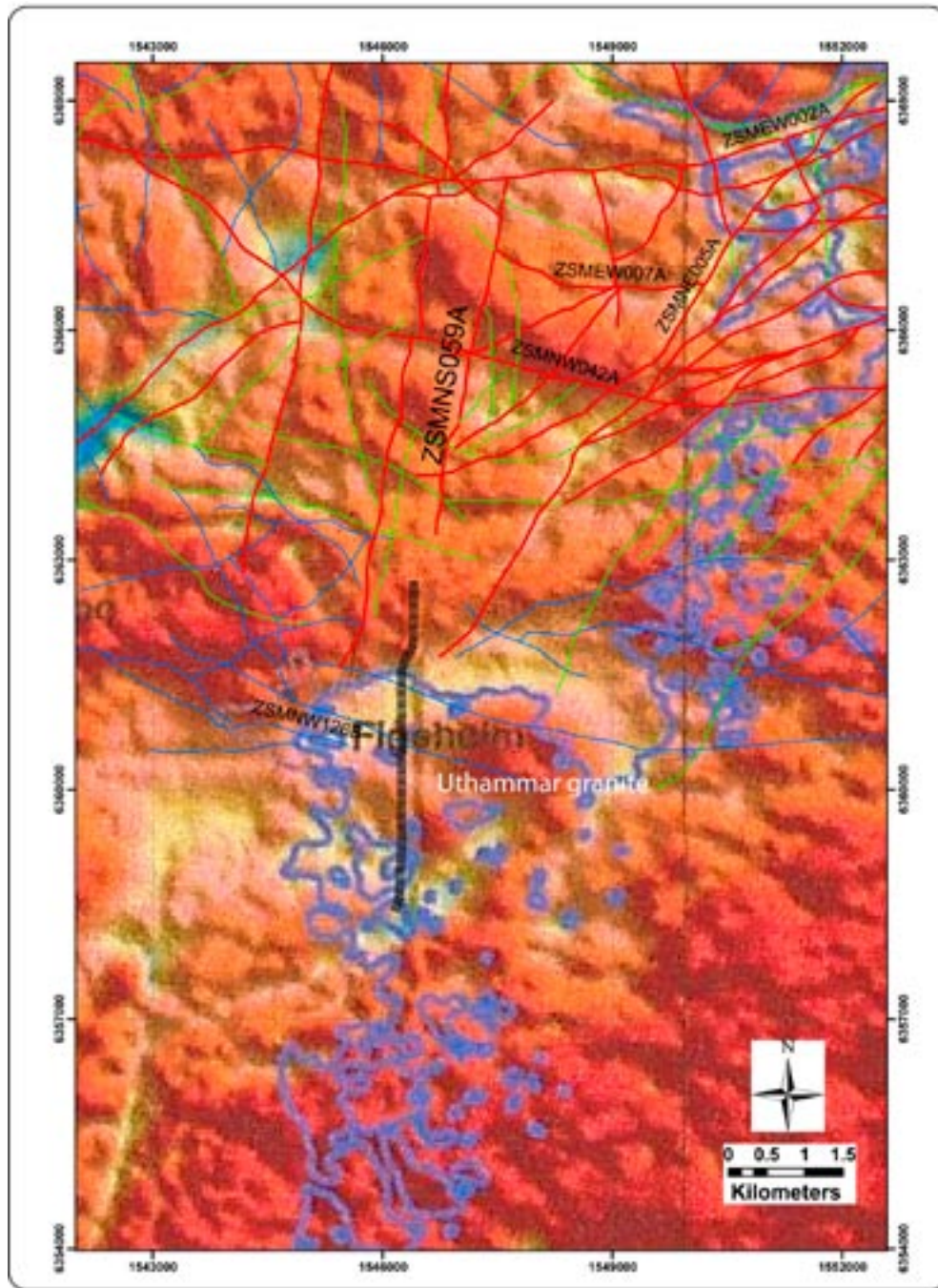
Figure 2-14. *Magnetic anomaly map of the southern part of the regional model area. Note how linea-ment ZSMNS059A, characterized by a ductile history overprinted at later stage by brittle deformation, apparently continues to the south and crosscuts the Uthammar granite at Figeholm. The dashed thick black line shows the interpreted trace of the southern continuation of the lineament but is slightly offset to the west to allow the unbiased identification of the lineament on the airborne magnetic map.*
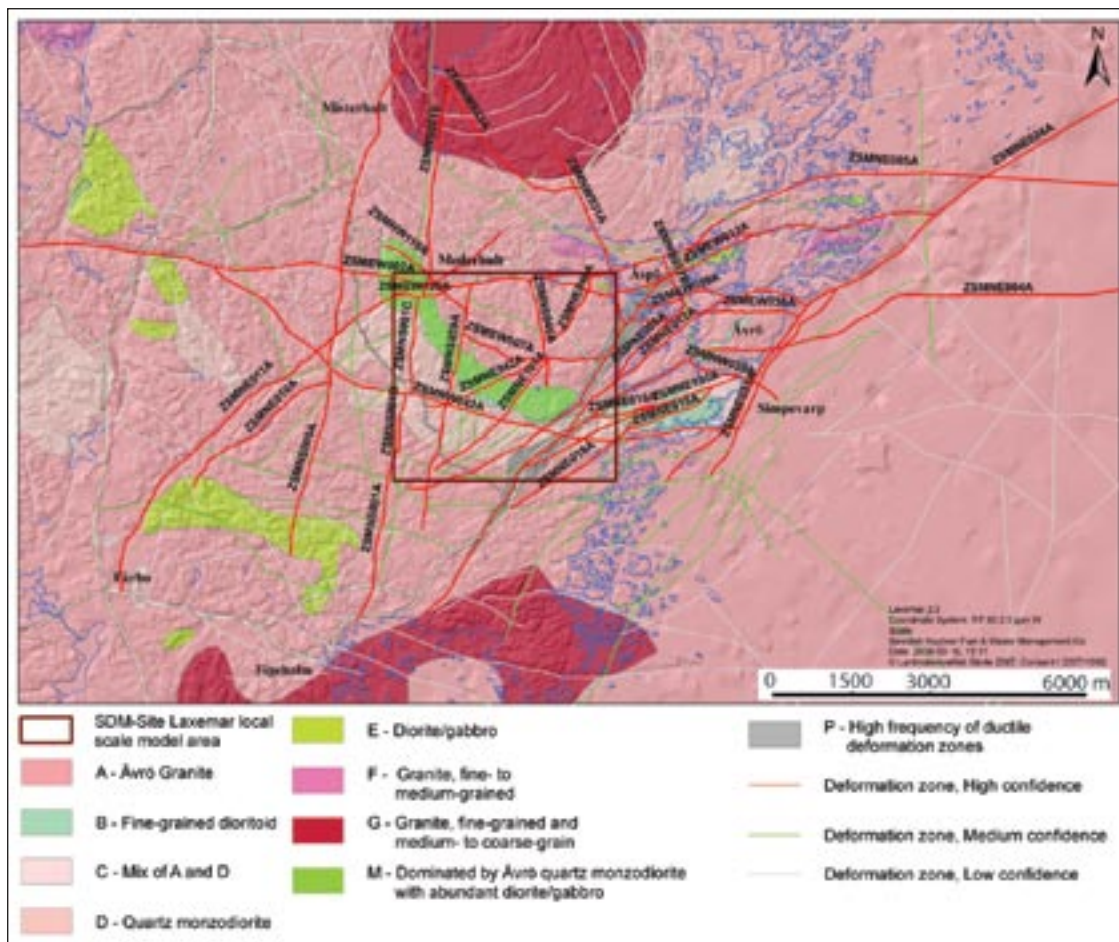
*Figure 2-15. Lineaments from the regional model area.*

It is presumably not a trivial task to distinguish the mylonitic fabric of the Äspö shear zone from the fabric of ZSMNE004A and 005A in the local model area and more investigations would be needed to validate this model. Moreover, unless more detailed structural information is gathered from ZSMNE004A, 005A away from the location of the Äspö shear zone, it is objectively not possible to know the exact characteristics of those lineaments, even whether they are actually mylonitic lineaments or not.

An important E-W-trending lineament of the regional and local model area is deformation zone ZSMEW002A, also referred to as the "Mederhult zone" (Figure 2-15). This is a very significant deformation zone, which strikes in the target area generally EW and is almost parallel with the northern boundary of the local model area. The zone has an estimated length of up to 30 km and a rather variable thickness, from 20 to 200 m, as indicated by the available topographic and geophysical data. The deformation zone has been studied by ground magnetic and VLF measurements /Stenberg and Sehlstedt 1989/, a refraction seismic survey /Rydström and Gereben 1989/, reflection seismic /Bergman et al. 2001/ and surface geology /Stanfors and Erlström 1995/. Results of these investigations plus detailed logging by /Braathen and Nordgulen 2005/ and /Viola and Venvik Ganerød 2007a/ indicate that the Mederhult deformation zone formed under ductile conditions but was repeatedly reactivated in the brittle field. Mylonitic foliation dips steeply to the south and a couple of sub-horizontal, W-plunging stretching lineations are reported by /Viola and Venvik Ganerød 2007a/, consistent with strike-slip kinematics.

More information on the Mederhult zone can be gleaned from the regional magnetic anomaly map of Figure 2-16. The westward continuation of the lineament is very obvious on the map, which portrays a slightly undulating, yet generally ENE-WSW oriented zone. Its overall orientation is similar to that of the OSZ, although the two tend to converge to the west. It is noteworthy that the Mederhult lineament forms the sharp northern boundary of a crustal block, which contains the Laxemar-Simpevarp area, characterized by several and significant low-magnetic belts. As shown by the inset of Figure 2-16, these corridors correspond to the ductile lineaments of the regional model area, including the Äspö shear zone, the possible westward continuation of ZSMNE011A (which seems to attain a more EW orientation to the west of the regional model area) and a few other lineaments not considered by SKB studies. The southern boundary of this block is not as continuous and obvious as the northern, Mederhult zone and is only tentatively drawn in Figure 2-16 by several segmented white lines.

The overall impression is that of a large crustal block, bound by ductile shear zones (some of which were reactivated in a brittle fashion during later structural episodes, such as, for example the Mederhult zone), which forms an internally sheared and strained "clast" within otherwise less deformed TIB granitoids. The shape of this "clast" is highlighted in the figure by a white shade, which is vaguely reminiscent of an asymmetric σ clast with two distinct tails, consistent with an overall sinistral sense of shear along a direction roughly parallel to the Mederhult zone and the OSZ. The location of the Götemar and Uthammar granites to the immediate north and south of this "clast" may be more than just coincidental.
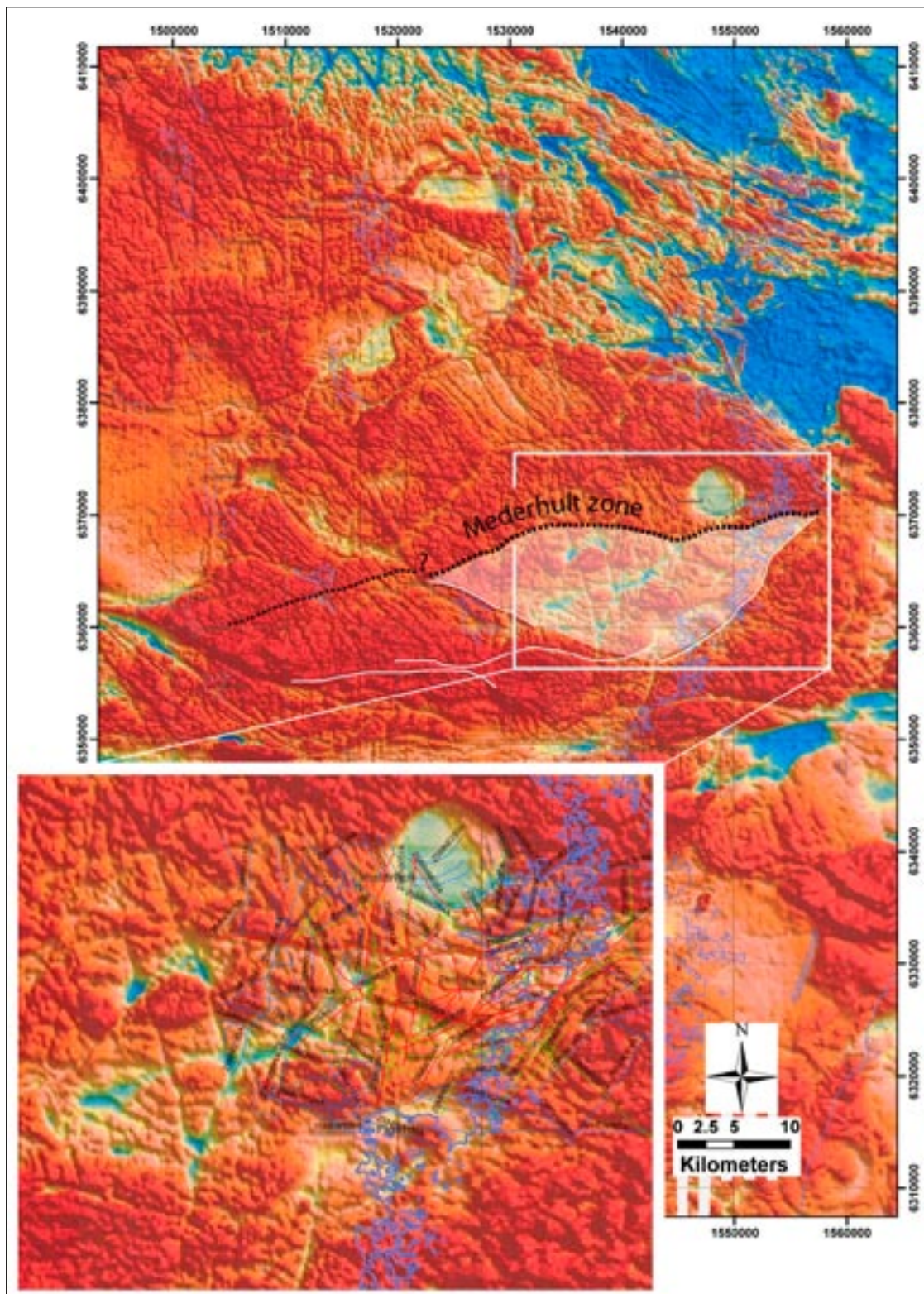
Figure 2-16. *Interpreted westward continuation of ZSMEW002A-Mederhult zone. Note that this lineament forms the northern boundary to a crustal block (which contains the Laxemar-Simpevarp area) characterized by very low-magnetic corridors (the block is highlighted by white shading). The inset zooms into the region containing these low magnetic belts and shows that they correspond primarily to identified ductile zones.*

3   Brittle evolution

3.1   Introduction and aim of the study

The previous chapter has served the purpose not only to discuss possible alternative models for the ductile evolution of the region, but also to lay the basis for the study and synthesis of brittle deformation in the area. The regional brittle fault and fracture pattern is the result of a long-lived geological evolution spanning almost one and a half billion years of complex events. As shown in Figure 3-1, the region is "saturated" by deformation zones that accumulated in the Precambrian basement of Sweden when several paleo-oceans opened and closed roundabout and by stress relief in the intervening periods of uplift and peneplanation /e.g. Munier and Talbot 1993, Söderbäck 2008/.

Unravelling such a long history of brittle deformation is a challenge, not only due to the large number of deformational episodes and hence the severe reactivation that most of the preserved structures underwent, but also because the paucity of post-Svecokarelian rocks seriously limits the understanding and constraining of the local geological evolution during more than 1,700 years of Earth history. The lack of reliable time constraints hampers assigning structures to episodes of well-constrained age.

The work presented below is based on a wealth of data from field observations (standard outcrops plus trenches and pavements polished and stripped from their soil cover so as to expose preserved structural relationships) and from several thousand meters of logged cores /Viola and Venvik Ganerød 2007ab, 2008/. Oriented structural features were systematically documented, described and characterized by those reports for a number of structurally relevant deformation zones. In addition to the mapping of planar structural features, particular attention was paid to shear striations along broken fault planes. These linear features were oriented and measured with the help of fracture orientation data from Boremap and a drill core holder, which
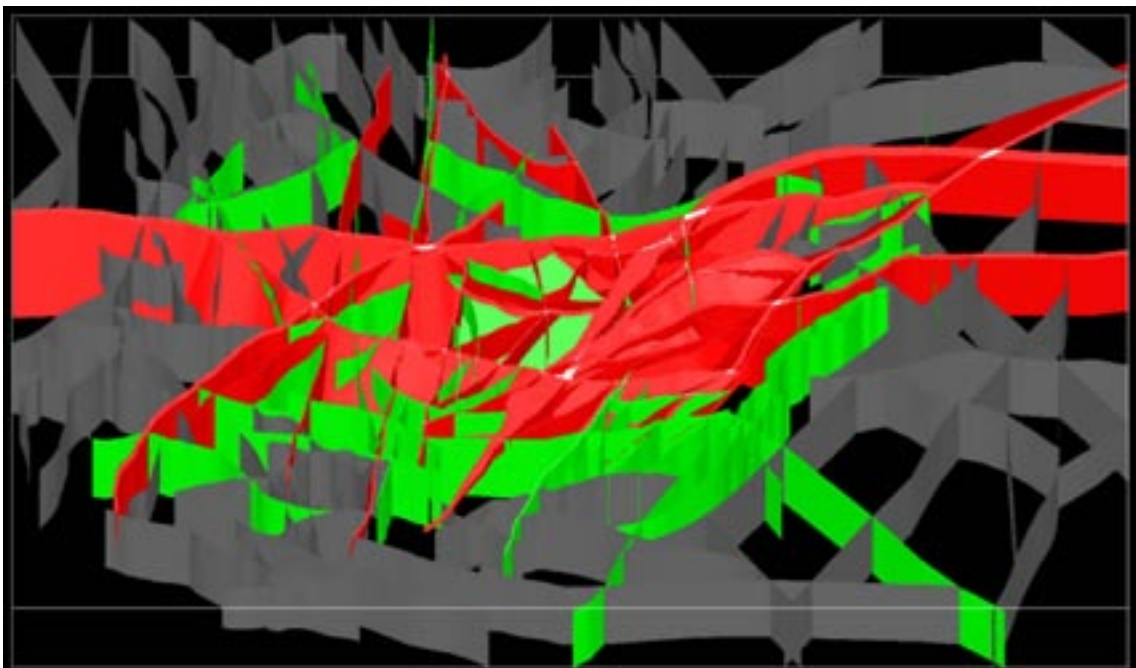
Figure 3-1. *3D diagram of version 2.3 of the deformation zones for the Laxemar-Simpevarp regional model area, with view to the north.*

allowed the core to be correctly positioned in 3D space. Statistically significant fracture and striation orientations and fault-slip data allowed the determination of the kinematics of many of the deformation zones investigated as well as the identification of multiple reactivation events.

The information gathered was not critically compiled in /Viola and Venvik Ganerød 2007ab, 2008/, though, and was never used to elaborate and propose a self-consistent scheme of deformational events. The aim of the following sections is thus to use that wealth of information, in addition to much more derived from other independent studies, to reconstruct and suggest an evolutionary scheme for the brittle evolution of the Laxemar-Simpevarp area.

Observations from the field are used to first generate a model for the local brittle evolution, based on geometric and kinematic inputs from well constrained outcrops. Data from boreholes are then used to integrate the results of the field study.

3.2 Fault-slip data analysis and stress inversion: a short introduction to the techniques used

Brittle kinematic indicators, crosscutting relationships between different generations of fractures, mineral infill and coating in tension gashes and along fracture planes, and fault-slip analysis on slickensided fault surfaces are the tools used during this study to unravel the local brittle history. The techniques of fault-slip analysis and stress inversion require a specific introduction.

Fault planes with slickenside lineations provide the direction and sense of motion on the specific fault. The collection of a fault-slip datum includes the fault plane orientation, the slip direction, and the sense of slip (reverse, normal, dextral, or sinistral). Senses of fault slip were determined by the growth direction of slickenside lineation fibres behind steps, Riedel shears and small-scale pull-apart structures /i.e. Hancock 1985, Petit 1987/. The reliability of slip-sense determinations was classified in three categories (excellent, good and probable).

Fault-slip data analysis allows the determination of the complete kinematics of fault trends (even major fault trends), a fundamental step in the unravelling of the kinematic evolution of an area. Even more importantly, fault-slip data analysis provides the basis for paleo-stress inversion calculations that aim at the reconstruction of the stress field evolution through time.

According to /Wallace 1951/ and /Bott 1959/, slip direction along a plane of known orientation under a given stress state can be determined provided that slip takes place in the direction of the maximum resolved shear stress. Also, a newly formed fault plane has an orientation that allows the relative magnitudes of shear stress τ and normal stress σ_n in this plane to meet with the Mohr-Coulomb yield criterion, $\tau = c + \mu\sigma_n$ where c is the cohesion and μ is the coefficient of friction. According to these principles, stress inversion techniques based on the Wallace-Bott criterion search for the stress state that best accounts for a given dataset by iteratively adjusting the theoretical slip pattern associated with a known stress state until it fits the slip pattern observed at the outcrop /Carey and Brunier 1974, Angelier 1979, 1984, Angelier et al. 1982, Etchecopar et al. 1981/. To this purpose, the orientation of σ_1, σ_2 and σ_3 (the greatest, intermediate and least compressive stresses) and the stress ratio $R = (\sigma_2 - \sigma_3)/(\sigma_1 - \sigma_3)$ are varied systematically to minimize the sum of all misfit angles with the misfit angle β, which represents the angle between the calculated maximum shear stress and the measured slip direction for an individual fault plane.

Methods based on this approach construct kinematic (or strain) axes for each individual fault plane assuming that in upper crustal deformation conditions, axes of strain coincide with axes of stress /e.g. Anderson 1951/.

In this study, kinematic axes (principal contraction and extension directions) were calculated by the inversion method of /Angelier et al. 1982/. This technique makes no assumption on the attitude of fault planes relative to stress axes. As a result, whether a fault plane is newly created by the tectonic stress itself or results from reactivation of an older discontinuity has no consequence for the reconstruction of the paleo-stress tensor. This is important because many fault movements have occurred along older fractures and inherited planar anisotropies.

Kinematic axes were computed using the direct inversion algorithm of the software package TectonicsFP v.1.65 /Reiter and Acs 1999/. The algorithm calculates the paleo-stress tensor (σ_1, σ_2 and σ_3) and the stress ratio R. Fault planes are displayed as great circles (Figure 3-2), upon which an arrow indicates the sense of movement of the hanging wall. The data calculated from fault planes are visualized as stress vectors on the lower hemisphere equal-area plots as σ_1, σ_2 and σ_3 stress axes (red circle, white square and blue triangle, respectively) combined with the associated dihedral plot, where the compressive field is shaded (Figure 3-3). In a dimensionless Mohr circle representing the σ_1–σ_3 plane, the normal stress σ (abscissa) and the shear stress τ (ordinate) are introduced by the stress tensor for each fault plane computed. The stress ratio $R = (\sigma_2-\sigma_3)/(\sigma_1-\sigma_3)$ defines the shape of the tensor. The dihedral angle between the measured lineation and the slip vector for each fault plane is displayed in a fluctuation histogram (Figure 3-3).
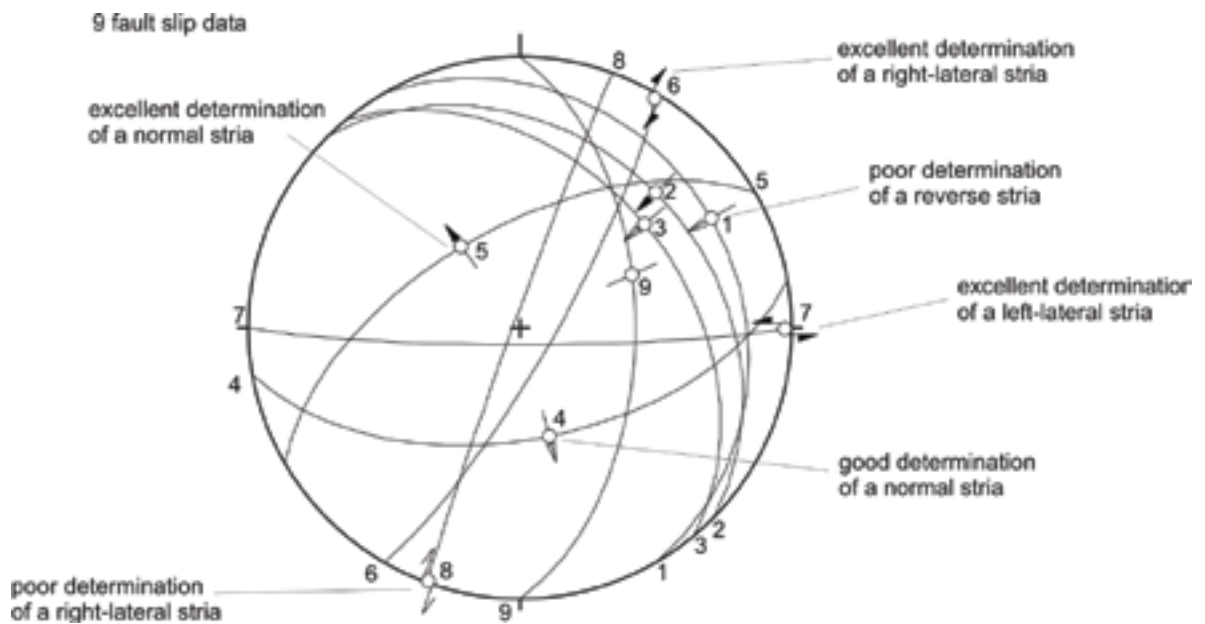
Figure 3-2. *Example of a stereogram plotting kinematic information for striated fault planes (Schmidt projection, lower hemisphere). Keys for striae: outward-directed arrow: normal striation (numbers 4 and 5 on the stereogram); inward directed arrow: reverse striation (numbers 1, 2 and 3); couple of arrows: strike-slip striation (numbers 6, 7 and 8); full black arrowhead: excellent constraints on the sense of shear (numbers 2, 5, 6 and 7); empty arrowhead: good constraints on the sense of shear (numbers 3 and 4); open arrowhead: poor constraints on the sense of shear (numbers 1 and 8); thin line without any arrowhead: no constraints on the sense of shear (number 9). Arrow indicates the sense of movement of the hanging wall.*
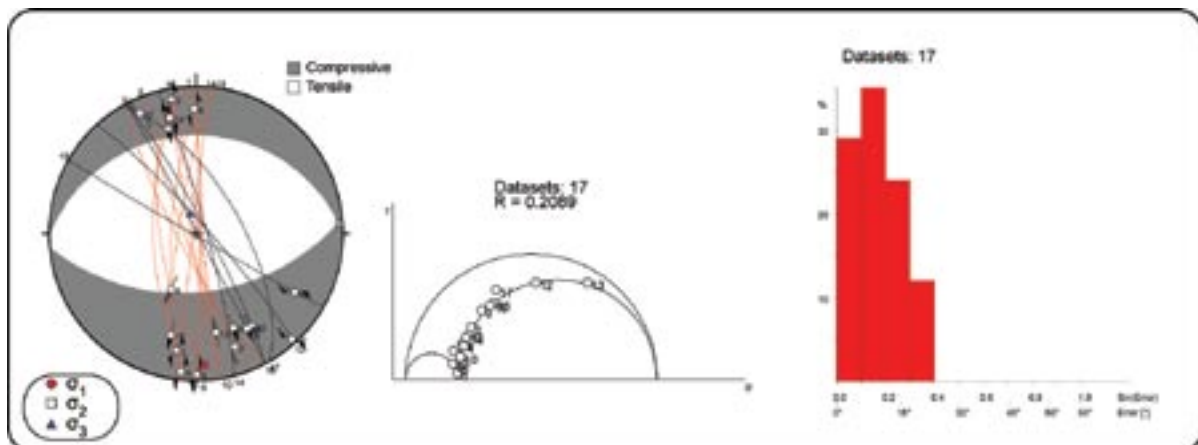
Figure 3-3. *Example of lower hemisphere, equal-area plot of brittle fault-slip striations with the associated stress axes and dihedral plot. Compression fields are shaded. Mohr circle diagram with computed stress ratio R and fluctuation diagram of misfit angle between the outcrop measured lineation and the predicted slip vector are also shown.*

### 3.2.1 Uncertainty linked with stress inversion studies: a cautionary note

Beside the crucial slip criteria mentioned above, fault-slip analysis methods are generally based on a series of other, major assumptions:

(1) The volume of rock affected by deformation is large compared to the scale of faults so that the computed stress tensor can be considered homogeneous on a macroscopic scale.

(2) During deformation the blocks bounded by faults are rigid and do not undergo rotations.

(3) Slip on different faults is mutually independent.

(4) Fault-kinematics is scale-invariant for the faults considered.

(5) Faults in a sample have movement directions that result from the action of a single uniform stress tensor.

Condition (5) is particularly relevant and when working in old, poly-deformed terranes, as in the case of the Precambrian of Southern Sweden, is rarely met. Thus, when outcrops contain fault sets with incompatible slip sense that can be ascribed to more than just one deformational event and stress tensor, it is necessary to separate heterogeneous data sets into homogeneous sub-sets before stress inversion by using field criteria (age relationships or type of mineralization) and visual and mathematical compatibility criteria (e.g. grouping of calculated individual axes, maximum angular deviation of axes from calculated sub-set means). Often, not even the application of these tools allows the confident sorting of complex and heterogeneous fault-slip data and numerical techniques may come to the rescue.

The software program TectonicsFP, for example, also incorporates a separate algorithm that performs a kinematic analysis of the dataset leading to the construction of contractional (P), neutral (B) and extensional (T; usually collectively referred to as PBT) axes for each individual fault slip datum. According to the Mohr-Coulomb failure criterion, the algorithm adopts a defined angle θ between the compression axis P and the fault plane accommodating slip, whereas axis B is constrained to lie in the fault plane itself. Experimental brittle deformation studies indicate θ = 30° as a reasonable value.

Results of PBT calculations, shown as clusters of kinematic axes (Figure 3-4) can be used to discriminate sub-sets of homogeneous stress datasets forming a heterogeneous dataset of otherwise difficult interpretation.
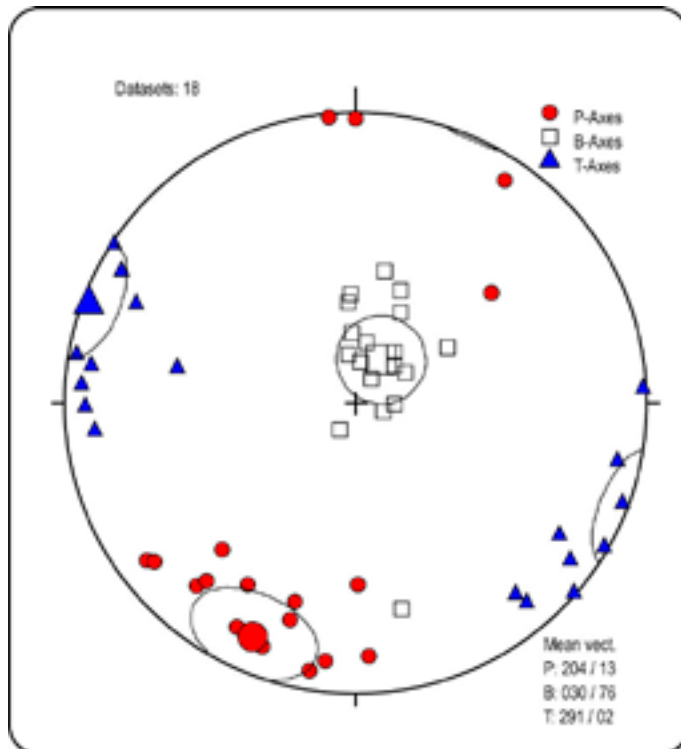
Figure 3-4. *PBT axes computed by the software program TectonicsFP. Each symbol triplet (circle, triangle and square) refers to an individual fault. Mean orientations for each cluster are indicated by the largest symbols and the corresponding orientation values are reported to the right of the stereogram.*

The Multi-Inverse Method approach (MIM software package; /Yamaji 2000a/) is the second alternative to the numerical sorting of heterogeneous datasets that was used during this study. The algorithm was developed specifically for the separation of heterogeneous fault-slip data and has been used in this study to validate some of the stress inversion procedures. The technique identifies paleo-stresses from heterogeneous fault-slip data in the absence of *a priori* information on the stresses themselves or on the faults. MIM represents a development of /Angelier's 1984/ inverse method. The details of the technique are described by /Yamaji 2000a, 2003/ and examples of applications to real field cases are given in, e.g. /Yamaji 2000b/ and /Yamada and Yamaji 2002/.

The MIM software was also used to verify, by means of unsupervised procedures, the validity of stress inversion computations obtained by the author in this study through the subjective sorting of the total fault-slip dataset. This was necessary in order to have an automatic and unbiased routine to select heterogeneous datasets.

Another important condition that has to be met is that the stress field at the time of faulting is uniform. This is, however, rarely the case and the introduction of this assumption in stress inversion computations clearly introduces uncertainty in the process.
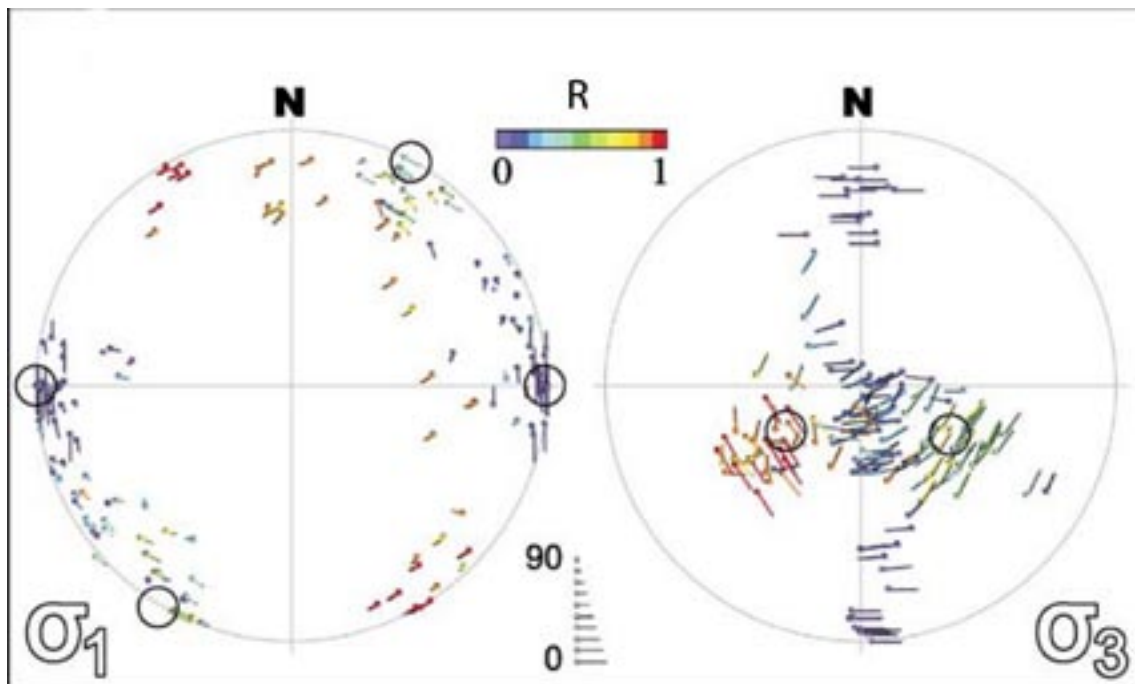
Figure 3-5. Results of multi-inversion applied to a dataset presented by /Yamaji 2003/. The directions of σ_1 and σ_3 are indicated by dots on the lower hemisphere equal-area projections on the left and right, respectively. In the left diagram, the direction of bars extending from the dots indicates the azimuth of the corresponding σ_3 direction. The length of the bar designates the plunge. On the right net, the role of the bar and dot are assigned inversely. The length and direction of the bar indicate the σ_1 direction. Open circles along the primitive circle indicate the direction of assumed stress axes. Clusters of dot-bar symbols with the same colour and same bar direction represent significant stresses. Each symbol represents a state of stress: stress ratio R is shown by colour, and the direction of stress axes is indicated by the position and direction of the symbol.

Analysis of stress inversion results from field fault-slip data benefits greatly from the direct observation of geometric and kinematic relationships among different fractures and faults. Direct observational data in drill cores that show the possible geometric relationship between shear fractures (minor faults) with different orientations (e.g. conjugate sets, Riedel shears) or between shear fractures and marker units are, however, more or less absent. In this respect, borehole data are of considerably less help to determine the kinematics along deformation zones compared with data from outcrops. As discussed in the next sections, this study relied therefore significantly on field observations to create an internally consistent deformational scheme and analysed the data extracted from the drill cores by using this scheme as a reference.

In addition, several other factors complicate the comparison of data acquired in the field with observations generated from drill core logging. Examples are:

• Different sampling scale.

• Outcrops are 2D planes, while boreholes are mostly a 1D record.

• Outcrops can be affected by superficial fracturing processes (tensional relief, weathering, shallow stress fields etc) that are not representative of the fracturing at depth.

In summary, it ought to be born in mind that there are several sources of uncertainty involved in the study presented in the remaining part of this report and that the results should be evaluated critically and cross-checked against independent observations and analyses.

## 3.3   Field kinematic study and stress inversion results

Fault-slip analysis and stress inversion was performed on several datasets obtained from a number of outcrops. Figure 3-6 shows field localities where data were obtained and the corresponding stereograms are shown in Figure 3-7 and Figure 3-8.

When dealing with sub-regional to regional datasets, the goal is that of obtaining an internally consistent kinematic and paleo-stress reconstruction. Individual anomalies do, however, occur, and result from, for example, discontinuities within the rock mass, complex deformational histories, modifications of stress direction close to large regional faults, fault block rotation and so on. These represent sources of variation in tensor orientation and ratio, but they do not influence the final result as long as the fault population considered is large enough. In order to have reliable local determinations, the local paleo-stress tensors obtained have to be consistent on a regional scale and be validated by independent field and geological constraints.

As shown in Figure 3-7 and Figure 3-8, many outcrops did not yield statistically significant datasets, as inversion on only a handful of fault-striation pairs would not lead to reliable results.

The necessary approach followed by this study was therefore that of merging in a first phase all field measurements in a single "regional" dataset and to consider it representative of the whole Laxemar-Simpevarp area (Figure 3-9). As can be seen from the stereogram generated, the dataset is highly heterogeneous and contains fault-slip data that obviously are the product of many, differently-oriented paleo-stress tensors and deformational episodes. The dataset had therefore to be sorted and individual homogeneous sub-sets were extracted. Sorting was based on geometric and kinematic compatibility criteria and on well-constrained structural relationships observed at individual outcrops.

A flow-chart illustrating the individual steps of the sorting procedure is shown in Figure 3-10. Two obvious fault families exist: steep to sub-vertical and relatively low angle faults. These are separated in the first step of the sorting process. Gently- to moderately-dipping faults are in turn sorted internally according to their normal or reverse kinematics (predominantly down-dip faults), whereas steep faults are split into three sub-homogeneous sub-sets, each characterized by differently-oriented groups of conjugate sinistral and dextral fractures and faults. Steep fractures bear sub-horizontal lineations, which indicate their strike-slip character. Only a limited number of steep faults contain steeply-plunging lineations and these are generally interpreted as being the result of structural reactivation with either normal or reverse kinematics along pre-existing steep planes (Figure 3-10).
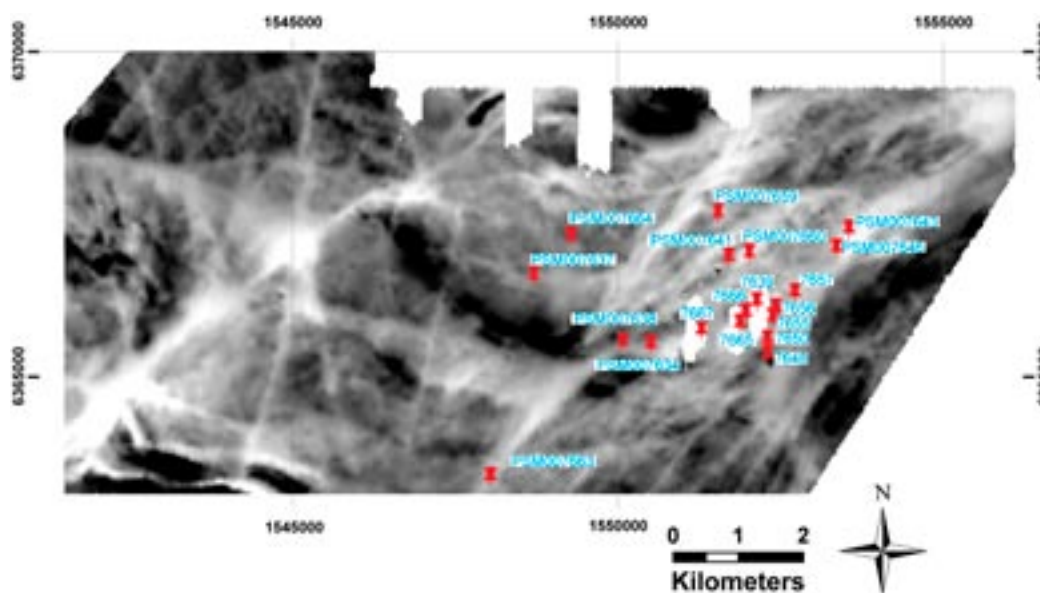

Figure 3-6. *Location of outcrops in the Laxemar-Simpevarp area where fault-slip data were acquired by /Viola and Venvik Ganerød 2007ab/. Background map is the total magnetic field. Please note that outcrop names were shortened to their last four digits in the Laxemar area due to lack of space.*
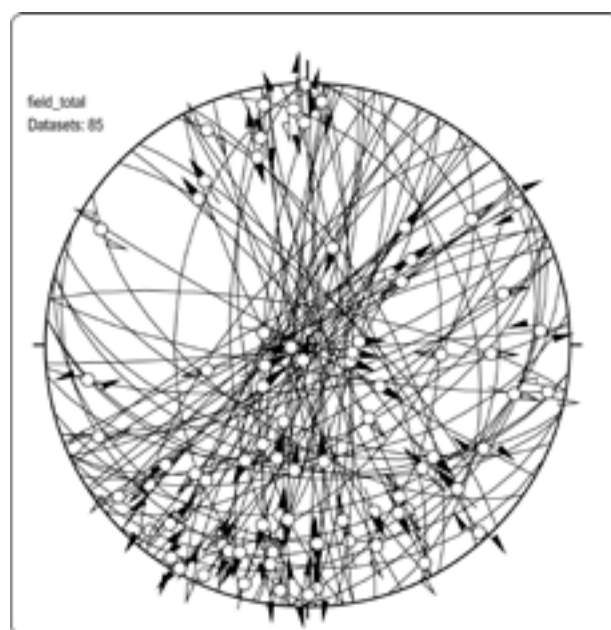
35
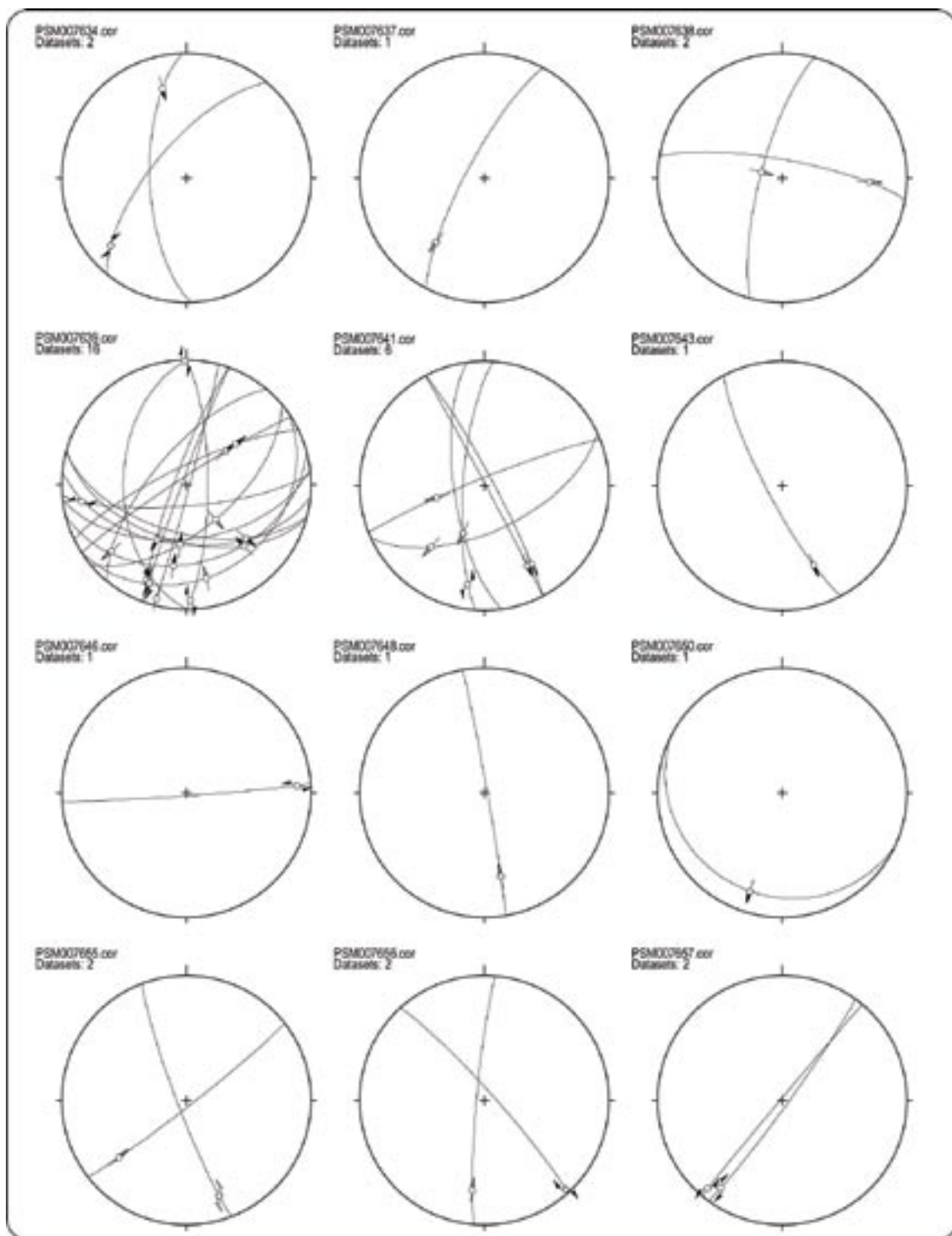
Figure 3-7. Kinematic information for striated fault planes (Schmidt projection, lower hemisphere) obtained from the localities of Figure 3-6 (continued in Figure 3-8).
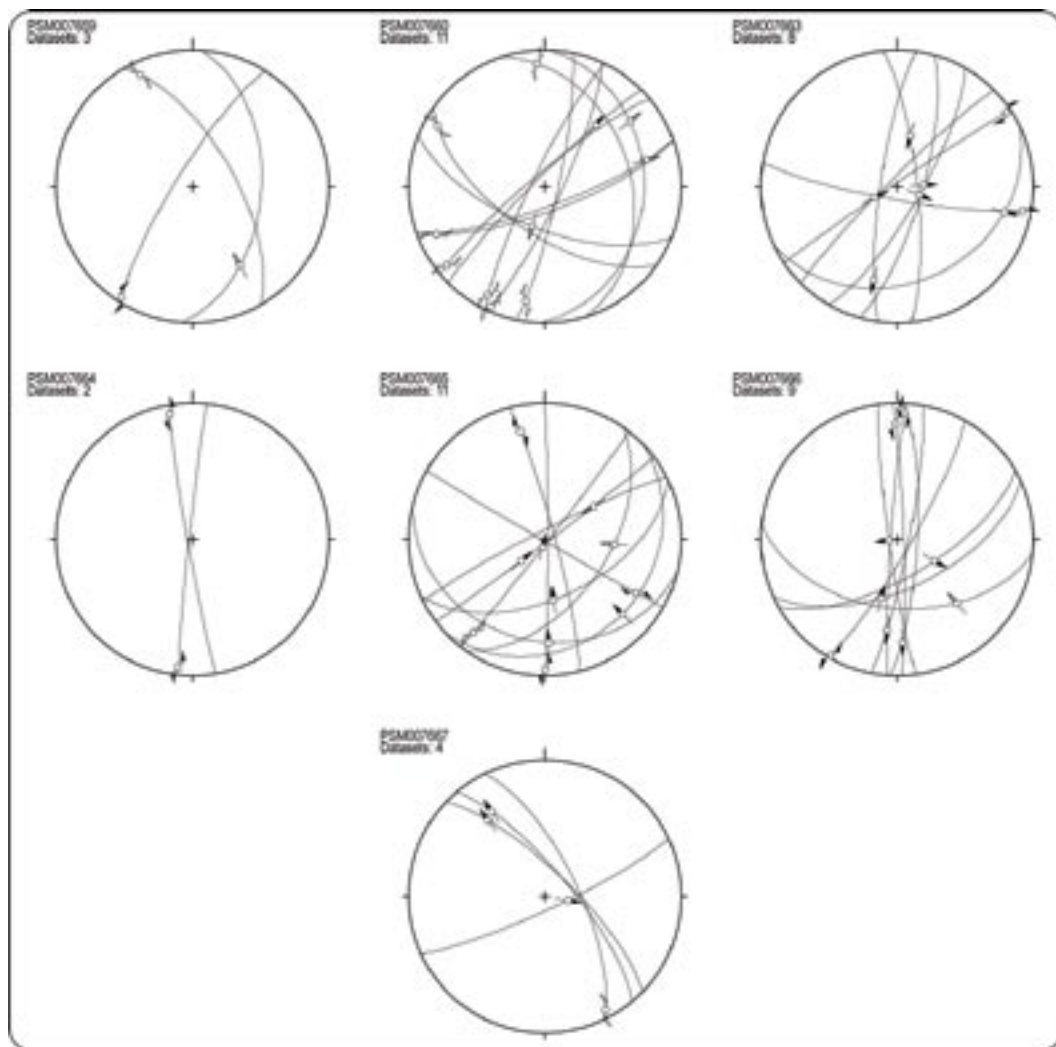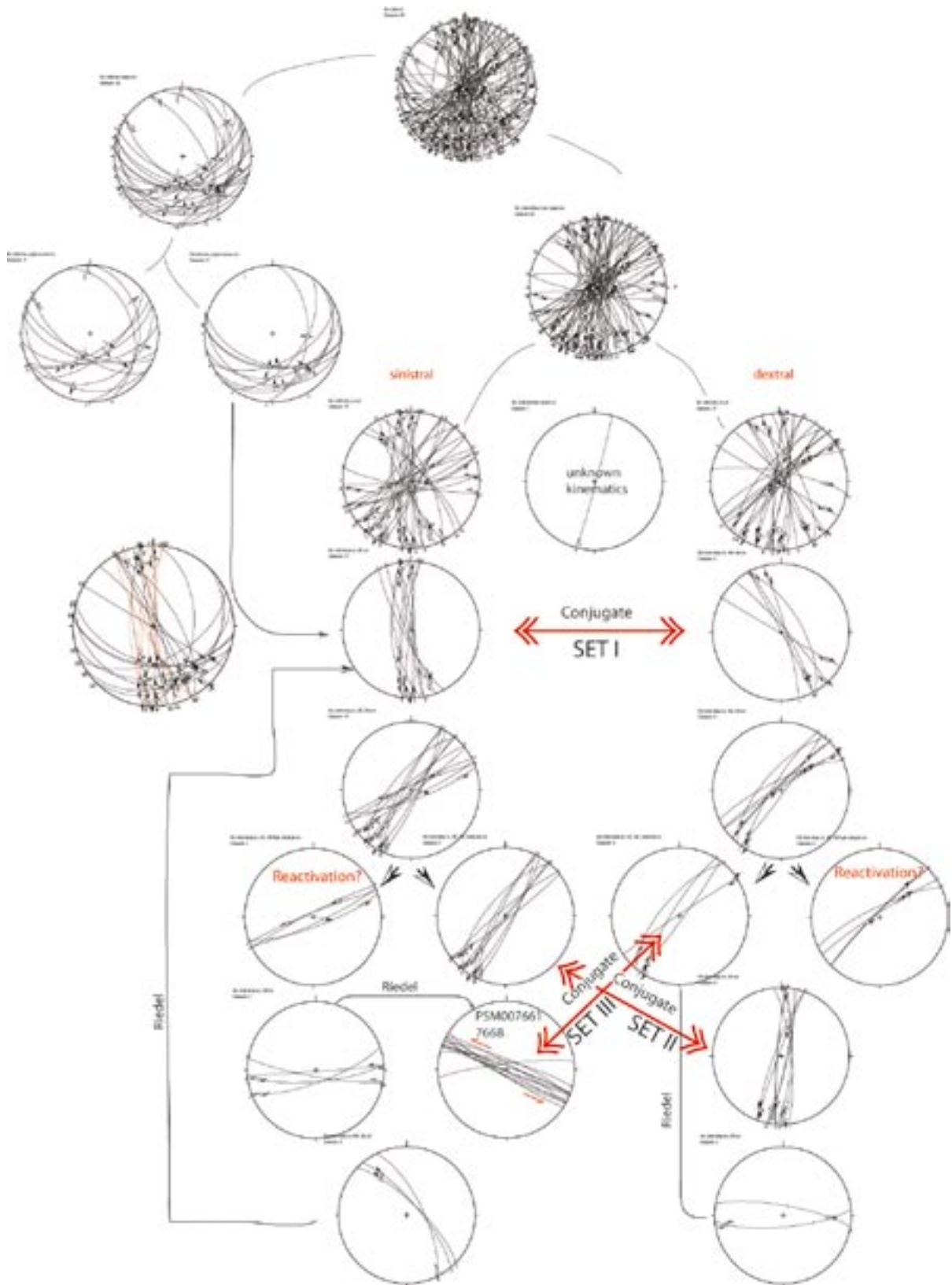
Figure 3-8. Kinematic information for striated fault planes (Schmidt projection, lower hemisphere) obtained from the localities of Figure 3-6.

Figure 3-9. Summary stereo plot of all fault-slip data collected in the Laxemar-Simpevarp area. The dataset is very heterogeneous and requires sorting in order to identify homogeneous sub-sets.

Figure 3-10. Sorting of the total field dataset according to geometric and kinematic compatibility criteria. Set I, II and III are discussed in detail in the text.

The most striking class of brittle features in the Laxemar-Simpevarp area is composed of systematic sets of conjugate and steep, sinistral and dextral brittle-ductile and brittle faults and fractures, dispersed at small angle about a N-trending axis. They are recognizable in the high-resolution DEM of the region, in the results of the airborne geophysics surveys and in any detailed field analysis and detailed fracture mapping (see, for example, Figure 3-6 and Figure 3-11). Complications in the interpretation of these fracture sets are that angles between the conjugate structures are generally small and a significant spatial overlap exists between sinistral and dextral fractures belonging to different sets. Moreover, reactivation is commonly observed. In order to understand this complex kinematic pattern, heavy reliance was placed on straightforward kinematic relationships observed at several outcrops.

3.3.1 Conjugate set I

Outcrop PSM007665 (Figure 3-6 and stereogram in Figure 3-8; /Viola and Venvik Ganerød 2007b/) contains a textbook case of a set of epidote-coated conjugate fractures, with a NS-striking sinistral and a NNW-SSE-striking dextral fracture. This spatial relationship is very commonly observed, especially when NS-oriented sinistral shear corridors in the area are considered. /Viola and Venvik Ganerød 2007a/, for example, describe a series of NS sinistral faults and fractures at site PSM007640, a polished pavement used to drill borehole KLX11A (Figure 3-12). Although no striated surfaces were observed at that very outcrop, the sinistral kinematics of the NS fractures and faults was determined on the basis of unambiguous kinematic criteria. It is also noteworthy that at the same outcrop thin synkinematic leucocratic dykes (upper left corner of Figure 3-12) occur in a bridge zone between two contiguous but laterally stepped NS-trending
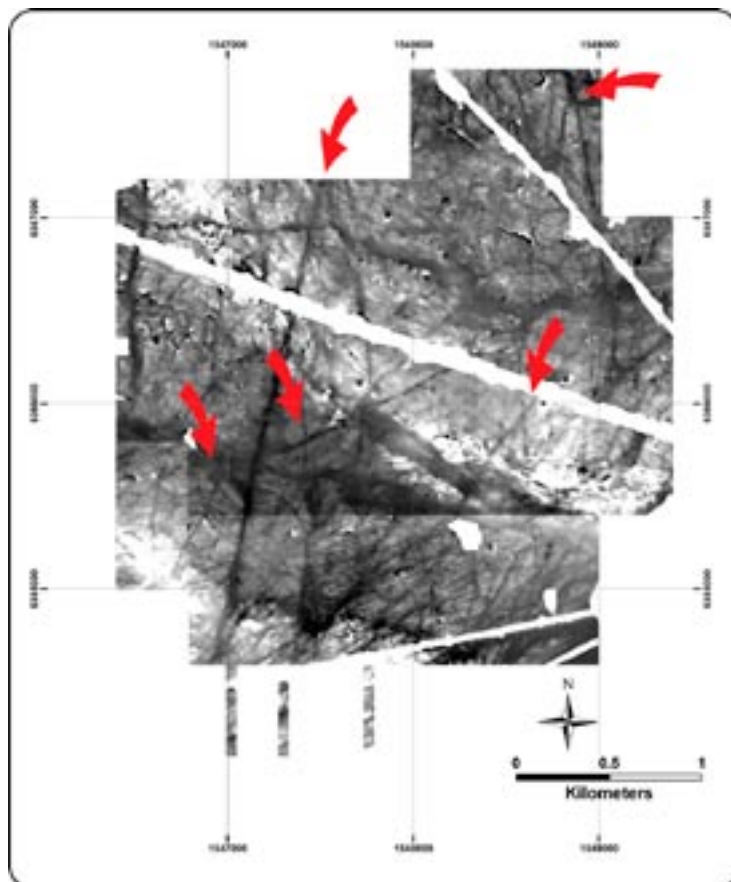
Figure 3-11. *High-resolution magnetic survey over central Laxemar. Red arrows point at selected examples of conjugate fracture sets. See Figure 3-6 for other examples from the entire Laxemar-Simpevarp area.*
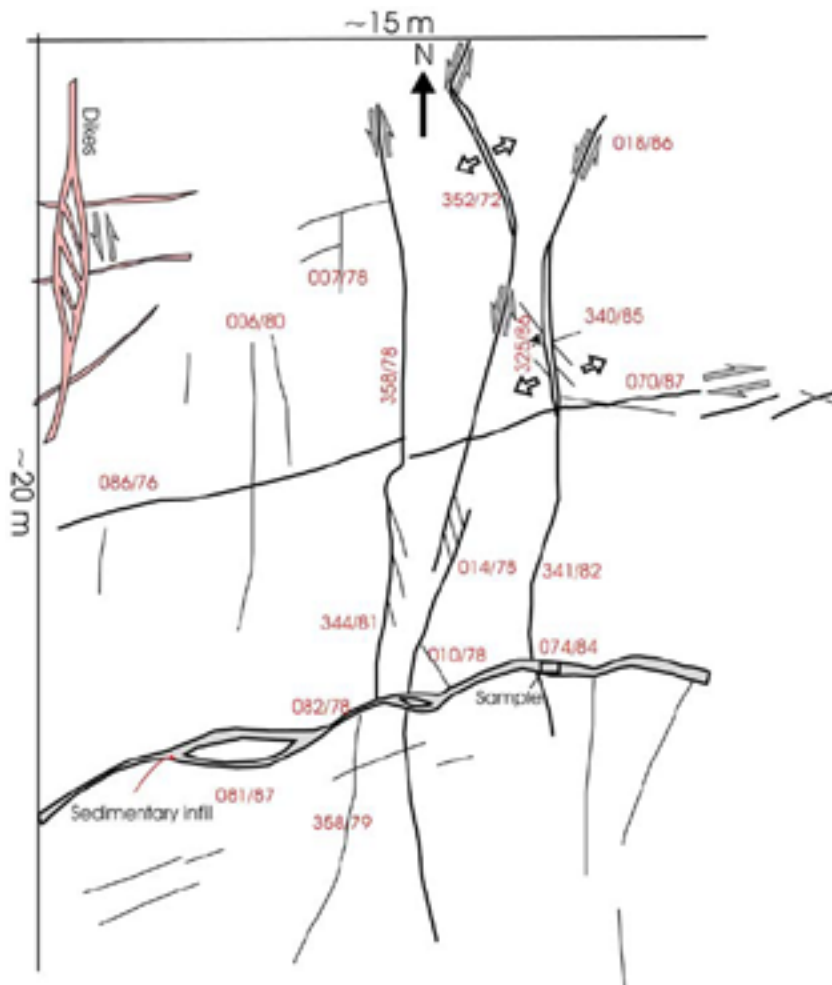
39

Figure 3-12. Sketch fracture map of drilling site KLX11A, from /Viola and Venvik Ganerød 2007a/.

segments of a fracture/dyke, again indicative of sinistral kinematics. Sinistral shear was therefore active at the time of granitic dyke emplacement, indeed relatively early in the evolution of the area, very likely prior to the intrusion of the Götemar and Uthammar granites.

NS trending fractures and faults were observed also at outcrop PSM007661 /Viola and Venvik Ganerød 2007b/.

N- and NW-striking brittle-ductile shear zones and fractures contain commonly idiomorphic epidote and quartz, and are probably amongst the oldest post-ductile features preserved in the area. Although the contemporaneity of N trending sinistral set with the NW striking dextral set is only explicit for a handful of observations, we consider them as generally due to the same shortening episode.

Striated fault planes belonging to this set were grouped in order to perform stress inversion and constrain the stress tensor (Figure 3-13).

Although the angular separation between the two families of faults is clear, there still exists overlap between some of the sinistral and dextral planes. Results of the stress inversion are shown in Figure 3-14a. A sub-horizontal maximum axis of shortening oriented 176/12 is calculated, with the least compressive stress oriented 345/78 and the intermediate axis 086/02. The Mohr diagram is not entirely satisfactory, with the majority of calculated normal and shear stress values plotting away from the failure envelope, thus indicating that development of newly formed fractures under the calculated stress condition is not mechanically favoured. On the other hand, the fluctuation histogram plots an acceptable misfit between calculated and measured slip direction.

40
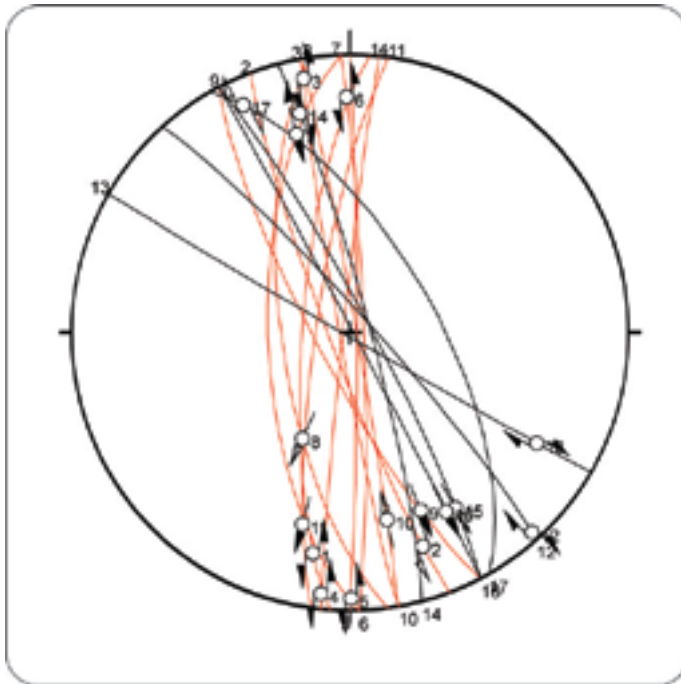
Figure 3-13. Striated faults assigned to conjugate set I. Red great circles: sinistral faults; black great circles: dextral faults.
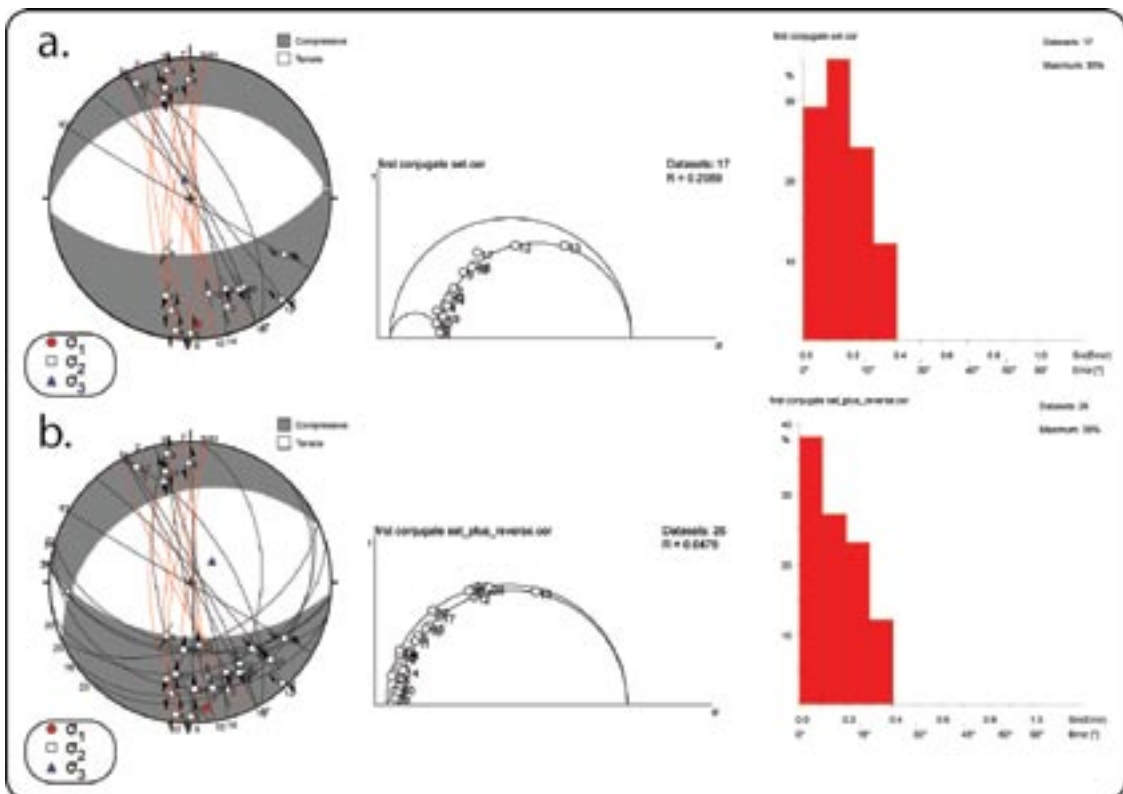

Figure 3-14. Stress inversion results for conjugate set I (a.) and conjugate set I plus top-to-the-N and NNW low angle reverse faults (b.).

Stress inversion results are, however, significantly improved when the steep fracture family is integrated with the low-angle reverse faults separated at the first step of the sorting procedure (Figure 3-10). As shown by Figure 3-14b, stress axes do not change significantly their orientation (σ_1: 173/11, σ_2: 265/14, σ_3: 045/72), whereas the stress ratio R decreases towards pure axial compression conditions and individual faults move in the Mohr diagram much closer to the ideal shear-normal stress condition on the failure envelope. The overall angular misfit also decreases, as shown by the histogram.

An unsupervised analysis of the dataset was performed by means of the PBT and MIM methods.

As shown in Figure 3-15, the direction of the compressive kinematic axes (red circles) does not vary between the two stereograms, with the mean value plunging very gently to the SSE for both the dataset containing only the strike-slip faults (to the left) and for the dataset including also the thrusts (to the right). There is, however, a moderate difference with respect to the orientation of the greatest compressive stress computed by the inversion method (Figure 3-14), with the mean kinematic axis offset by c. 20° to the east. Tensional axes have their mean vector plunging horizontally to the SW for both datasets, and are thus in contrast with the sub-vertical orientation of the least stress derived from the inversion method (Figure 3-14). In the case of the dataset containing strike-slip and thrust faults, however, they also form a second, minor sub-vertical cluster, in line with a thrust regime. As shown in the Mohr diagram of Figure 3-14b, the introduction of the thrusts is such that differences in value between σ_2 and σ_3 are very minor, leading to their possible orientation permutation in time, reflected by oscillatory thrust and strike-slip conditions.

The results of this independent approach can be considered satisfactory and help constrain a phase of SSE-NNW oriented compression. Low-angle, top-to-the-N and NW reverse faults were likely formed together with steep NS sinistral and NNW-SSE dextral strike-slip faults. It should be noted that this conclusion only states the geometric, kinematic and dynamic compatibility of steep fractures belonging to set I and low-angle, top-to-the-N and NW reverse faults, but does not constrain by any means the relative abundance of steep vs. low-angle faults.
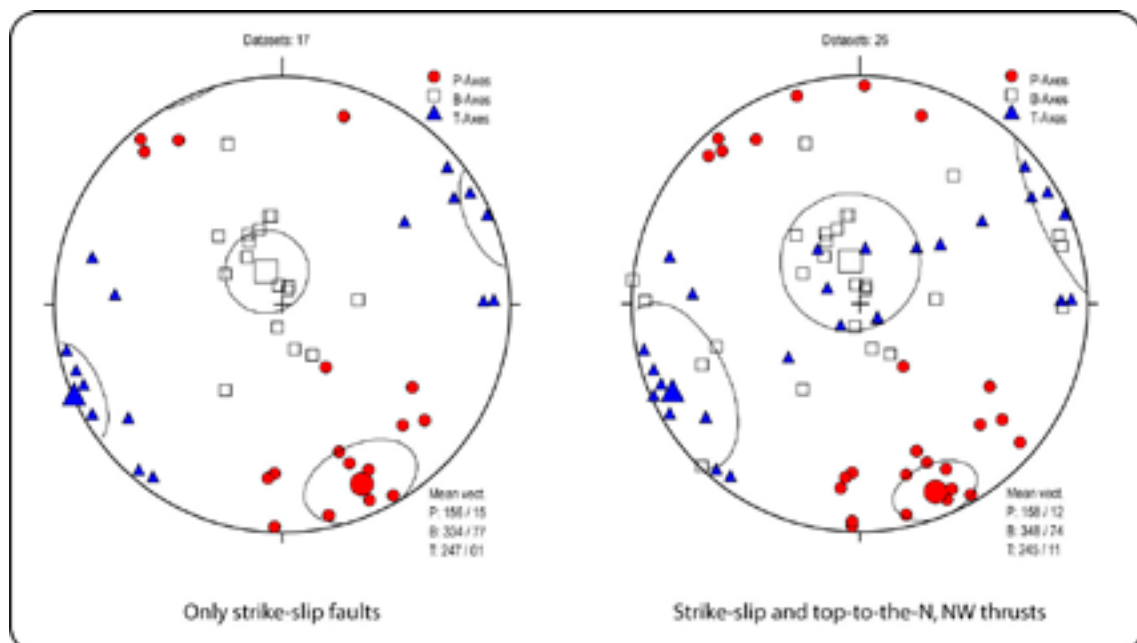
Figure 3-15. *PBT axes for the conjugate set I dataset. The stereogram on the left (17 striated planes) plots only strike-slip faults, the stereogram on the right adds also the top-to-the-N, NW thrust faults.*

3.3.2   Conjugate set II

A second, distinct set of steep, conjugate strike-slip fractures can be easily recognised in the area. Sinistral NE-trending faults are conjugate to dextral, NS oriented faults (Figure 3-16).

Most of the conjugate sets visible on the airborne geophysics survey results can actually be ascribed to this set (e.g. Figure 3-11). Stress inversion results are shown in Figure 3-17. Figure 3-17a shows the results for the inversion of just the steep strike-slip fractures. σ_1: 180/10, σ_2: 047/76, σ_3: 272/10 are calculated, defining a stress ratio R = 0.35, and constrain a NS-oriented compression accommodated primarily by strike-slip structures (see the beach volley diagram of Figure 3-17a). Individual faults plot along or not far from the failure envelope on the normal vs. shear stress plane of the Mohr circle and satisfactory misfit angle values are calculated. In order to verify whether the low-angle reverse faults could fit this stress regime better than the one that generated set I, stress inversion was also computed for a new dataset that includes not only steep strike-slip faults but also top-to-the-N and NW reverse faults. Results are worse in this case, though, and deteriorate the quality of the stress inversion procedure for set II, as indicated by many faults moving away from stress conditions close to the failure envelope and by the significant increase of faults with higher misfit angle between observed and calculated slip direction (Figure 3-17b).

The results of the PBT approach on conjugate set II are shown in Figure 3-18. Results are generally in line with the stress tensor computed by the inversion method, with only a moderate rotation to the west, as indicated by a mean P axis plunging to 204° versus a S-plunging σ_1 (Figure 3-17).

In order to validate the stress inversion procedure run for set II (and indirectly for set I as well) and to verify whether the two sets were split according to valid criteria, the MIM approach was used on a single database containing all steep strike-slip faults (i.e. set I and II) with and without the top-to-the-N, NW thrusts. The results, shown in Figure 3-19, confirm that two different stress regimes, with a maximum compressive stress plunging sub-horizontally to the SSE and SSW, respectively, can explain satisfactorily fault-slip data for these two sets. Moreover, results improve when the thrusts are also considered.

NS-trending dextral and NE-SW sinistral features belonging to set II are observed not only as striated planes, but also as proper mesoscopic faults. NS faults were described by /Viola and Venvik Ganerød 2007b/ for example at outcrop PSM007661 (Figure 3-6 and see also Figure 3-16), where dextral kinematics along c. NS-trending fractures was established on the basis of the finite dextral offset of microgranitic dykes and abundant Riedel shears. A spectacular sinistral NE-striking strike-slip fault is described by /Viola and Venvik Ganerød 2007a/ from the coast of the Simpevarp peninsula (outcrop PSM007657, Figure 3-6). A discrete, c. 0.5 m thick brittle fault zone, bearing sub-horizontal SW-plunging striations, contains evidence of several episodes of cataclasis, overall sinistral sense of shear (as shown by a granitic dyke offset by c. 3 m across the fault) and later dilation oriented c. NW-SE.

As in the case of set I, set II contains brittle-ductile, epidote-quartz shear zones (for example, outcrop PSM007634, /Viola and Venvik Ganerød 2007a/). Metamorphic conditions during fracturing and shearing, as constrained by the epidote and quartz mineral coating of the striated planes, are thus similar for both sets.
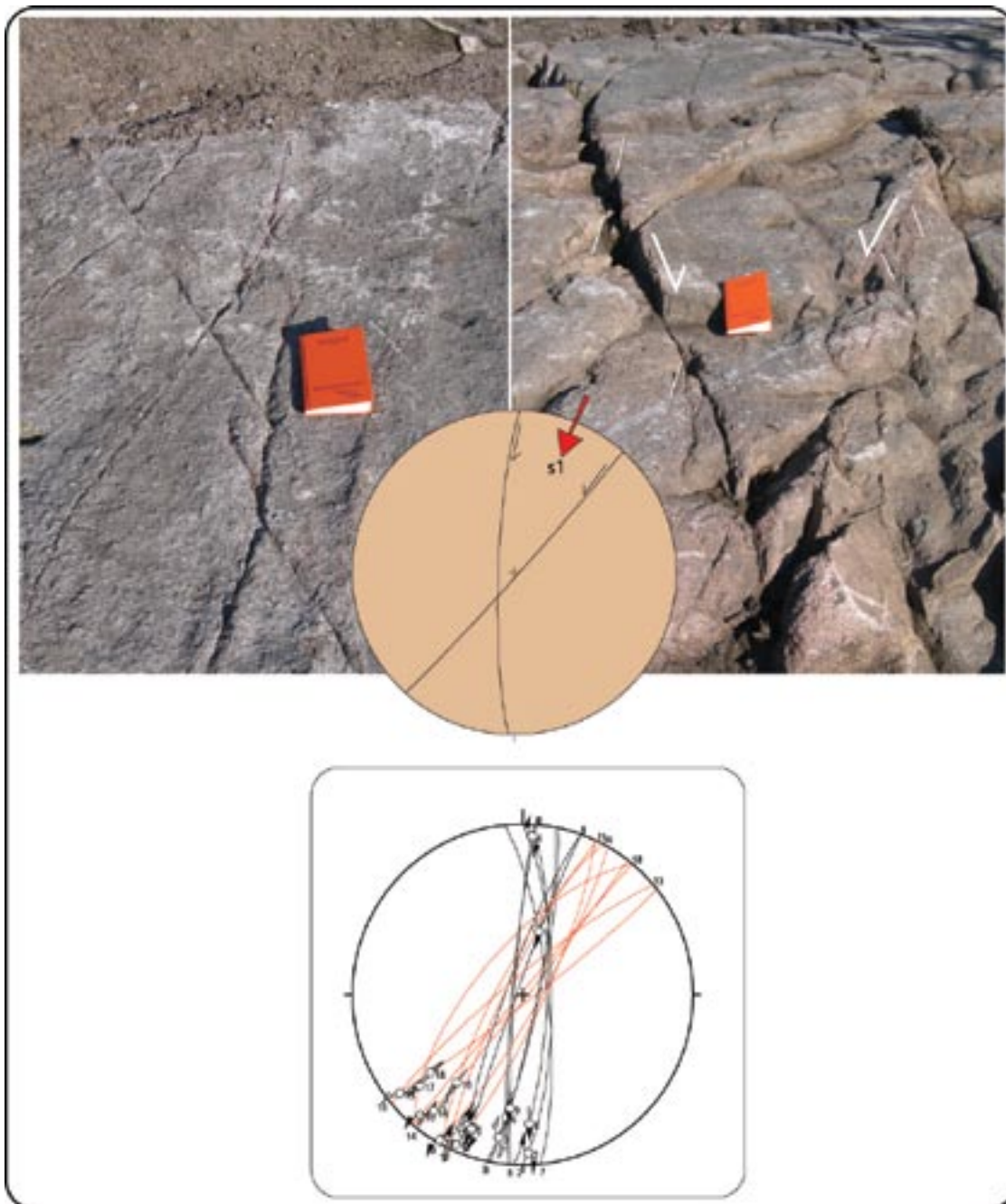
**Figure 3-16.** *Field photos looking to the northeast of sinistral and dextral fractures (kinematics established with Riedel fractures) belonging to set II (outcrop PSM007661 /Viola and Venvik Ganerød 2007b/).The lower stereogram displays all striated faults measured in the Laxemar-Simpevarp area that can be assigned to conjugate set II. Red great circles: sinistral faults; black great circles: dextral faults.*
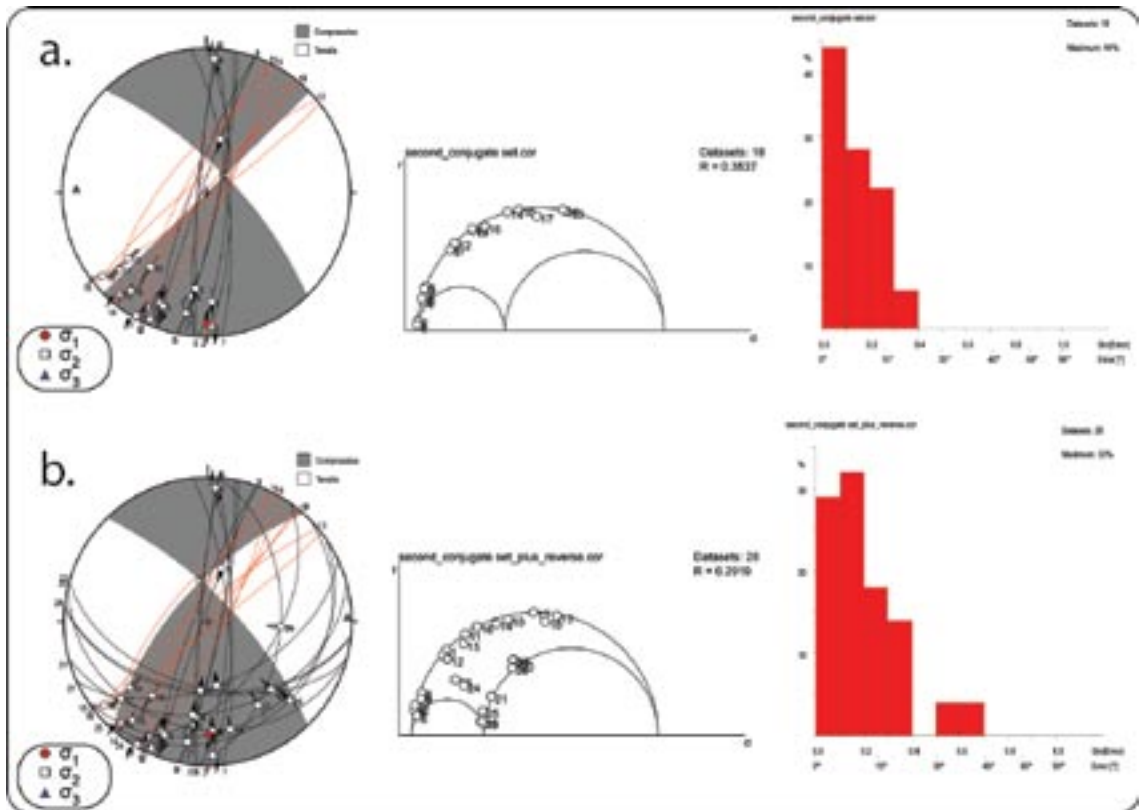
Figure 3-17. *Stress inversion results for conjugate set II (a.) and conjugate set II plus top-to-the-N and NW low angle reverse faults (b.).*
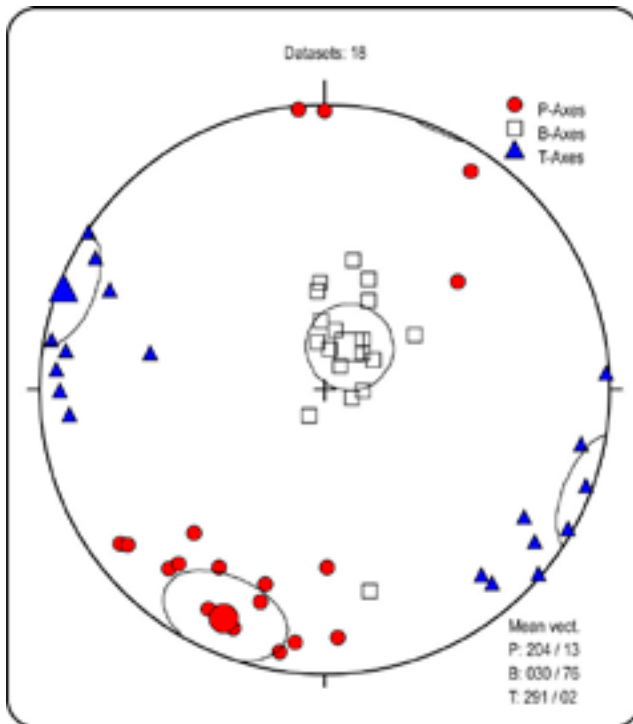
***Figure 3-18.*** *PBT axes for conjugate set II.*
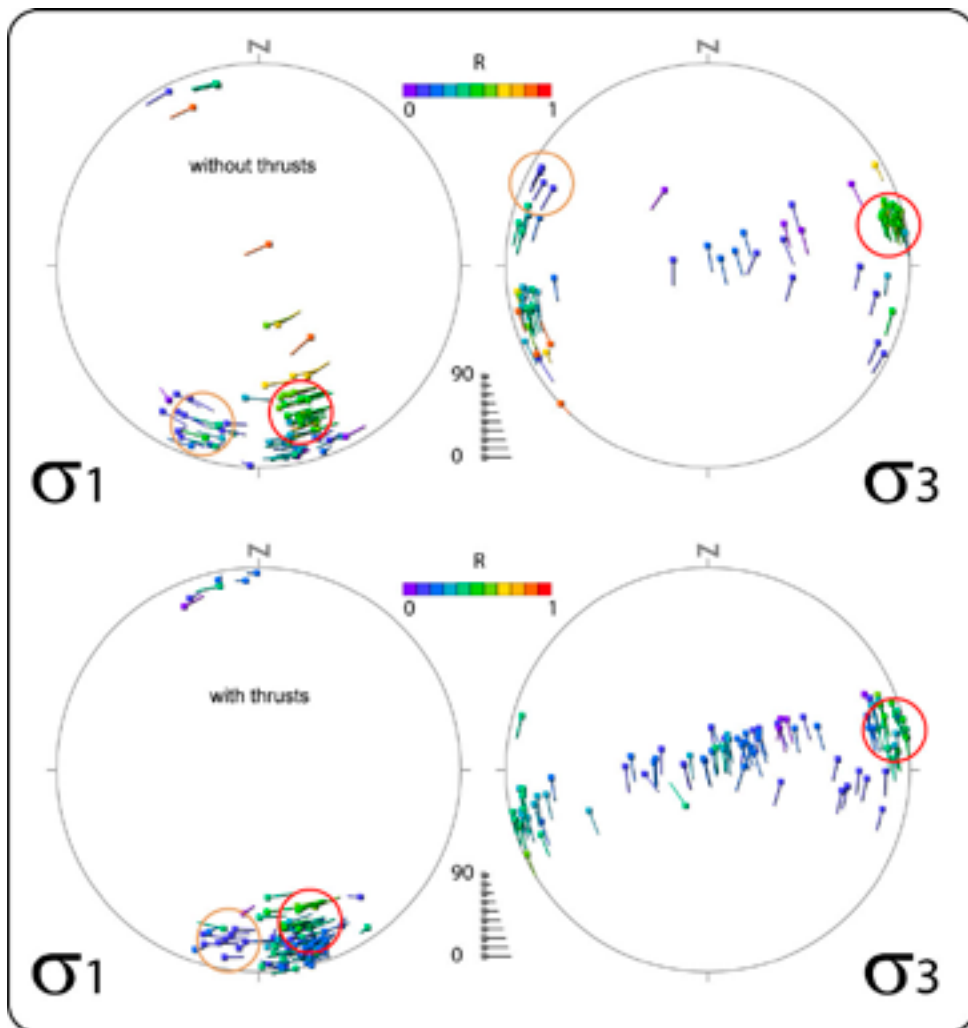
Figure 3-19. *Results of multi-inversion applied to a dataset containing the steep strike-slip fractures of set I and II (upper line) with the addition of top-to-the-N, NW thrusts (lower line). Results from the direct inversion and PBT methods applied separately to the two datasets are confirmed, with two distinct shortening episodes oriented SSE-NNW and SSW-NNE respectively. See caption of Figure 3-5 for guidelines on how to read these diagrams.*

3.3.3   Conjugate set III

A third, quite differently oriented and less common set of conjugate fractures was identified by the sorting procedure of Figure 3-10. It contains ENE- to NE-trending dextral and ESE-WNW-oriented sinistral faults. Although not as common and obvious in the field as the two sets described above, conjugate fractures spread about the EW directions can still be recognised at a variety of scales (Figure 3-20). An example is outcrop PSM007640 /Viola and Venvik Ganerød 2007a/, containing a significant ENE-trending dextral fault and several associated Riedel fractures. /Viola and Venvik Ganerød 2007ab/ describe several outcrops containing fractures and small-scale faults that can be ascribed to this set of conjugate features. However, not always were both orientations observed and some localities preserve either sinistral or dextral faults only. Moreover, second order Riedel shears are very common and complicate significantly the overall picture. As shown in Figure 3-10, a few striated planes, which do not belong to statistically significant populations, were interpreted as Riedel fractures subordinated to the dominant directions of set III.
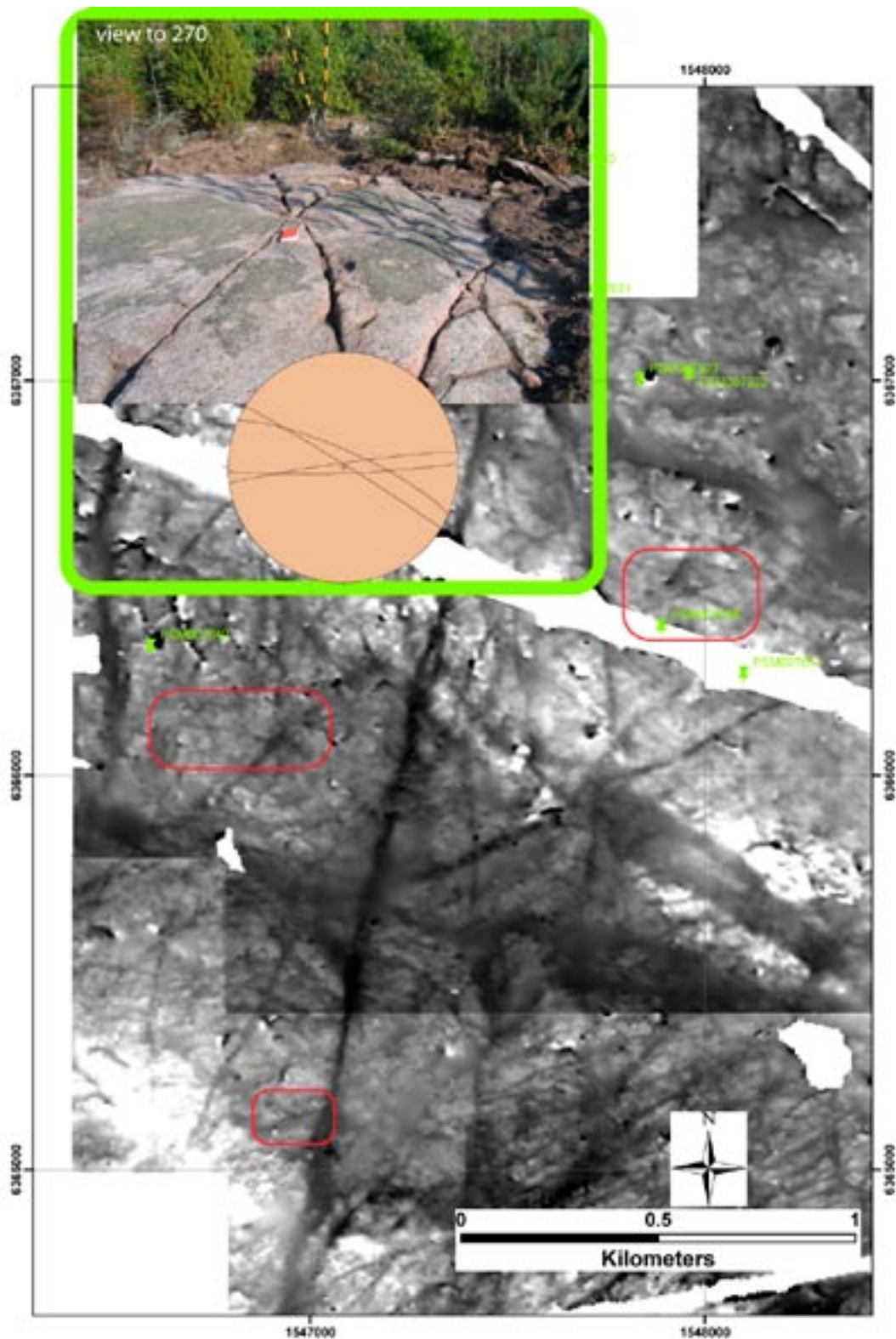
Figure 3-20. Inset: field photograph with view to the west of outcrop PSM007668 /Viola and Venvik Ganerød 2007b/ showing a set of conjugate fractures whose intersection defines an acute angle bisected by the EW direction. The background image is the total magnetic field of central Laxemar. Red rectangles highlight areas with clear sets of conjugate fractures oriented as those shown in the inset photograph.

Unfortunately, insufficient striated fault planes with ESE-WNW strike and sinistral kinematics were found in the field. The flow-chart of Figure 3-10 was thus integrated with information from faults whose sinistral kinematics was derived from Riedel geometries and not from slickensided planes. No stress inversion could be calculated for this set of field fault-slip data, although a c. EW maximum shortening direction is to be expected, i.e. the orientation of the bisecant of the acute angle defined by the intersection of the conjugate fractures.

3.3.4 Low-angle normal faults

Moderately-dipping normal faults form another distinct population within the fault-slip dataset measured in the field. The sorting procedure of Figure 3-10 defined 11 extensional striated planes. Although striated normal faults do not represent a statistically robust dataset, they are important structural features in the Laxemar-Simpevarp area and are the focus of much attention also in the light of the fact that there exist important low-angle seismic reflectors that cut across the Laxemar target area, which could be expression of extensional structures. Moreover, extension was suggested by /Viola and Venvik Ganerød 2007a/ for lineament ZSMEW007A, based on observations made in a trench dug across the moderately N-dipping gouge core of the fault.

Fault-slip data are not internally consistent and do not allow the definition of a single, well-constrained extensional regime. Inversion leads to a loose stress tensor, characterized by a high average misfit angle and unsatisfactory normal versus shear stress conditions for the majority of the faults. Figure 3-21 shows the dataset used, which consists not only of the low-angle extensional striated planes but also of all steep faults with steeply plunging striations and extensional kinematics.
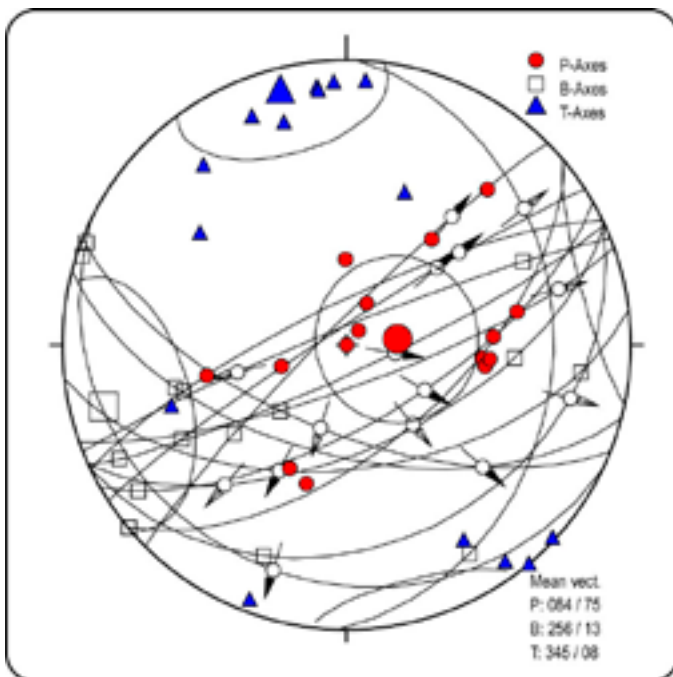

Figure 3-21. PBT axes computed for normal faults from the field dataset.

PBT axes were calculated for all faults (Figure 3-21). A large spread is observed although a very steeply E-plunging compression- and a sub-horizontal NNW-plunging tension axis are the strain axes that best fit the dataset, thus suggesting NNW-SSE oriented extension. The large scatter probably indicates that the analysed dataset is heterogeneous, formed by more than just one sub-set. Information from the numerous normal faults measured in the oriented drill cores (section 3.4.6) is therefore necessary to investigate further and interpret the data.

A possible independent indication of extension is seen in numerous Cambrian dykes, up to a few decimetres wide and a few meters long, which occur commonly in the area with mainly a NE strike, indicative of NW-SE-oriented extension. Figure 3-12 shows one of these dykes from the Laxemar area injected in the southernmost part of the polished pavement of drill site KLX11A /Viola and Venvik Ganerød 2007a/.

3.4 Kinematic study and stress inversion results on oriented drill cores

3.4.1 Data acquisition

An identical approach to that employed for the interpretation of the field data was used on fault-slip data gathered by /Viola and Venvik Ganerød 2007ab, 2008/ during the detailed structural logging of several kilometres of oriented cores from the Laxemar-Simpevarp area.

The standard procedure for obtaining the true orientation of linear structures (lineations, striations, etc) on fault surfaces in drill cores with known orientation was as follows:

- Fractures of potential interest were identified by visual inspection of drill cores from selected deformation zones, as defined previously by the geological single hole interpretations.

- Individual fractures were identified on the BIPS image of the borehole wall, which provides a mirror image of the core itself. Care had to be taken to ensure that the fracture selected on the image matched the one from the drill core. In some cases this was challenging, particularly where abundant fractures cut the core at different angles. Independent checks that the correct fracture was chosen could be carried out by using information contained in the drill core database, as, for example, the properties of the fracture itself, the acute angle α between the fracture and the core axis, and the angle β, which is the angle (measured counter-clockwise) from the lower intersection of the fracture with the core wall, to the top of the drill core.

- Having identified the fracture of interest, the top of the drill core was marked based on visual inspection of the BIPS image and on the angle β. The fracture orientation was obtained using the information contained in the drill core database.

- The core was positioned the right way up and at the true inclination using a core holder supplied by SKB. This device allowed the accurate adjustment of the core inclination as given in the database.

- The orientation of the linear structure was determined by measuring its trend and plunge.

- Once the sense of slip was determined with confidence, the true movement of the hanging wall with respect to the footwall of the fault was established.

- Relevant data were recorded in a database.

An extra source of uncertainty

It has to be pointed out that during an internal investigation of uncertainties connected with the orientations of mapped geological features, a particular problem concerning the orientation of the borehole TV-image (BIPS) was discovered. The problem was related to the rotational orientation of the probe, which sometimes resulted in errors and unacceptable uncertainties in the orientation of mapped geological features in the boreholes /Döse et al. 2008/, and as a result, in the possible misorientation of some of the slickenlines measured during this study.

On the basis of a preliminary investigation of the extent of the problems, a revision of the orientations from the BIPS-loggings was carried out for 48 prioritized boreholes in Oskarshamn. The BIPS-images were divided into the following groups according to the method of orientation: bubble level (x boreholes), steel ball (y boreholes) and compass oriented BIPS-images (z boreholes).

For revision of BIPS-images oriented with bubble level clinometer or compass, the raw data tapes were investigated. On the raw data tapes the compass or bubble level could be observed as well as the pointer which determines the rotational orientation of the BIPS-image. The relation between the bubble level clinometer or compass versus the pointer was documented and the resulting data was used to correct the orientations of mapped geological features. The uncertainties of the corrected orientations were also estimated.

The raw data tapes could not be used for revision of BIPS-images oriented with steel ball clinometer because of the unreliable clinometer type. Instead, the BIPS-images were revised by comparison with Acoustic Televiewer-images. The results from these comparisons were used to correct the orientations of mapped geological features and to estimate the uncertainties of the corrected orientations.

The BIPS-images oriented with steel ball clinometers were unequivocally marred by greater errors in the rotational orientation, compared to the bubble level oriented images which were relatively well oriented. The rotational corrections of BIPS-images oriented with steel ball clinometer are mostly within $\pm 20°$ (uncertainty $\sim \pm 10°$) whereas the rotational corrections for BIPS-images oriented with bubble level clinometer are generally within $\pm 5°$ (uncertainty $\sim \pm 3°$). Compass oriented BIPS-images from vertical boreholes also show larger errors in rotational orientation with correction values of about $\pm 15°$ (uncertainty $\sim \pm 10°$).

In some boreholes no correction of the orientation of mapped geological features was performed. The reason for this was that the boreholes were of lower priority, the raw data tapes were missing or defect or that the revision of bubble level oriented BIPS-images in similar boreholes showed that the original orientation was generally good. For these boreholes a general uncertainty value of the BIPS orientation was calculated, based on the results from the revision of BIPS-images from similar boreholes.

The final calculated uncertainties of the orientations of geological features are not affected by the BIPS-image orientation alone, but also by the mapping procedure and the deviation measurement of the borehole. These factors have also been evaluated within SKB, but these evaluations are outside this project.

The problem with the orientation of the borehole TV-image was discovered only at a stage when the logging work reported by /Viola and Venvik Ganerød 2007ab, 2008/ was almost complete. Correction of the acquired dataset at that late stage would not have been possible and this study uses therefore the same uncorrected datasets discussed in those three reports. Obviously this introduces additional uncertainty in the analysis described below, although, given the significant similarity between the results derived from the field observations and those derived from the drill cores, it is believed that this uncertainty does not affect the reconstructions and models presented here.

3.4.2   Sorting procedure

The bulk of the data is shown in the uppermost stereogram of Figure 3-22. Geometric and kinematic criteria were used to separate this extremely complex set of information into two main fault groups. Steep faults with dip angle greater than 60° were isolated and interpreted as belonging to three different conjugate sets of strike-slip faults (Figure 3-22). These sets are comparable to those identified from the field observations.

Shallow to sub-horizontal striations confirm the strike-slip character of these faults. There are, however, numerous steep to sub-vertical faults that bear steeply-plunging striations. As in the case of the field data, these are interpreted as potential indicators of kinematic reactivation of pre-existing steep fault planes under later normal and thrust stress regimes. A number of WNW-ESE dextral strike-slip faults (bottom stereogram in the right-hand side column of Figure 3-22) do not apparently belong to any systematic conjugate set, but can be interpreted as Riedel faults to, for example, the SW-NE striking dextral faults of set III. Other kinematically possible combinations (for example as conjugate dextral faults to the sinistral striated planes of set III) are not considered likely on the basis of the lack of such geometric relationship in the field. Field investigations, where 3D outcrop relationships are visible, were used in this study as a validating tool for observations made on the cores and are generally assigned greater weight than conclusions drawn from relationships observed in the cores.

3.4.3   Conjugate set I

Figure 3-23 shows the results of stress inversion and PBT axis calculation for the striated planes defining conjugate set I. Results are remarkably similar to those obtained for the field measurements, with a c. NNW-SSE-oriented compression direction. The Mohr diagram, though, portrays a not fully convincing situation (despite the relatively low average misfit angle), with fault stress conditions away from the failure envelope. This is very likely due to the fact that several striated planes (especially the dextral fractures) are not perfect strike-slip faults, but bear instead moderately plunging lineations.

As mentioned above, the many reverse faults populating the dataset of Figure 3-22 are of difficult interpretation due to the large scatter in strike and transport direction. Nonetheless they can be sorted according to their orientation, so that, for example, ENE-WSW-striking thrusts are chosen and implemented into set I dataset, similarly to what was done for set I field observations.

The final results are shown in Figure 3-24. Here, set I conjugate strike-slip fractures and conjugate ENE-WSW-striking thrusts were merged and processed as a homogeneous dataset and, in addition, they were also merged to the field data of Figure 3-14. Inversion results for this very large dataset are satisfactory and improved significantly compared to Figure 3-23, with good normal versus shear stress conditions for the processed faults and angular misfit values not in excess of 35°.

This dataset is used as an example to demonstrate that low-angle thrusts, if selected properly, can be used to strengthen the results of the inversion procedure run on the strike-slip conjugate fractures and faults. Moreover, this inversion procedure confirms the results obtained from the field data, indicating that structural information from the cores is fully compatible with field data and can therefore be used to refine and strengthen models calibrated upon field observations.
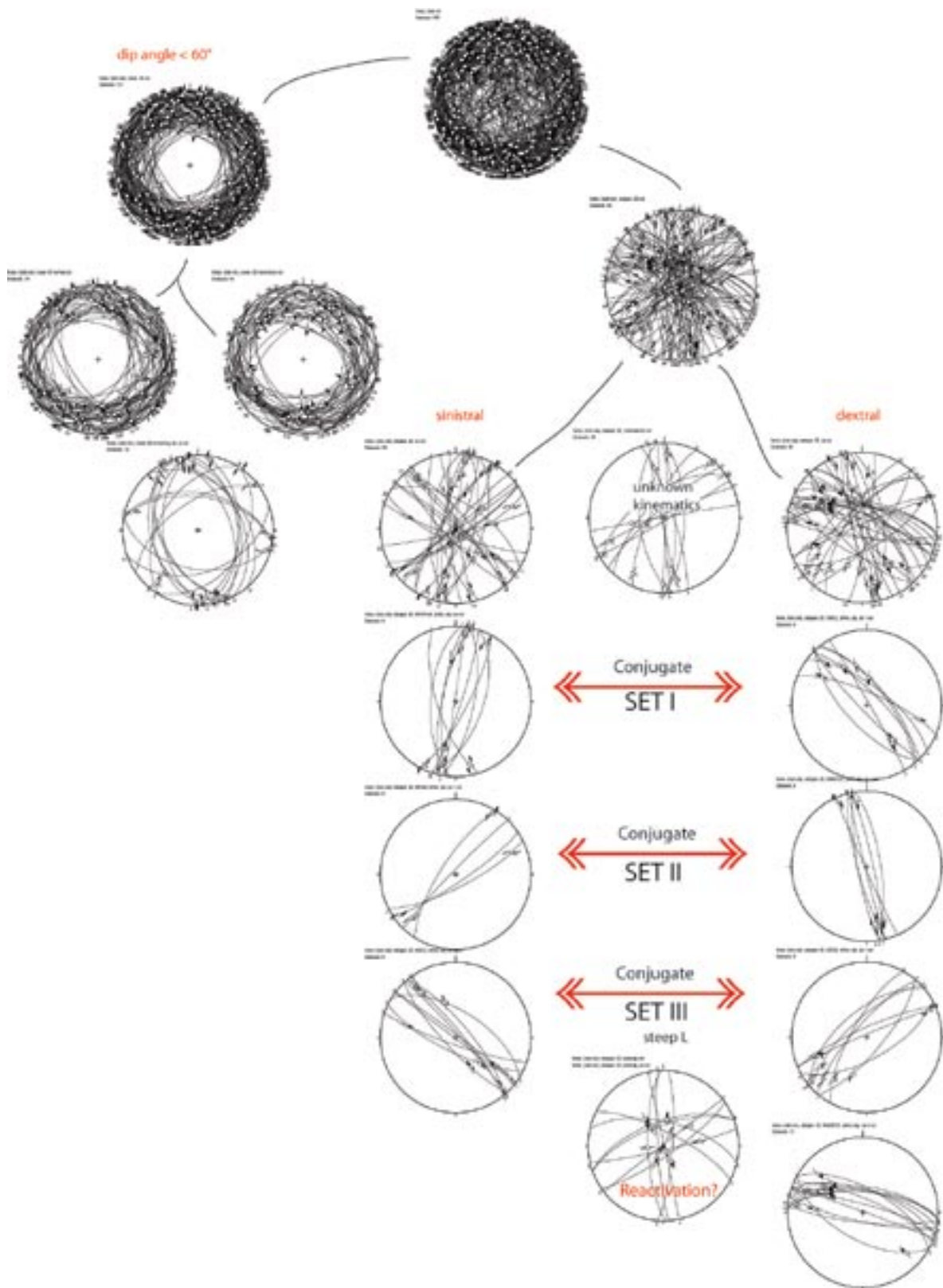
Figure 3-22. Sorting of fault-slip data collected from structural logging of the cores studied and described by /Viola and Venvik Ganerød 2007ab, 2008/ according to geometric and kinematic compatibility criteria.
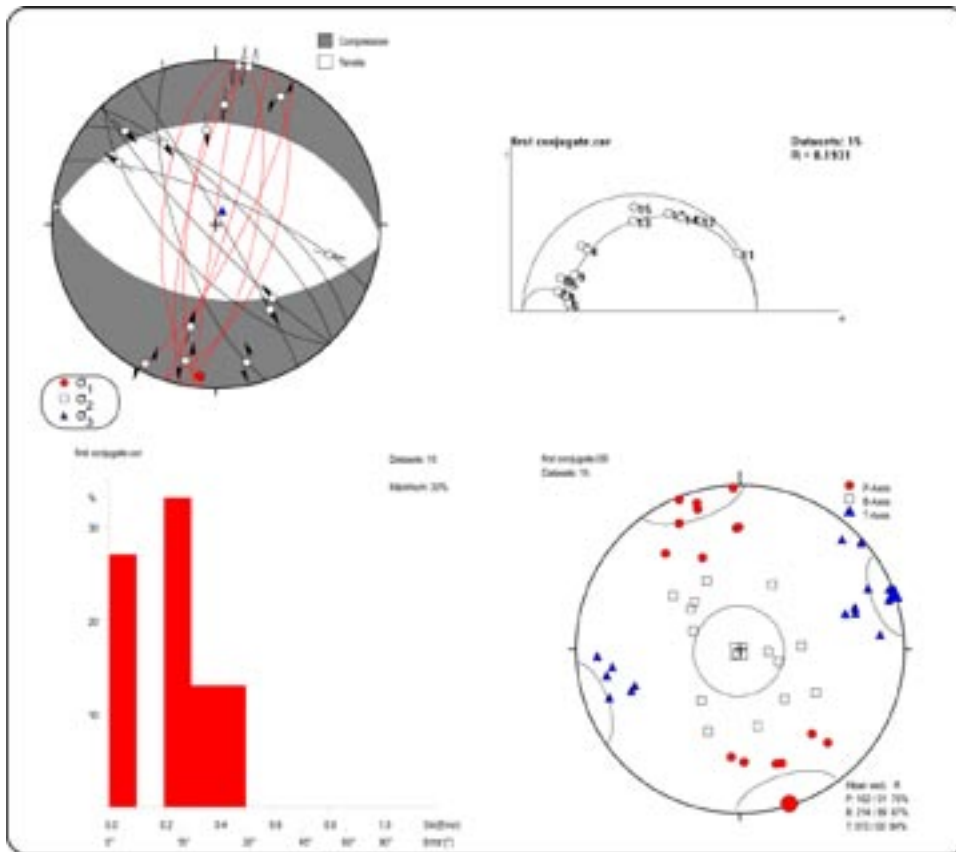
Figure 3-23. *Stress inversion results and PBT axes for conjugate set I as per data from the analysed cores.*
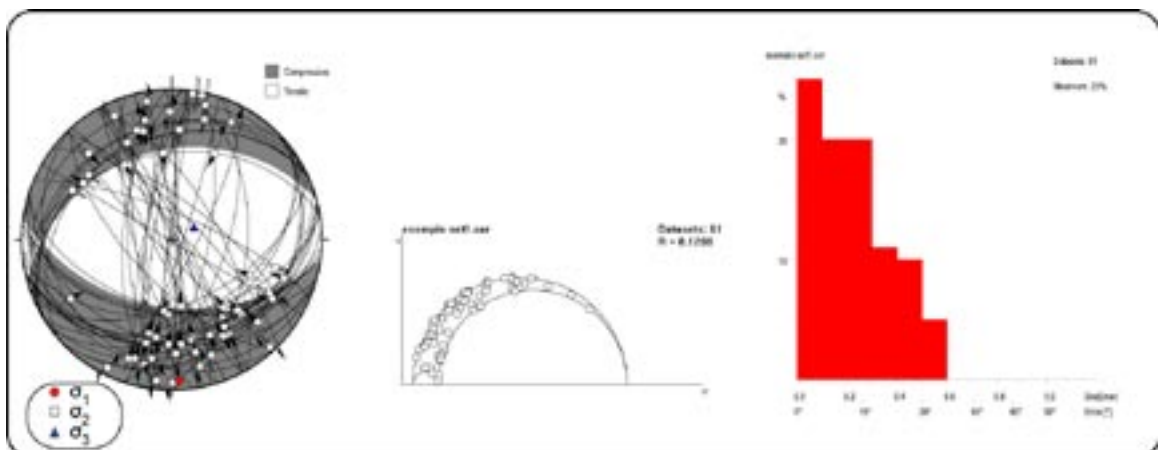
Figure 3-24. *Stress inversion results from a dataset containing set I conjugate strike-slip faults, top-to-the-N-NW and S-SE thrusts and the complete field set I dataset.*

3.4.4 Conjugate set II

Robust results were also obtained from the inversion of fault-slip data belonging to conjugate set II extracted from the bulk drill core data (Figure 3-25). Very low average angular misfit and close to ideal normal versus shear stress conditions strengthen the results derived from the field study of a SSW-NNE-oriented shortening episode in an overall strike-slip regime.

As for the field study, the addition of WNW-ESE-oriented thrusts to set II deteriorates the results of the inversion procedure.

In addition, an integrated dataset was produced by merging field- and drill core-conjugate set II fault-slip data. Results are even more robust because generated from a statistically strong fault population and are therefore assumed to be very representative of this specific deformational episode (Figure 3-26).
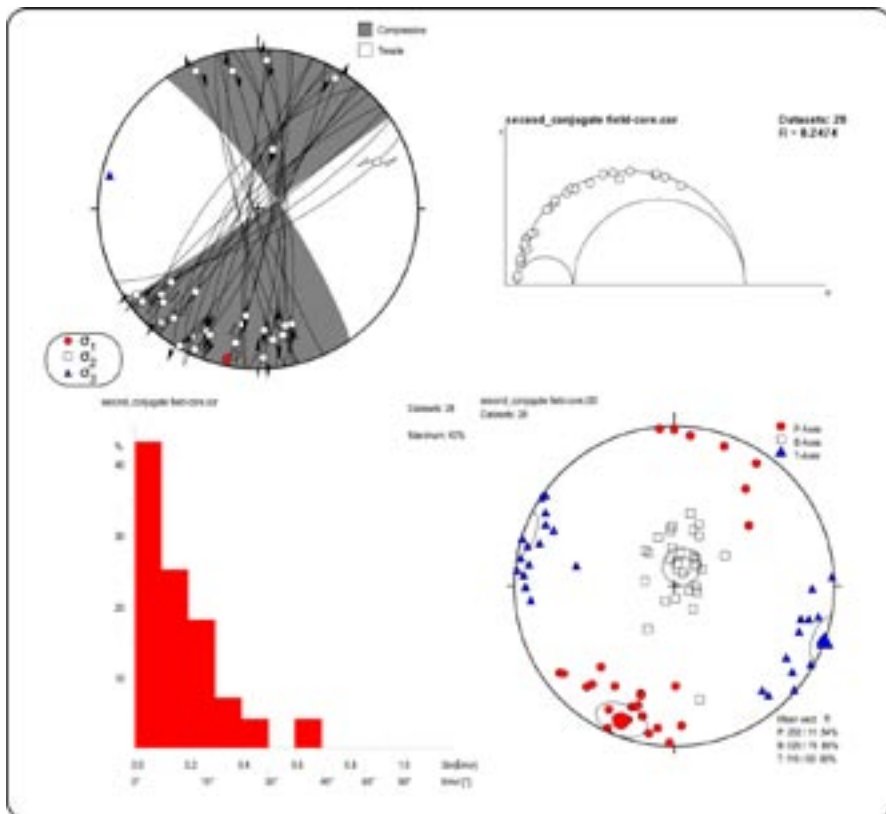
3.4.5 Conjugate set III

As mentioned above, no stress inversion could be performed on field fault-slip data belonging to conjugate set III due to the lack of sinistral ESE-WNW-striking striated planes. Drill core data come, however, to the rescue and contain a population of strike-slip fractures with this orientation. Figure 3-27 shows the results of the stress inversion procedure, which confirm a distinct thrust shortening episode characterized by a c. E-W-trending compressive stress. The addition of N-S- to WNW-ESE-striking thrusts leads to an even better resolved state of stress.

The coating of the vast majority of these fractures is chlorite, calcite and epidote, suggesting faulting under lower T conditions than set I and II, hence a possibly younger age for this deformational episode.
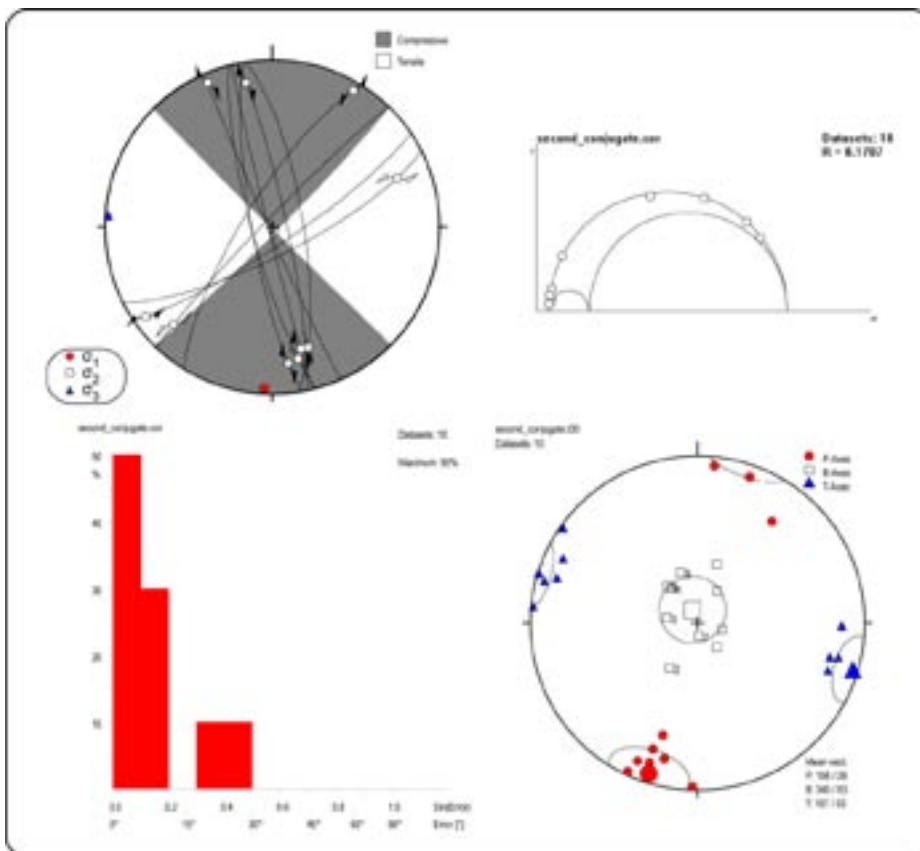
Figure 3-25. *Stress inversion results for the drill core fault-slip data that define conjugate set II. SSW-NNE-oriented shortening under strike-slip conditions is proposed.*

Figure 3-26. Stress inversion results and PBT axes for the "total" conjugate set II dataset, containing both field and drill core fault-slip information.
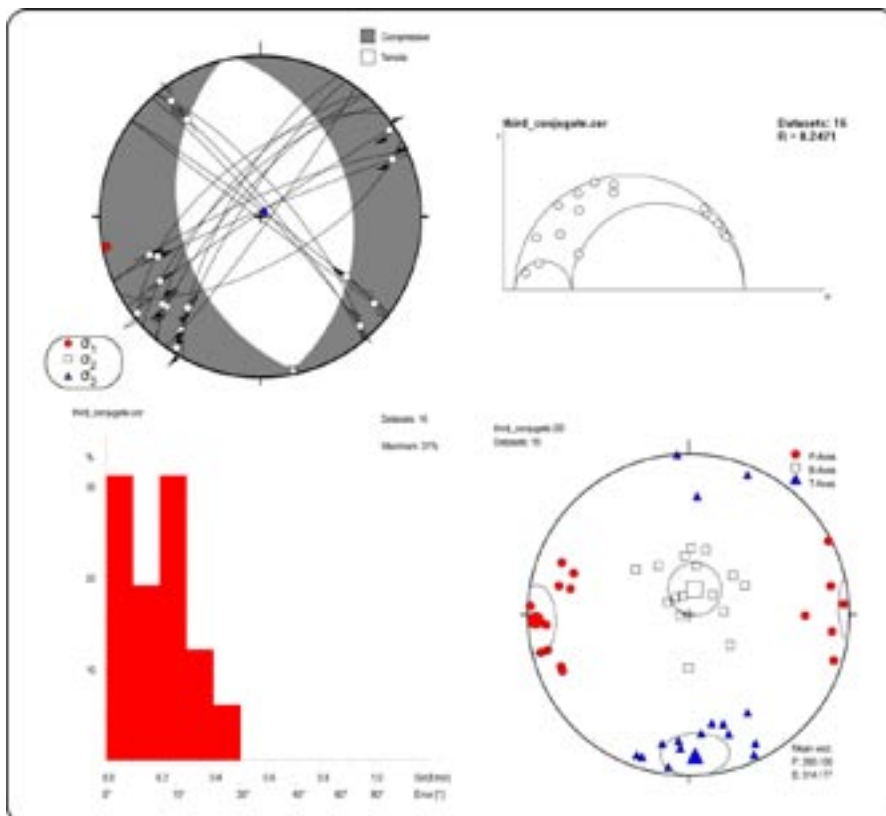
Figure 3-27. Stress inversion results and PBT axes for the "total" conjugate set III dataset, containing both field and drill core fault-slip information.

3.4.6 Low-angle normal faults

Logging of drill cores allowed the identification and kinematic analysis of many more "low angle" than steep striated fracture planes, reflecting the bias due to the very steep attitude of the borehole axes.

It was already discussed how some of the thrusts can be genetically assigned to some of the conjugate sets and are thus liable to be interpreted as the expression of the stress regimes presented and documented above.
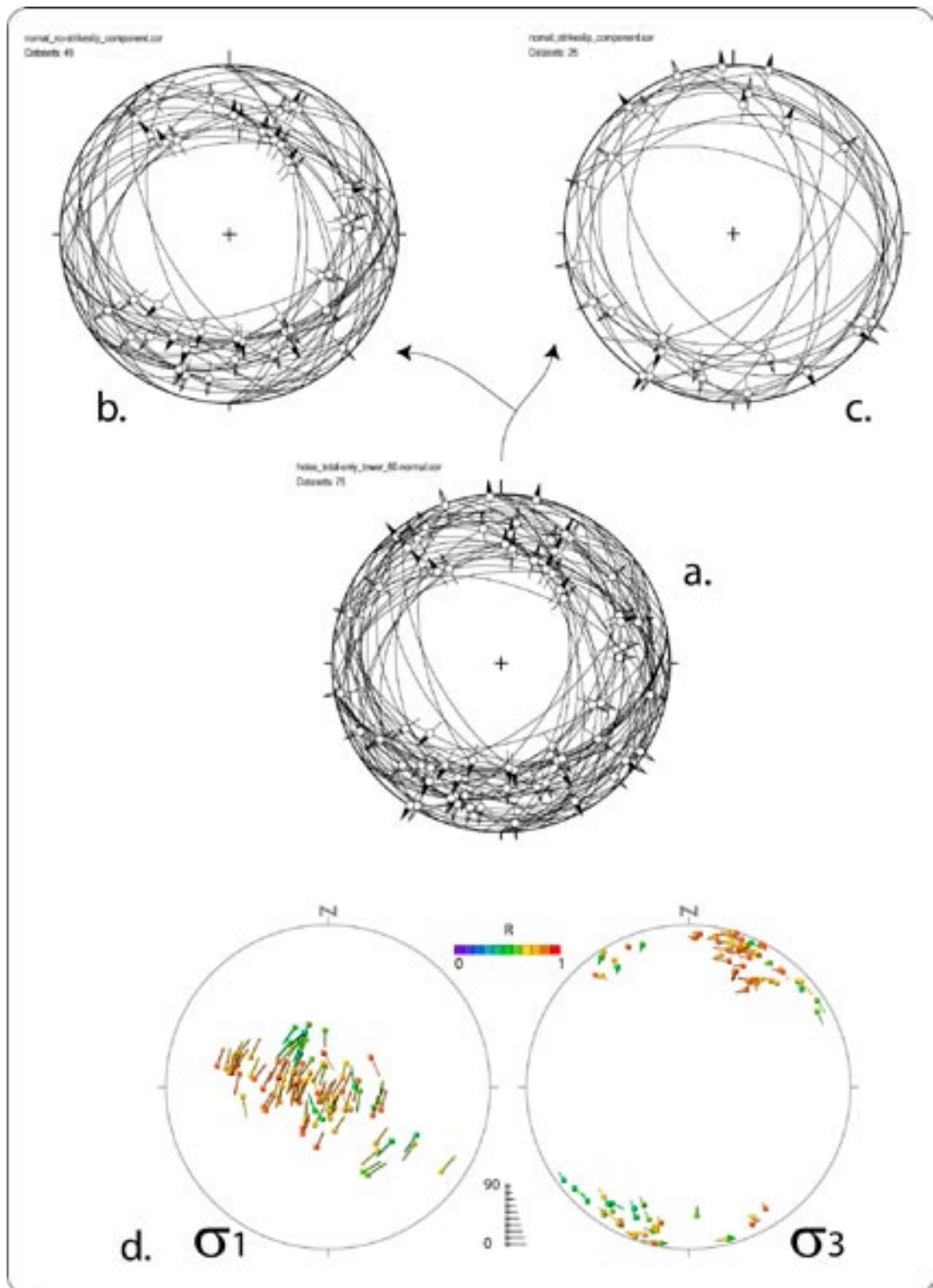
Low angle- to moderately–dipping normal faults are, on the other hand, of difficult interpretation and their sorting is not a straightforward procedure. The MIM procedure was run on the dataset of Figure 3-28a, which contains dip-slip (Figure 3-28b) and extremely high-obliquity (Figure 3-28c) normal faults. It is clear that the dataset is heterogeneous and contains fault planes belonging to more than just one extensional episode. Even the multiple inversion technique, though, fails in isolating obvious sub-sets (Figure 3-28d). This is particularly true when the orientation of σ_1 is considered, whereas more information is extracted from the σ_3 stereogram, which clusters data into two separate groups (although very heterogeneous internally), one prominent oriented NNE/NE-SSW/SW and a second, more subdued, oriented NNW/NW-SSE/SE.

This information was used in an advanced sorting procedure, which split the normal faults of the dataset of Figure 3-28b according to kinematic criteria. Two sub-sets were identified, with antithetic top-to-the-NE and -SW and -NW and -SE normal displacement, respectively (Figure 3-29 and Figure 3-30). These two stress tensors account very satisfactorily for almost all normal faults containing down-dip or high-angle striations. Results of the inversion procedure constrain very robust paleo-stress states, as indicated by the very positive stress conditions for failure for individual faults in the Mohr circle diagrams and by the histograms plotting the mismatch angles between predicted and measured slip direction.

The two datasets were also integrated with some of the steep faults with normal kinematics that were isolated through the preliminary sorting procedure of Figure 3-22. Figure 3-30, for example, contains two sub-vertical fault planes (numbered 16 and 17, respectively), which, based on their orientation, could be the result of faulting during the development of some of the conjugate sets described above. Their recorded kinematics, however, and the steep plunge of the striations they bear are incompatible with those sets; these faults can instead be easily interpreted as pre-existing steep fractures reactivated during subsequent extension. Incidentally, the Mohr diagram of Figure 3-30 shows that faults 16 and 17 plot indeed far from stress conditions typical for failure of a newly formed fault and are instead characterized by stress conditions which are in line with their reactivation.

A point to be stressed in this section is the fact that many of these normal faults dip at moderate to very low angle, thus not compatibly with brittle field Mohr-Coulomb failure conditions for newly formed normal faults. This especially applies to the family of top-to-the-NW and -SE normal faults (Figure 3-31b), which, albeit with very variable dip angles, dip as low as 10° and even less. It is very likely that these extremely low dip angles result from reactivation of older structures (possibly even ductile), from block rotation during the long-lived deformational history of the region or from a combination of the two factors. Very gently-dipping structures could have initially formed as dilational joints oriented sub-parallel to the topographic surface in response to stress release in the bedrock during unloading cycles in the area.

Transtensional faults (Figure 3-28c) are not interpreted here as representing a distinct event, and are instead read in terms of reactivation of low-angle faults under subsequent strike-slip shear episodes.

Figure 3-28. a.: Fault-slip data for all normal faults measured in the drill cores logged by /Viola and Venvik Ganerød 2007ab, 2008/. The data contain moderately to gently-dipping and sub-horizontal normal faults with down-dip or high-plunge angle striations (b.) and faults bearing very oblique striations (c.). d.: Results of multi-inversion applied to the dataset of a. See caption of Figure 3-5 for instructions on how to read these diagrams.
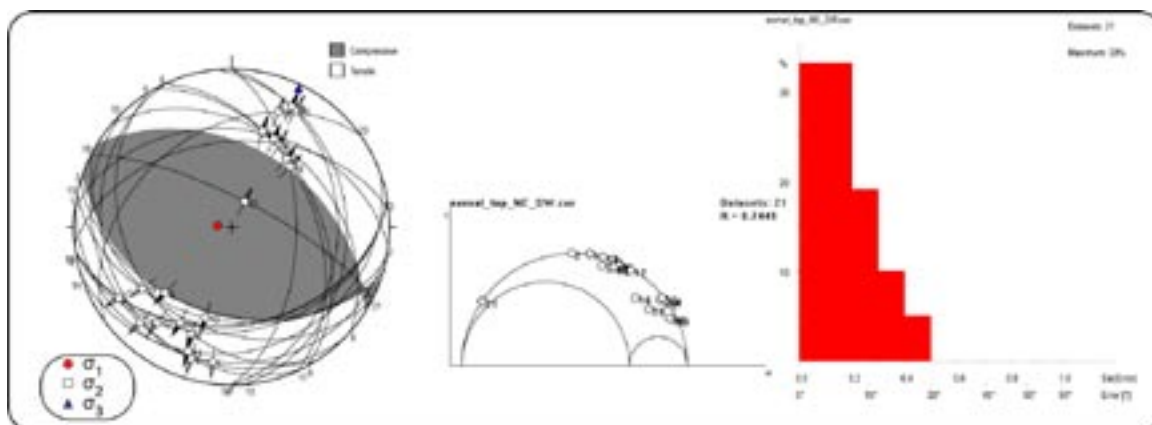
Figure 3-29. *Stress inversion results on a fault population characterized by antithetic top-to- the-NE and –SW extensional kinematics. A stress tensor is identified with σ_1 oriented 276/83, σ_2 116/07 and σ_3 026/02.*
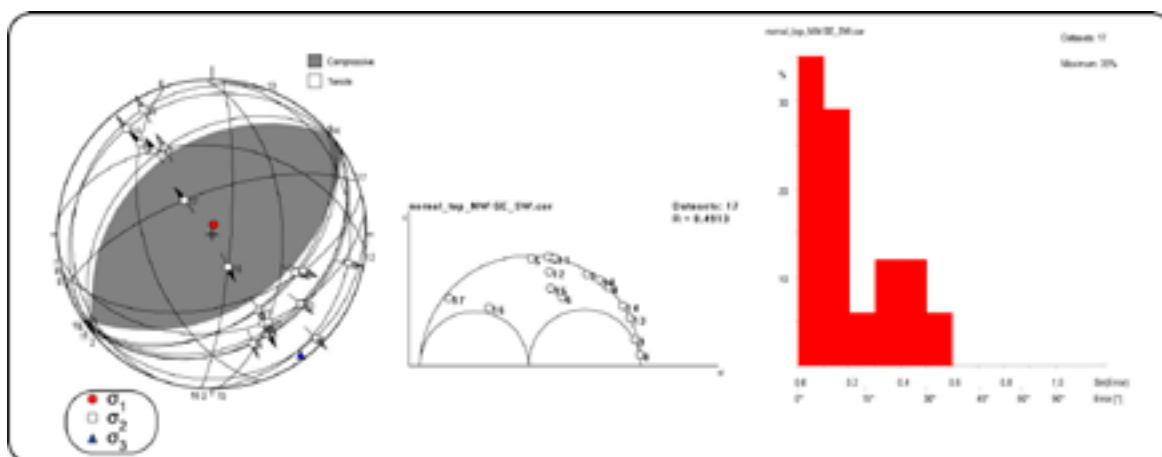

Figure 3-30. *Stress inversion results on a fault population characterized by antithetic top-to- the-NW and –SE extensional kinematics. A stress tensor is identified with σ_1 oriented 010/85, σ_2 234/04 and σ_3 144/03.*

3.5 Analysis of fault-slip data from the Ordovician limestones of Öland

3.5.1 Introduction and summary of existing studies

The paucity of post-Svecokarelian rocks in the study area seriously limits the understanding of the local geological evolution during more than 1,700 years of Earth history. The Ordovician limestones exposed on the neighbouring island of Öland represent therefore an extremely valuable possibility to look at the effect of brittle deformational phases that occurred after the Ordovician. Although the time elapsed since the Ordovician represents only a limited time sequence compared to the 1.5 Ga of brittle evolution of the basement exposed in the Laxemar-Simpevarp area, studies of brittle deformation accommodated by the Öland limestones help reduce the uncertainty necessarily involved in this paleo-stress tensor study.

An SKB progress report by /Talbot 1990/ reported a superbly exposed fault zone along the west coast of Öland, characterized by various generations of carbonate fibres grown in dilation and shear fractures. Fault-slip data are, however, not presented nor illustrated by that study.
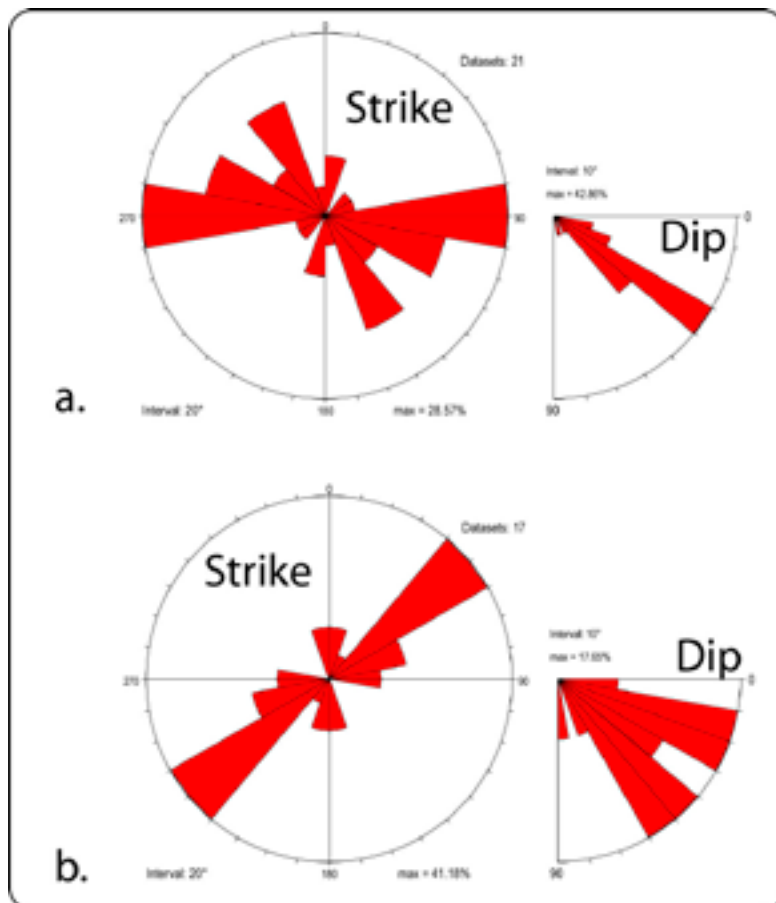
Figure 3-31. *Rose diagrams plotting the strike of the normal faults of Figure 3-29 (a.) and Figure 3-30 (b.) together with their dip angles. Note the extremely flat attitude of many of the normal faults, especially among those of dataset b.*

A detailed analysis of fracturing in the lower Ordovician limestones exposed along the western coastline of the island was carried out by /Milnes and Gee 1992/. Their study dealt with the geometrical arrangement and the investigation of the amount of movement on fractures mapped in quarries and on continuously exposed shore platforms. No systematic kinematic analysis of striated fault planes was done, though, and no fault-slip data are available for paleo-stress analysis. Their conclusions were that the lower Ordovician limestones suffered remarkably little deformation since deposition, i.e. over the last 500 million years.

/Munier and Talbot 1993/, on the other hand, acknowledged the fact that in the absence of post-Cambrian marker rocks it is not possible to be certain which fracture sets from the Laxemar-Simpevarp-Äspö area formed or reactivated later than about 500 Ma and therefore, in the hope of distinguishing post-Cambrian deformation, investigated fault-slip data in the Cambro-Ordovician platform sequence of Öland. Their conclusions are that the measured dataset is incompatible with one single stress field, but it can be readily accounted for by two different (but of unknown relative and absolute age) stress fields characterized by ENE and WNW-oriented σ_1, respectively.

Several well-exposed sites on the island were studied during this study (Figure 3-32) in order to compute paleo-stress states for the post-Ordovician deformational phases in a consistent fashion with the study of the Laxemar-Simpevarp area.
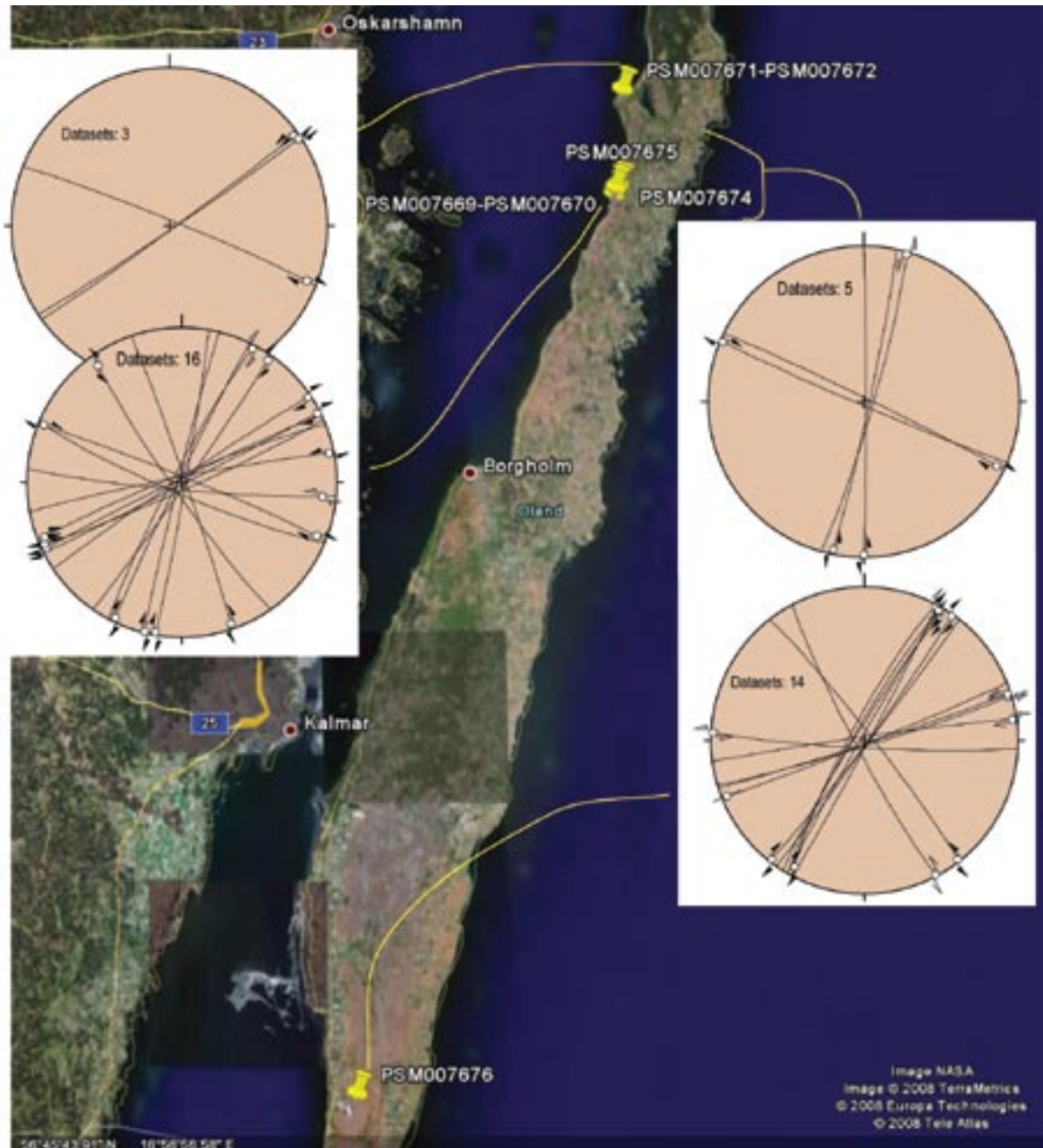
Figure 3-32. *Observation localities studied on the island of Öland and measured fault-slip data. Given the extremely flat morphology of the island, covered by horizontal Ordovician limestones, measurements were taken in active (PSM007674, 75 and 76) and abandoned (PSM007669, 70, 71 and 72) limestone quarries.*

60

3.5.2 Site description

**PSM007669 (6330620, 1565515) and PSM007670 (6331254, 1565598)**

These two sites represent the southern- and northernmost termination of a traverse at a locality called Jordhamn (location shows in Figure 3-32). The section consists of a continuous seies of abandoned quarries right along the coast in an area that contains otherwise no shore exposures (Figure 3-33). Bedding is preactically horizontal (Figure 3-33). The limestones exposed in the quarries contain superb striated fault planes. The quality of the kinematic indicators is such that almost all data were constrained kinematically with the highest degree of confidence, thus reducing significantly one of the elements of uncertainty introduced into the paleo-stress computations (Figure 3-34 and Figure 3-35).

Figure 3-35 plots the measured fault-slip data for this continuous exposure. The dataset looks rather heterogeneous and not of straightforward interpretation. The observation of clear examples of sets of conjugate fractures in the field, however, is an important tool to better understand the coexistence of several subsets in the outcrop fault-slip population. Figure 3-36 plots two such sets, whereas Figure 3-37 shows the procedure followed to sort the outcrop dataset. When faults that are kinematically and geometrically compatible with these subsets are removed and plotted separately (set a and b in Figure 3-37b), a possible third set is identified (set c, Figure 3-37c). This is defined by very well constrained sub-vertical dextral faults striking ENE-WSW and a single E/ESE-W/WNW sinistral striated plane (Figure 3-37c).

Figure 3-33. View to the south of the abandoned quarries of Jordhamn. Note the horizontal bedding planes.
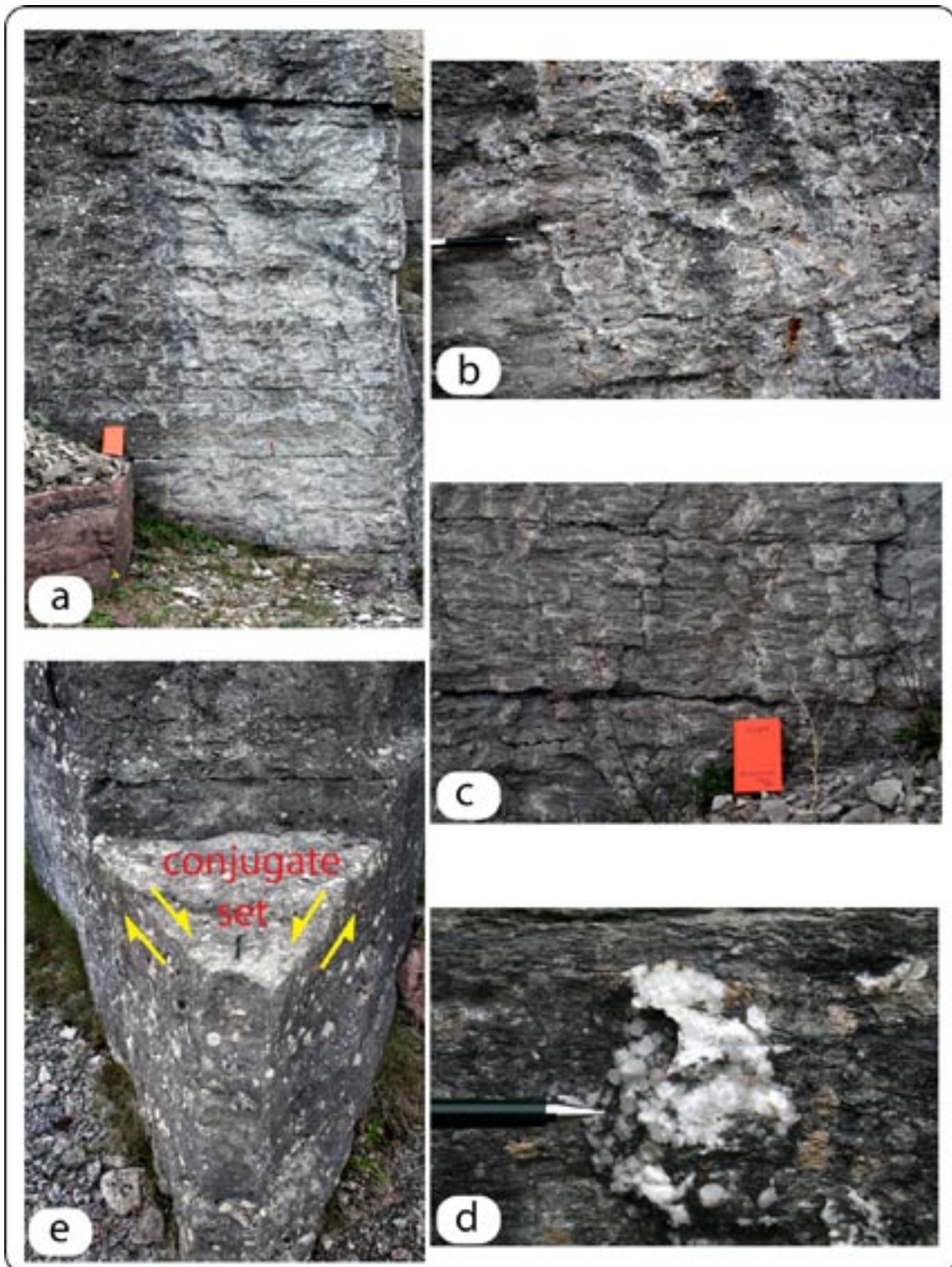
Figure 3-34. (a.), (b). and (c.): Examples of striated fault planes with pronounced secondary calcite steps from the Jordhamn section. (d.): Internal structure of a step on a dextral fault plane. Coarse-grained, euhedral calcite crystals are found in the step strain shadow, whereas fine-grained and sheared calcite coats the sheared part of the step. (e.): Mesoscopic set of conjugate fractures, the orientation of which is shown by the red great circles in Figure 3-36. View to 070°.
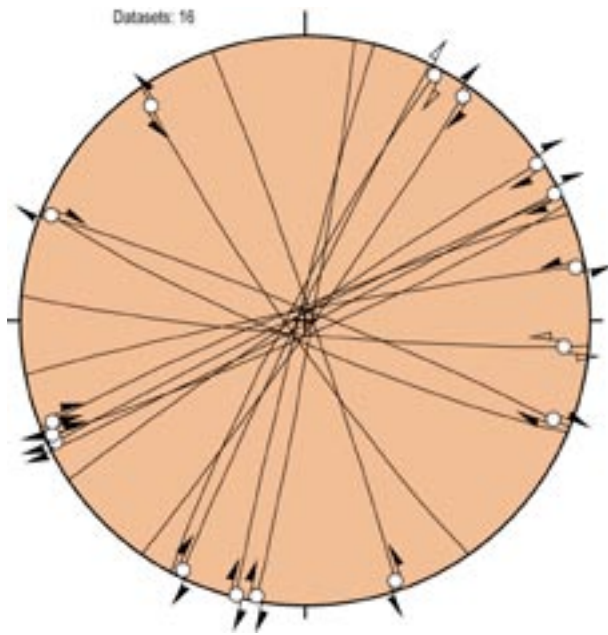
Figure 3-35. *Fault-slip data from the abandoned quarries of Jordhamn.*
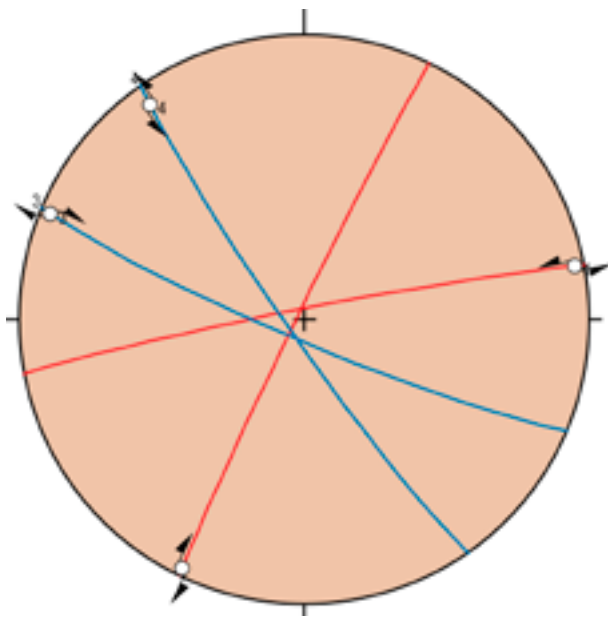
Figure 3-36. *Orientation and kinematics of two sets of conjugate fractures directly observed in the field. The red great circles correspond to the set visible in Figure 3-34e.*
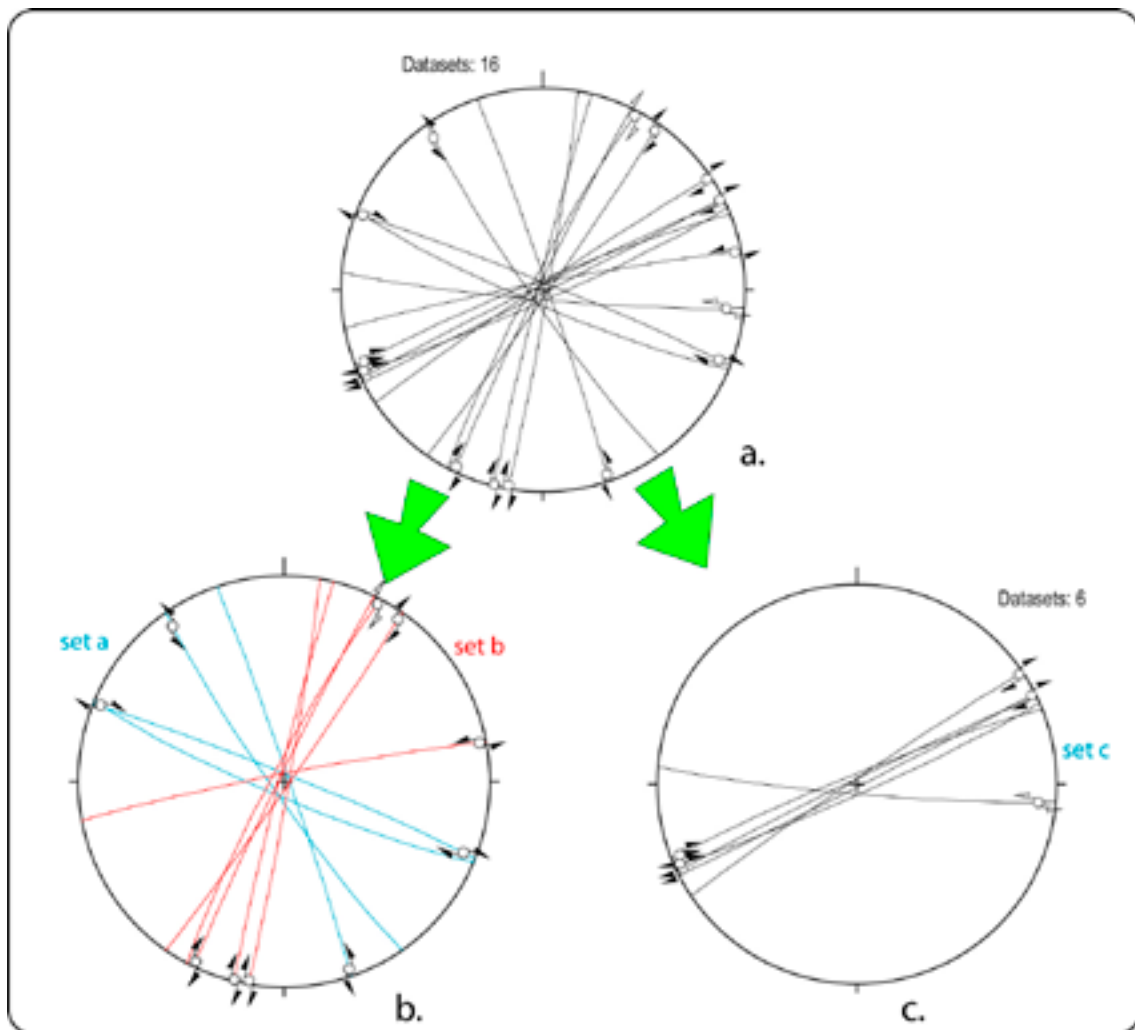
Figure 3-37. *The total fault-slip data (stereogram a.) is sorted by using geometric and kinematic criteria and by referring to field observations of sets of conjugate fractures. Dextral and sinistral faults are thus assigned to three distinct sets of conjugate fractures referred to as set a, set b and set c (blue, red and black great circles; stereograms b. and c.).*

It is obvious that the E/ESE-W/WNW striking sinistral fault of this set is very similar in orientation to the E/ENE-W/WSW sinistral fault of set b (Figure 3-37b), and uncertainty may therefore exist for this reconstruction. On the other hand, set b is constrained tightly by direct field observations. If the sinistral fault of set c was assigned to the latter, there would then remain a significant set of dextral faults striking ENE-WSW of no simple interpretation. It is concluded, therefore, that a third conjugate set of strike-slip fractures also is recognizable at this locality.

Due to the limited number of data in set a, paleo-stress inversion could be computed only for set b and c.

Figure 3-38 presents the results of a very solid inversion procedure for set b. Inversion establishes a horizontal and c. SW-NE trending σ_1 that bisects the acute angle defined by conjugate fractures oriented similarly to those of Figure 3-34e, in an overall strike-slip faulting regime. The extremely low mismatch angle between predicted and observed slip direction and the good stress conditions plotted by the Mohr circle diagram indicate a robust inversion procedure. PBT axes indicate an only slightly misoriented average greatest horizontal compressive direction, plunging 02° towards 054°.

64
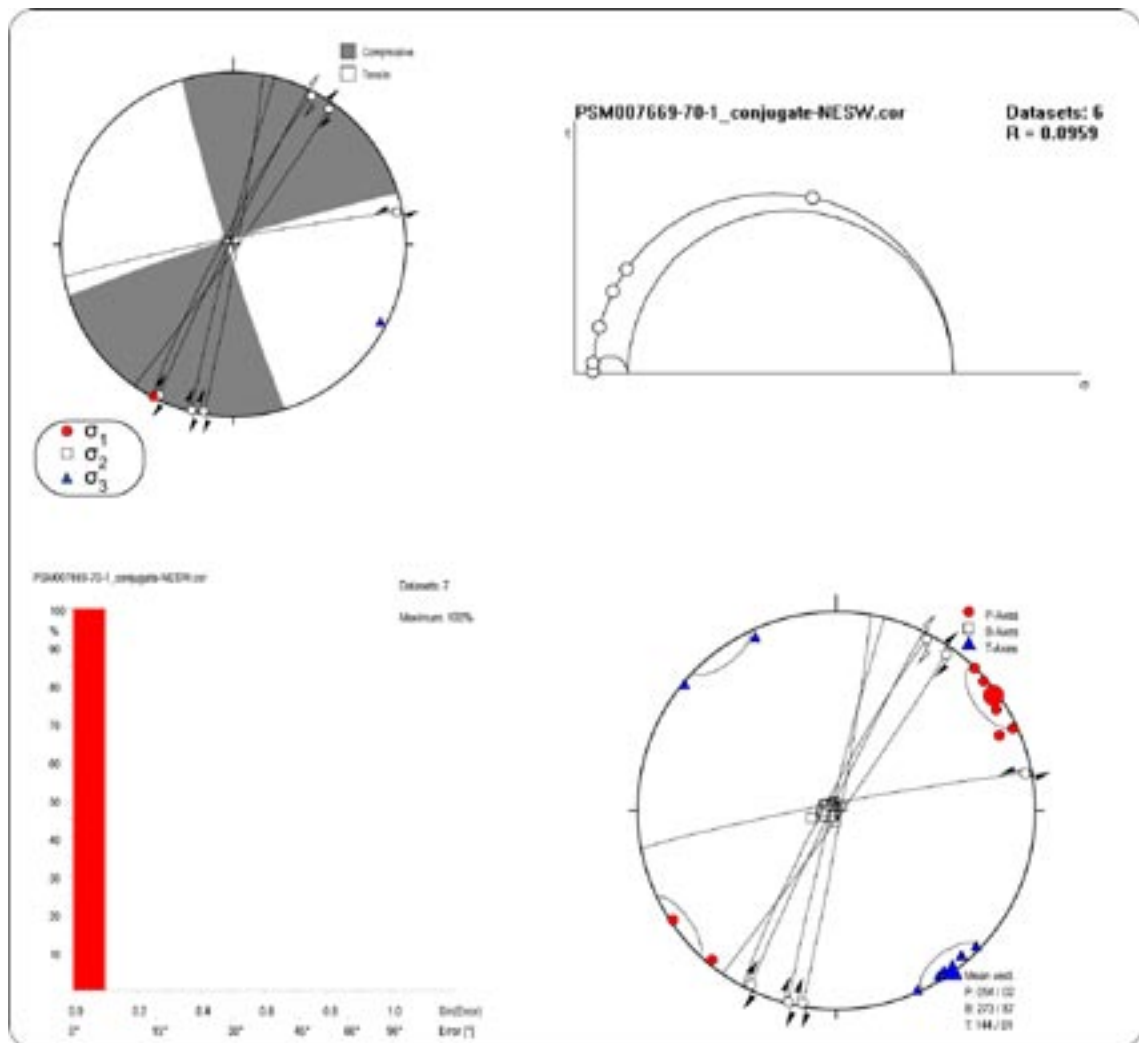
Figure 3-38. *Stress inversion results and PBT axes for set b from PSM007669–PSM007670 that defines a strike-slip faulting regime with a horizontal σ₁ oriented 208°.*

Results of stress inversion on set c are shown in Figure 3-39. PBT axes were also computed. Results are in general agreement, with a sub-horizontal σ_1 oriented c. E-W.

PSM007671 (6431232, 1566398) and PSM007672 (6341597, 1566474)

Fault-slip data shown in Figure 3-40 were measured in a series of abandoned quarries that are referred to as the "Hagudden section" by /Milnes and Gee 1992/. Unfortunately, many of the quarries were recently filled with aggregate material and only an extremely limited number of observations could be made. No stress inversion can be computed with the three striated planes documented.

PSM007674 (6331618, 1565740) and PSM007675 (6332012, 1566067)

A very large and operative limestone quarry is located at locality Gillberga. PSM007674 and PSM 007675 were taken in the southernmost (now apparently not actively exploited) and norternmost part of the pit. Figure 3-41 shows one spectacular sinistral fault plane with N-S strike from the active part of the quarry.

Only a few striated planes were measured and results are shown in Figure 3-42. A well defined set of N-S striking sinistral fault planes is observed, together with WNW-ESE trending dextral planes.
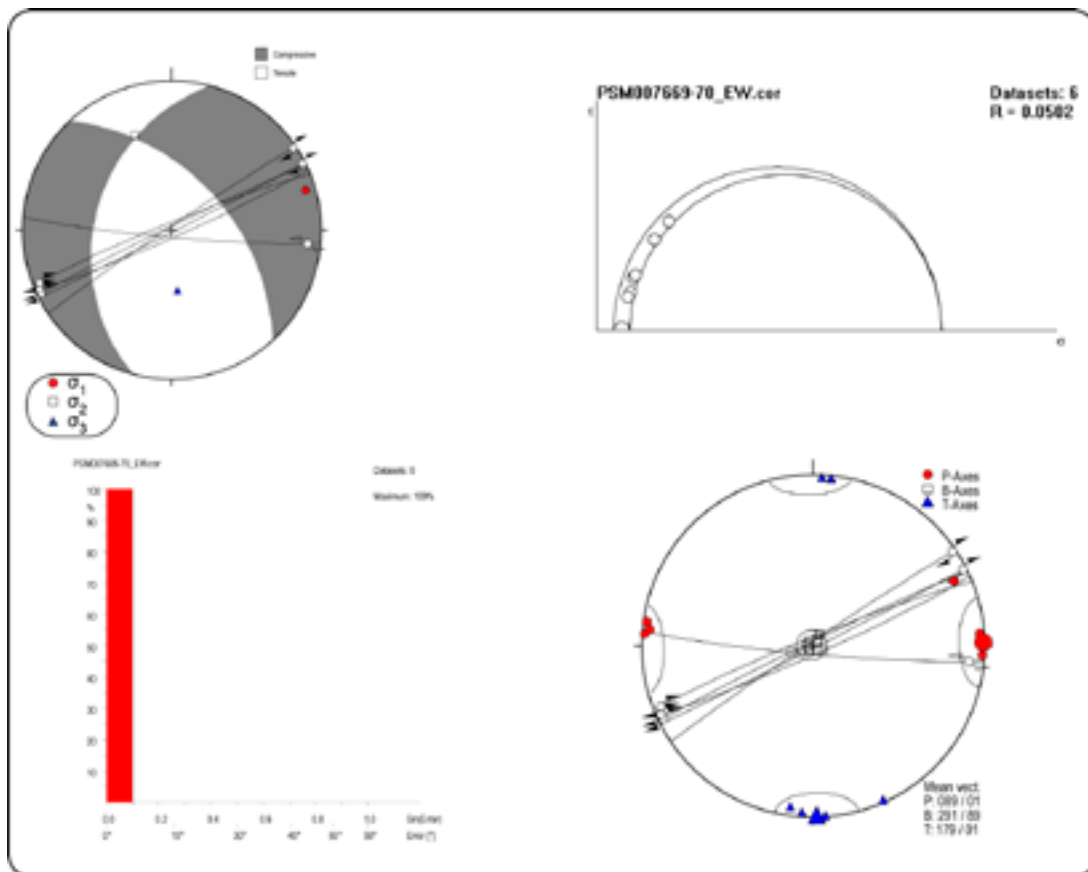
Figure 3-39. *Stress inversion results and PBT axes for set c from PSM007669–PSM007670. Inversion constrains a σ₁ plunging 07° towards 073°. σ₂ and σ₃, however, are inclined, 339°/32° and 174°/57°, respectively. PBT axes were also calculated, and constrain a strike-slip fault regime with sub-horizontal maximum and least compressive stress directions.*
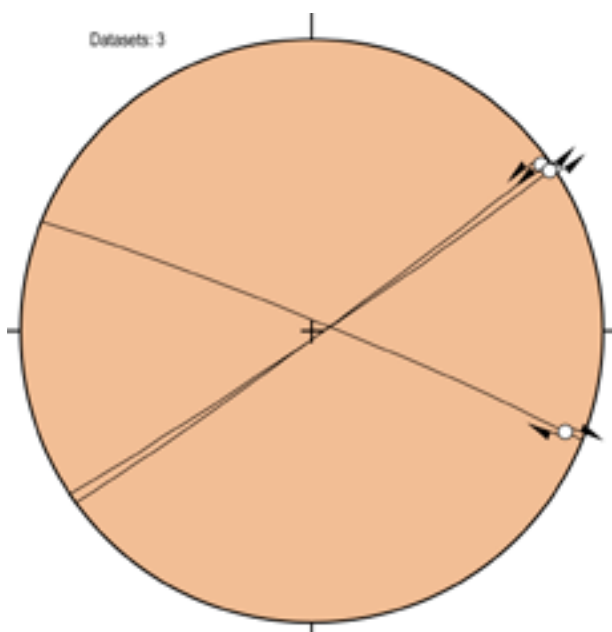
Figure 3-40. *Only three fault planes were constrained kinematically at localities PSM007671 and PSM007672.*

Figure 3-41. *Large fault plane with very pronounced slickensides and striations. The plane strikes N-S and is a sinistral fault. View to 090°.*
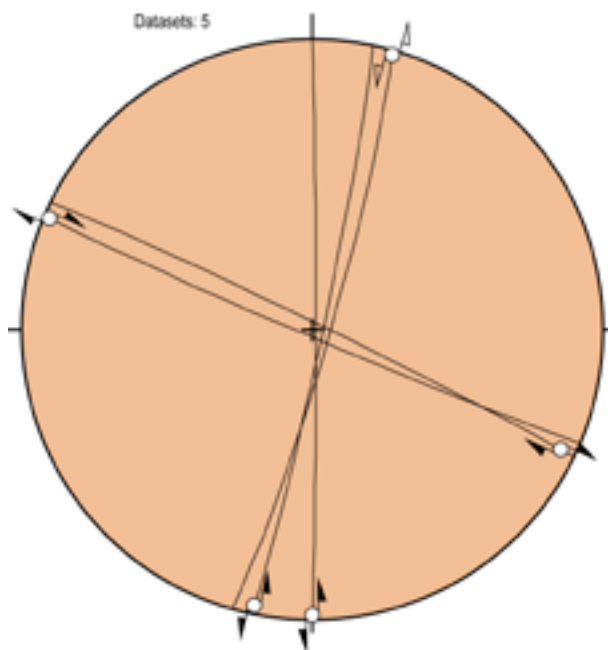
Figure 3-42. *Fault-slip data from the limestone quarry at Gillsberga.*

The large quarry at Albrunna, in the southern part of the island, provides limestone to a nearby cement factory. Fresh rock cuts allowed the detection of a very pervasive set of conjugate fractures (Figure 3-43). The ENE-WSW trending sinistral fractures are very systematic and occur regularly with spacing on the order of c. 70 m. Their sinistral kinematics could be easily determined, but the quality of the indicators was worse than in the case of the conjugate dextral fractures, with several fault planes presenting contrasting kinematic indicators. Moreover, a sinistral E-W trending fault plane displays a geometric arrangement with respect to the other sinistral, systematic fractures that recalls the situation discussed for the Jordhamn section, with a subtle orientation difference between the sinistral faults of set b and set c.

Stress inversion was computed on the subset shown in Figure 3-44. The procedure yielded a sub-horizontal σ_1 oriented 030° (Figure 3-44), which is comparable to the results obtained for set b from Jordhamn.

3.5.3 Discussion of fault-slip data from Öland

Given the similarities among some of the stress states discussed above for several localities in Öland, it was decided to merge the data and to proceed to stress inversion on a single, statistically more robust dataset. The sorting procedure for the total, merged dataset is shown in Figure 3-45 and it is based on geometric and kinematic criteria (as in the case of the analysis for the field and drill core data from the Laxemar-Simpevarp area discussed above). It confirms the results obtained for the individual observation sites and it identifies the same three conjugate sets. Only five fault planes (Figure 3-45) could not be fitted in the three conjugate sets.

Inversion results are summarised in Figure 3-46. Satisfactory stress conditions and very good fluctuation histograms indicate that the obtained results are robust. As mentioned earlier, direct field observations support the identification of sets a and b, whereas set c remains more speculative.

The significance of each of these paleo-states of stress and their role and connection to what has been documented for the Laxemar-Simpevarp area is discussed in the next section.
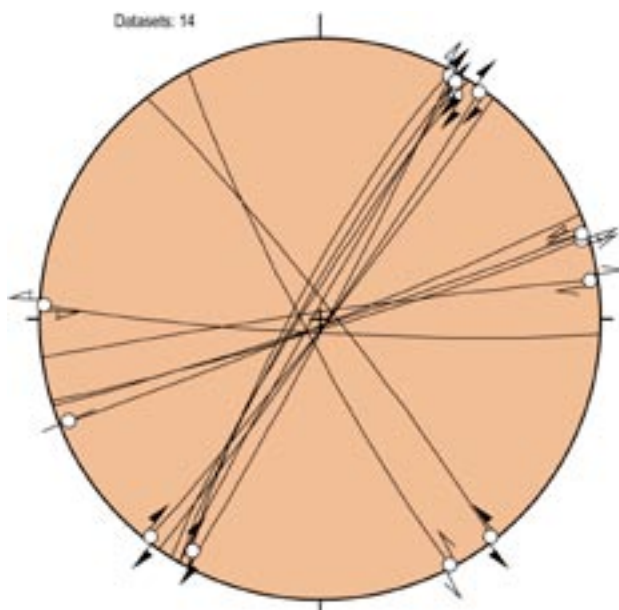
Figure 3-43. *Fault-slip data from the Albrunna limestone quarry. A prominent set of conjugate fractures is present in the dataset.*
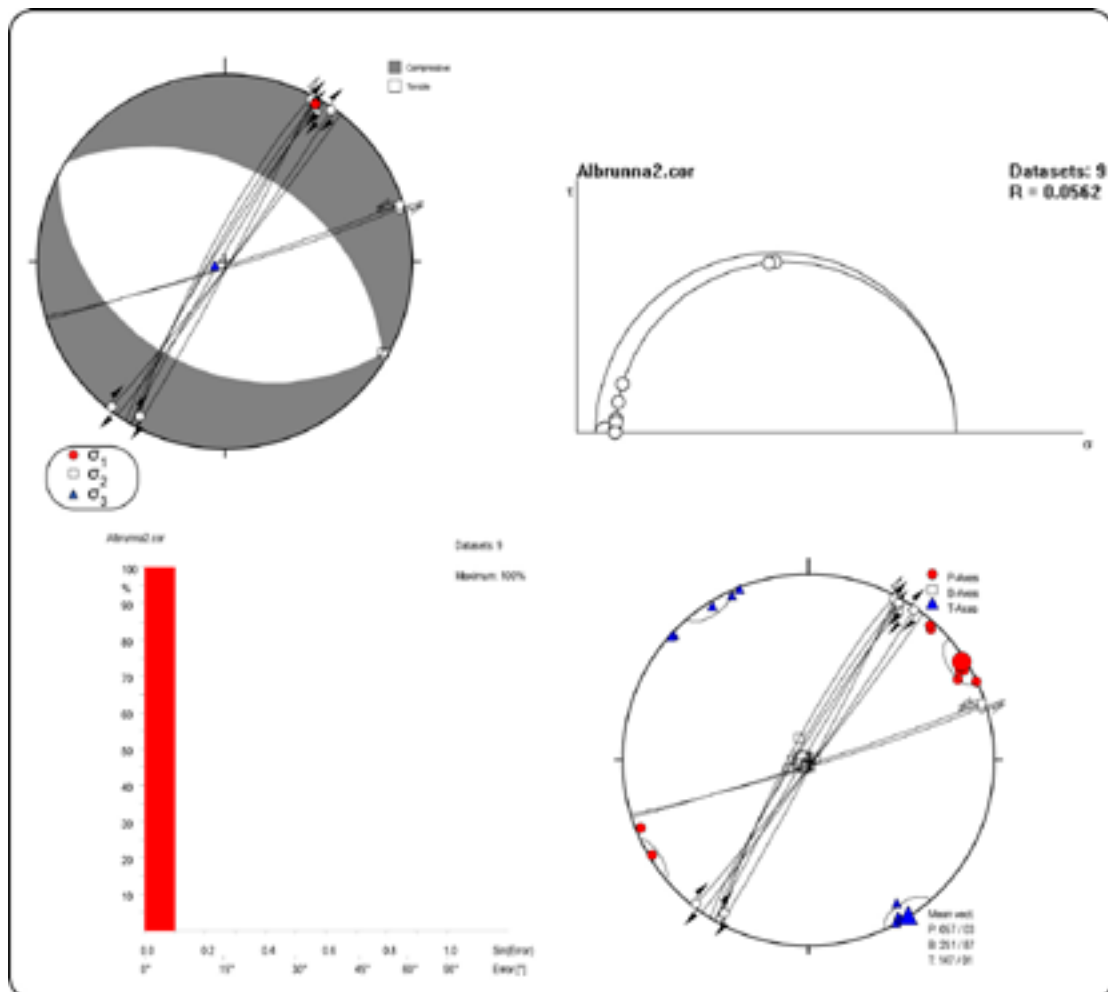
***Figure 3-44.** Stress inversion from the Albrunna limestone quarry that defines a thrust faulting regime with a sub-horizontal (04°) σ_1 oriented 030°. σ_3 dips 85° towards 248°. PBT axes are also shown.*

3.6 Discussion and conclusions

3.6.1 The regional framework and the ductile evolution

An attempt is made here towards the construction of a deformational scheme that accounts for the data elaborated so far. The information derived from the field study is tentatively integrated with the lessons learned from the detailed logging of the oriented drill cores.

The main obstacle is the unfortunate lack of constraints on the absolute and, at times, also relative timing of the identified deformational events. In order to provide the necessary boundary conditions for an understanding of the bedrock geological evolution of the Laxemar-Simpevarp area, the reconstructed sequence of events is therefore viewed in a broader geological perspective. Two existing models/reconstructions are shown in Figure 3-47. The orogenic events that shaped southeast Sweden are summarised with their associated stress fields. It is not the aim of this work to provide a description and summary of the principal local orogenies and the reader is therefore referred to, for example, the very thorough synthesis provided in /Söderbäck 2008/.

Here it is interesting instead to note the proposed stress fields for each tectonic pulse, in that some of these are the trigger of the brittle deformational phases characterized in this study. In general there is good agreement between the two reconstructions, although the model of Figure 3-47a, benefiting from 15 more years of research, portrays some additional elements that were not acknowledged by /Munier and Talbot 1993/, such as the Gothian and Hallandian events. Stress orientation also differs somewhat for the Caledonian event.

69
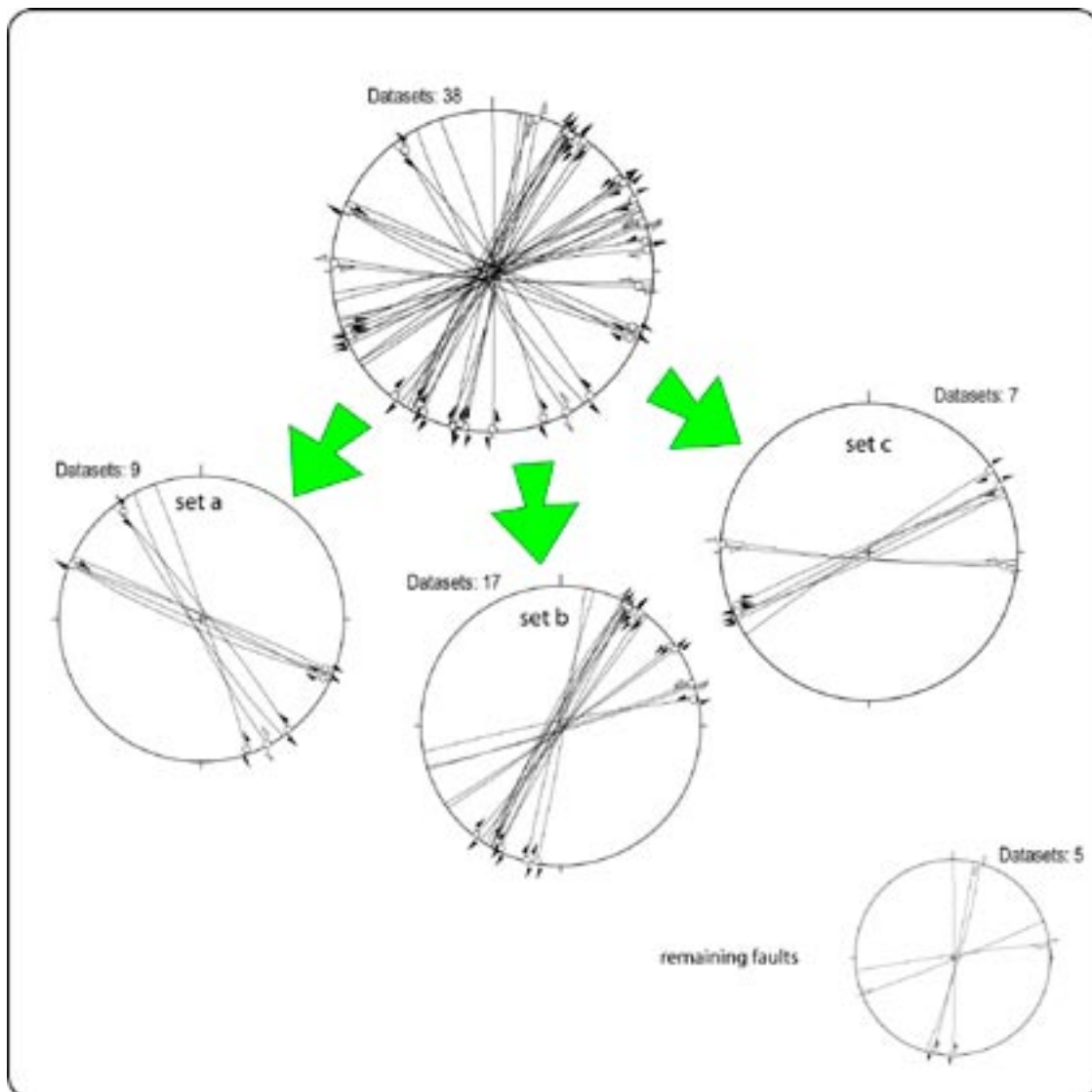
Figure 3-45. *Sorting of the merged dataset from Öland on the basis of geometric and kinematic compatibility criteria.*

In order to fit the results of this study in those reconstructions, it is necessary to have direct or indirect time constraints so as to be able to pinpoint the abscissa (time) for each episode. Unfortunately, there are still many unsolved issues concerning the timing of events and as a consequence this study limits itself to a working hypothesis, which could be turned into a robust model only if more accurate constraints were available.

The bedrock at the present level of erosion in the Laxemar-Simpevarp area cooled below 500°C by 1.76 Ga. The Svecokarelian orogeny imposed a weak foliation on the 1.8–1.7 Ga TIB rocks. This foliation generally trends NW along the belt elsewhere but, as shown above, has an unusual EW and even NE-SW strike in the study area, where it is proposed here it was deflected by shearing along the OSZ system.

There still remains, however, a great uncertainty concerning the post 1.76 Ga cooling history, in particular the time when the bedrock passed through the brittle-ductile transition in the crust and entered the brittle realm. $^{40}Ar/^{39}Ar$ ages by /Söderlund et al. 2008/ indicate that the bedrock in the area responded brittly to deformation at least as early as 1.62 Ga and that the Hallandian Götemar and Uthammar granites were emplaced at c. 1.45 Ga above the brittle-ductile transition. /Söderlund et al. 2008/ also suggest that these granites cooled below c. 300°C at 1.42 Ga.
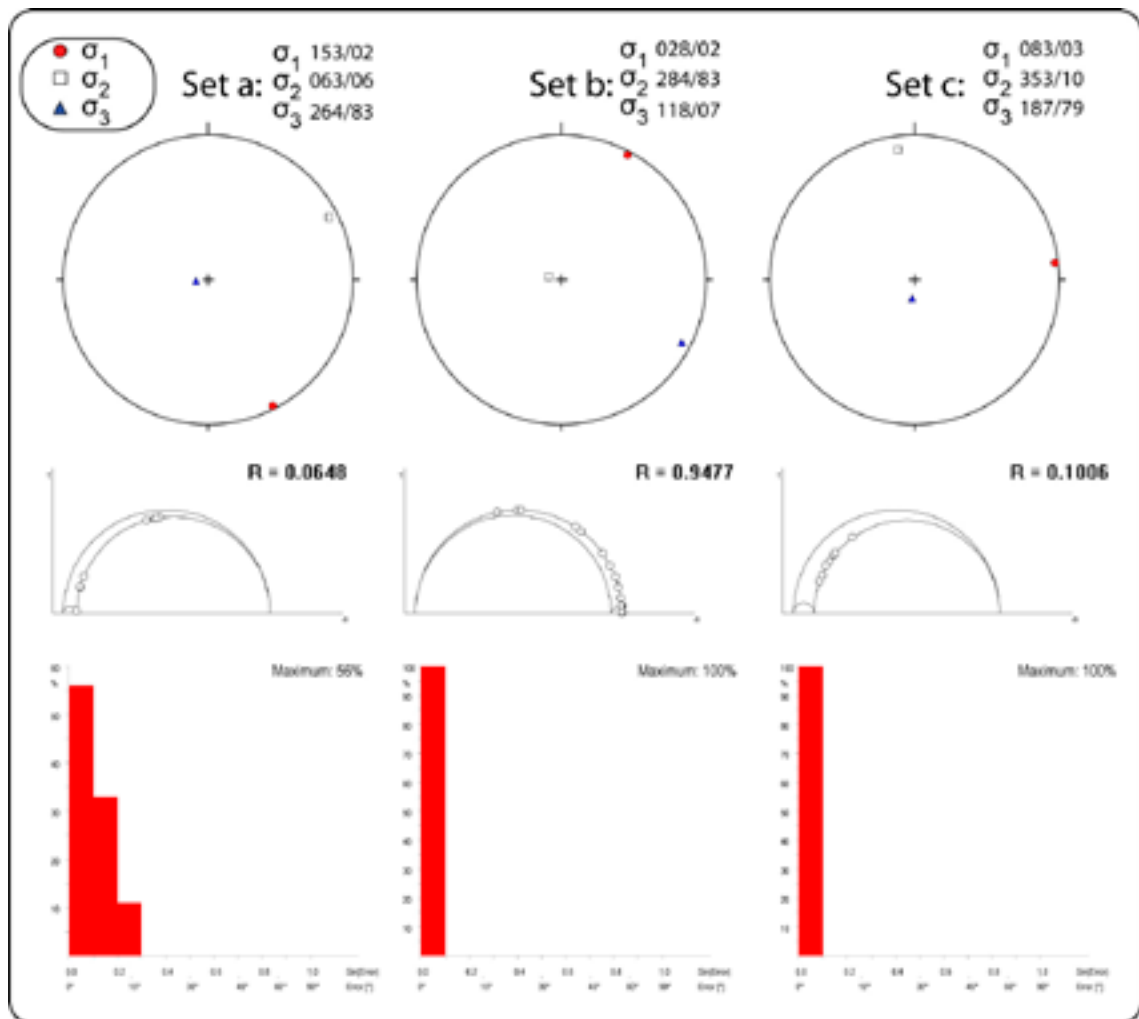
Figure 3-46. *Summary of stress inversion for each of the three conjugate sets from Öland.*

On the other hand, as discussed in detail in the section dealing with the ductile regional history (section 2), a $^{40}Ar/^{39}Ar$ muscovite age of c. 1.4 Ga was obtained from a pervasive mylonitic fabric of the Äspö shear zone /Drake et al. 2007/, and, in disagreement with the interpretation of this age representing post Hallandian granites cooling or late hydrothermal fluid circulation, it is tentatively suggested that it may represent a formation age, i.e. the timing of a second and distinct ductile episode. Structural evidence also supports in part this model. With this in mind, it may therefore be necessary to envisage a model in which a first ductile episode, followed by cooling and accommodation of subsequent strain by brittle structures, was overprinted, at least locally, by a second ductile/brittle cycle.

In this scenario, an early exhumation/cooling phase (leading to the bedrock containing the Svecokarelian ductile signature crossing a first time the brittle-ductile transition) would have occurred prior to the emplacement of the Hallandian granites; A second, distinct ductile episode (OSZ-Äspö type of shearing?) would have instead postdated the Hallandian granites, although direct observations of mylonitised Hallandian granites are not reported. In the absence of more compelling information on the kinematic history and temporal evolution of many of the lineaments and shears of the area, it is therefore hard to draw certain conclusions.
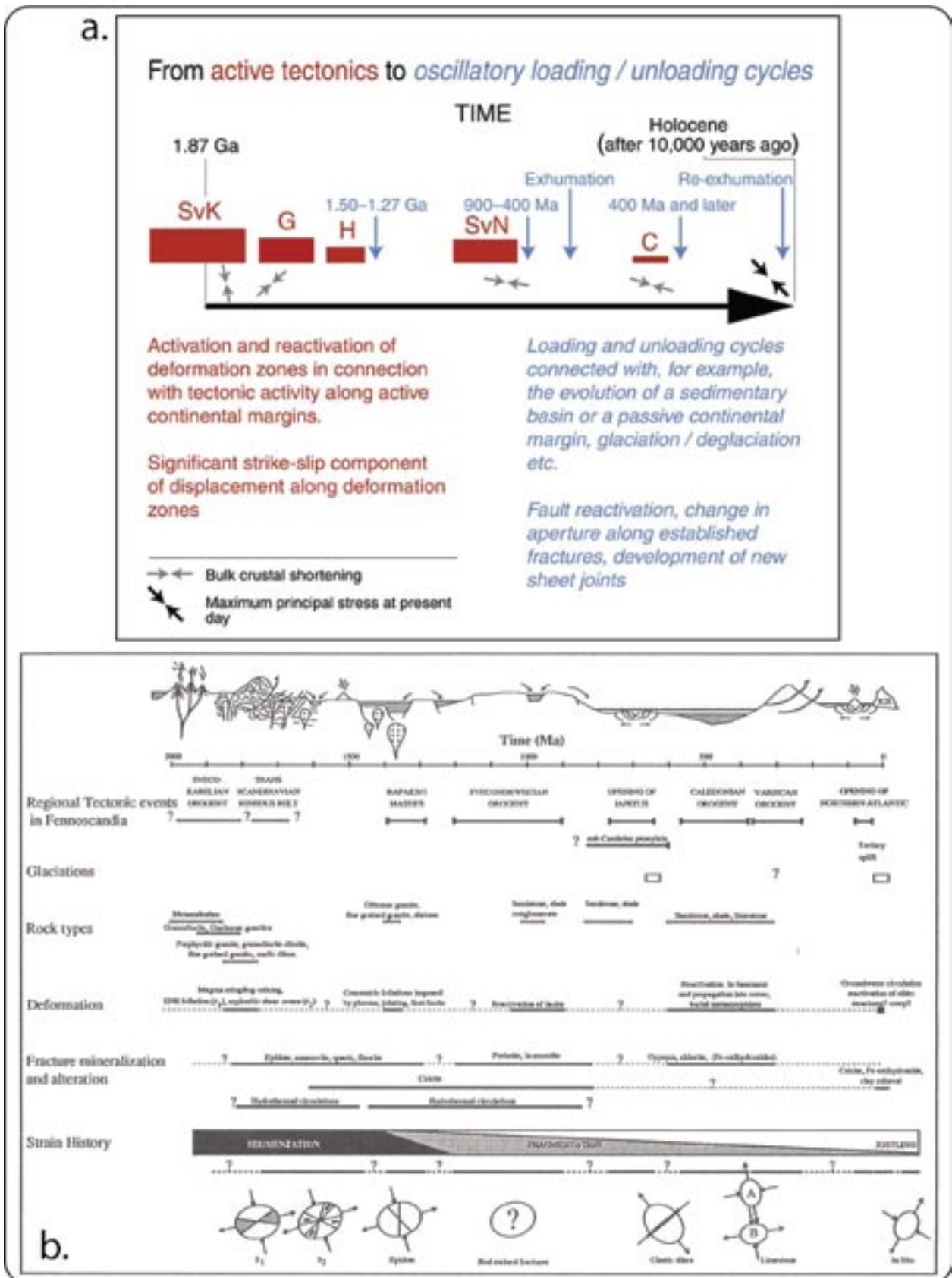
Figure 3-47. *Two proposed schemes of the geological evolution of southeast Sweden. a.): Diagram adapted from /Söderbäck 2008/, summarizing active tectonics (red) and oscillatory loading and unloading cycles (blue) during geological time. SvK: Svecokarelian orogeny, G: Gothian orogeny, H: Hallandian orogeny, SvN: Sveconorwegian orogeny, C: Caledonian orogeny. b.): Tentative chronological scheme summarizing the main lithological units and tectonic events affecting the Baltic shield according to /Munier and Talbot 1993/.*

72

3.6.2 The brittle evolution

Conjugate set I and II are no doubt some of the most prominent brittle features observed in the Laxemar-Simpevarp area (Figure 3-48). As shown above, set I formed in an overall thrust regime and moderately-dipping NE-SW striking thrusts were also formed together with the steep fractures of set I. Crosscutting relationships were not observed directly in the field, although several outcrops show evidence for dextral reactivation (NS-striking fractures of set II) of earlier NS-trending sinistral fractures (e.g. PSM007661, /Viola and Venvik Ganerød 2007b). Interpretation of the magnetic pattern shown in Figure 3-49, however, supports the interpretation of set II (drawn in yellow) postdating set I (in black), as shown by the displacement of a dextral set I fracture across a sinistral set II lineament.

Direct chronological constraints on these two sets are not available and we can therefore only speculate on their age. Based on the mineralogy (quartz, epidote and chlorite) of fault plane coatings and on the observation that several brittle-ductile shear zones have kinematics and orientation compatible with these sets, it could be argued that they both formed early in the regional evolutionary scheme (> 1.45 Ga?). The results of stress inversion and the calculated PBT axes are indeed in good agreement with the bulk stress orientation suggested for the Svecokarelian and Gothian orogenic phases in Figure 3-47a. On the other hand, it is also common to observe later chlorite coating on some of these fractures, which points to later reactivation. Moreover, similarly oriented striated planes were observed deforming Sveconorwegian dolerite dykes, implying that at least some of these fracture sets were formed later or were reactivated and deformed rocks genetically linked to the waning stages of the Sveconorwegian orogeny (c. 900 Ma). For example, Figure 3-50a and b show some key structural relationships described by /Viola and Venvik Ganerød 2007b, 2008/ respectively. In KLX20A steep fractures, the orientation and kinematics of which suggest them to belong to conjugate set II, crosscut at times low angle faults, but are in turn also cut by the gently dipping faults. Both normal and thrust faults were documented in DZ1 of KLX20A (Figure 3-50a). These relationships are in any case important in that they demonstrate that set II (or at least reactivation along set II) is post c. 900 Ma, the inferred age of the Sveconorwegian dolerite dykes. The fact that crosscutting relationships are not consistent, with steep fractures cutting and being cut by the low-angle fractures, is of difficult interpretation, because the kinematics of the latter could not be established for those fractures observed directly as interacting with their steeper counterparts.
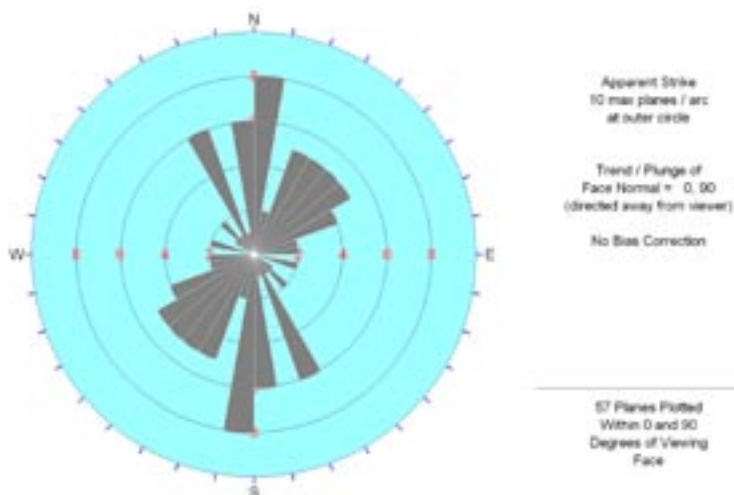
Figure 3-48. *Rose diagram of fractures from the field study belonging to conjugate set I and II.*
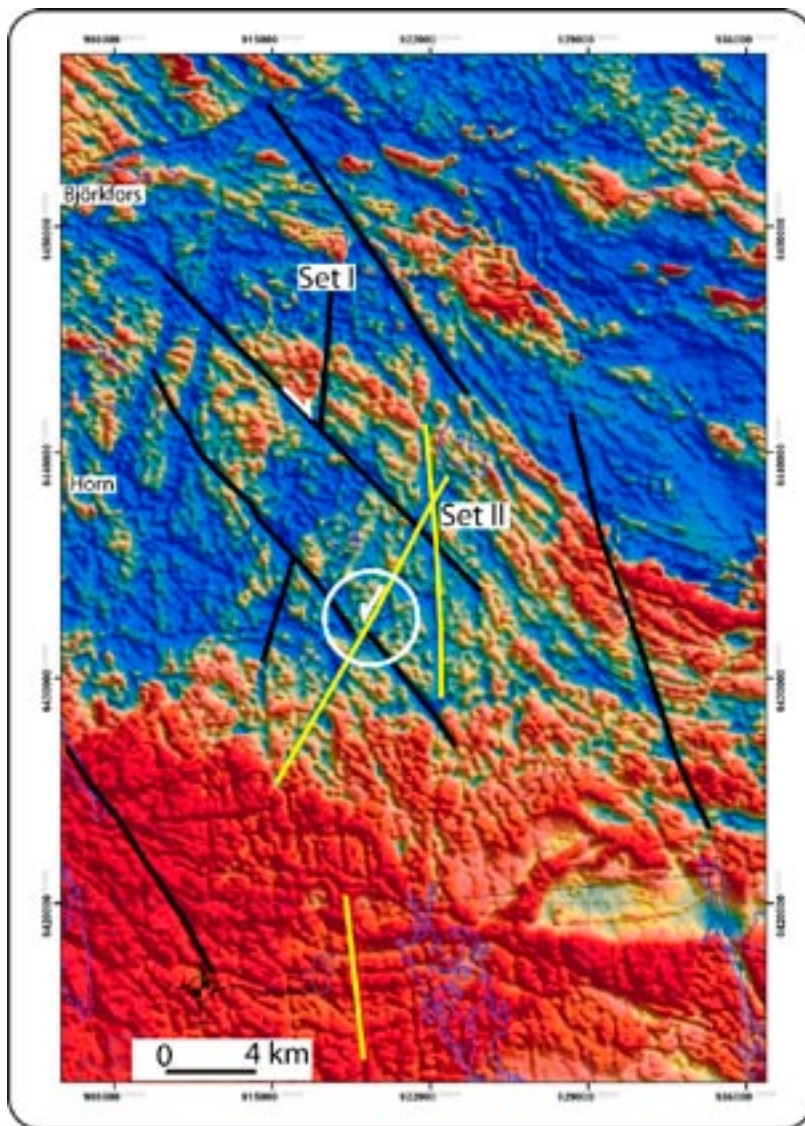
Figure 3-49. *Crosscutting relationships between conjugate set I (black lines) and II (yellow lines) suggesting set II to postdate set I.*

A slightly different situation was documented by /Viola and Venvik Ganerød 2008/ for DZ5 in KLX19A (Figure 3-50b). Here, low-angle extensional faults cut across a quite variable set of steep fractures. Unfortunately not enough faults could be measured to draw any conclusion if not that at least one extensional phase post-dated the intrusion of the dyke and the formation of earlier steep fractures.

A viable explanation for the absence of consistent temporal relationships between the steep and the low-angle fractures within the dykes is their formation under overall transtensional or transpressional conditions. When strain is accommodated in transtension or transpression it is common to have strain partitioning and localisation in strike-slip and normal or reverse structures that transiently overprint each other, thus generating rather ambiguous crosscutting patterns.
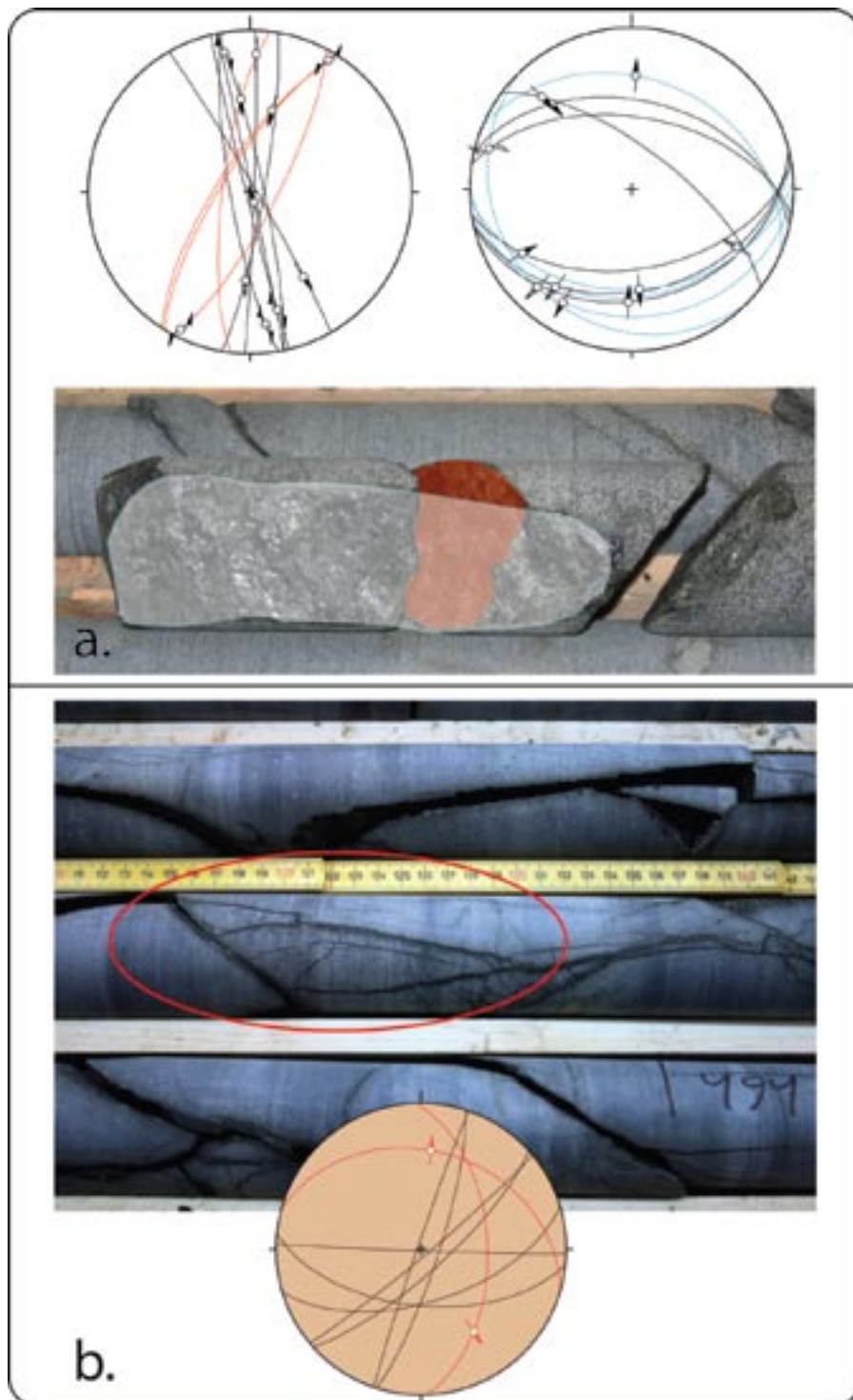
Figure 3-50. a.): Fault-slip data for part of DZ1 in KLX20A sorted to separate steep, NNW-to NNE-trending sinistral (red great circles) and dextral (black great circles) striated faults (top left stereogram) from moderately N- and S-dipping normal (blue) and thrust (black) faults. The steep fractures locally cut across the flatter ones (shaded in white and red, respectively, in the bottom photograph), although it was not established whether the latter are normal or thrust faults or both. Figure taken from /Viola and Venvik Ganerød 2007b/. b.): DZ5 of KLX19A: The circled area in the photograph highlights an example of shallow, high α fracture, crosscutting earlier steep, low α fractures. This geometric relationship is commonly observed in DZ 5. The stereogram plots the orientation and normal kinematics of two of these low dip angle fractures (red great circles) and several steeper fractures cut across by the former. Figure taken from /Viola and Venvik Ganerød 2007b/.

DZ7 in KLX19A was also logged by /Viola and Venvik Ganerød 2008/, but no kinematic analysis was carried out due to the high level of uncertainty encountered while trying to identify fractures in the BIPS image. Similarly to DZ5, DZ7 is entirely located within a doleritic dyke of inferred Sveconorwegian age, which hosts numerous striated faults. These, although not reported in /Viola and Venvik Ganerød 2008/, were used in this study with the goal of adding more constraints to our understanding of the brittle deformational history of the area. In spite of the uncertainty associated with the positive identification of core fractures in the BIPS image, the analysis of Figure 3-51 suggests that the observations made are, after all, correct and can be used in the independently-established structural framework. DZ7 fault-slip data contain several steep fractures that define a conjugate set, which is identical to conjugate set II. Stress inversion on the data defines a paleo-stress tensor that is indeed very similar to that computed independently for set II. It appears therefore that both KLX20A and KLX19A suggest set II or its partial reactivation to be post dyke intrusion.

/Viola and Venvik Ganerød 2007a/ reported that at the drill site for boreholes KLX11A and KLX20A in western Laxemar, NS-oriented fractures with a sinistral component of movement do not displace ENE-trending dextral fractures and a similarly oriented dilatant fracture infilled by Cambrian sandstone (sedimentary dyke?). This suggests that the former are Precambrian in age and at this site were not reactivated during the Phanerozoic. The former can now be assigned to conjugate set I, whereas the ENE-trending dextral structures belong very likely to conjugate set III and the sandstone filled fracture may be the expression of a separate extensional phase. Some of the kinematic and geometric relationships among these structural elements are not of easy
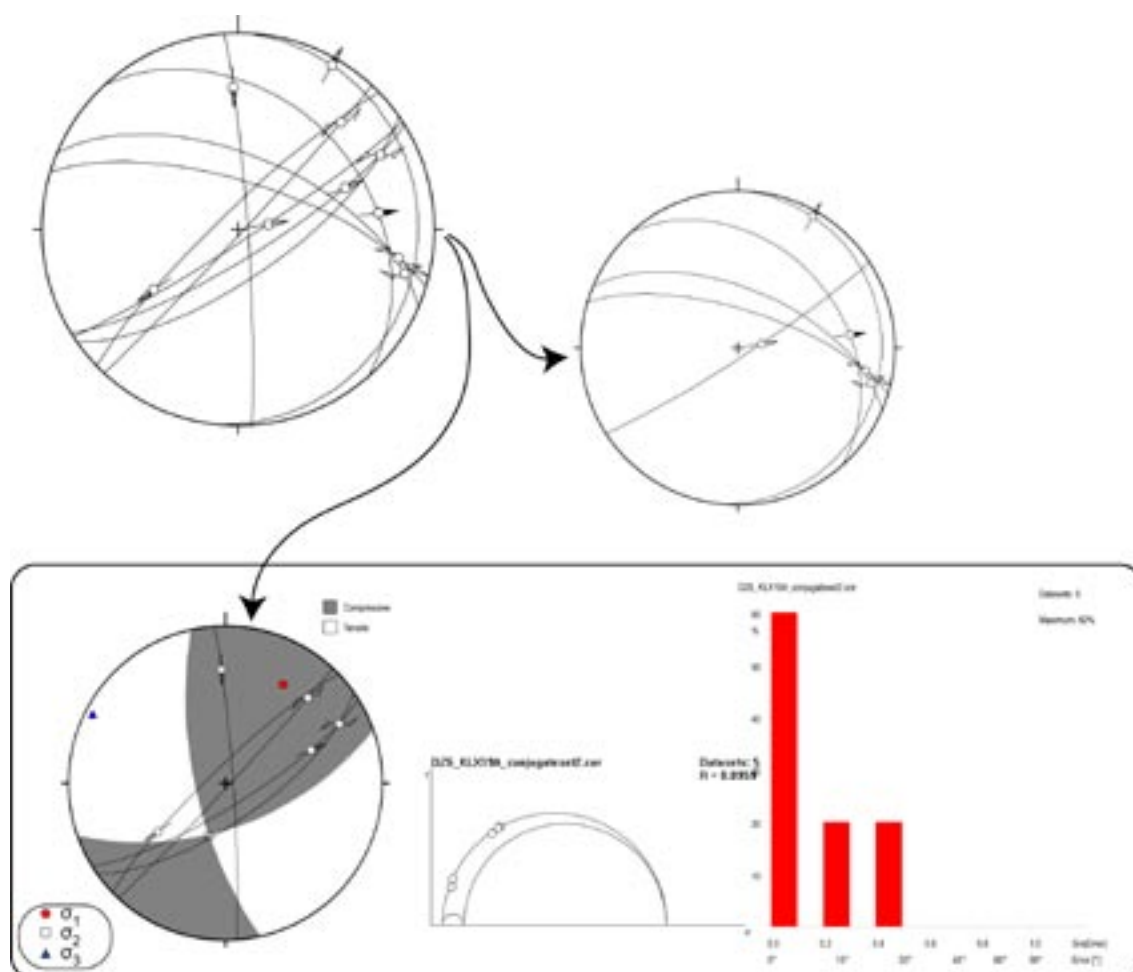
Figure 3-51. *Geometric and kinematic sorting of DZ7 in KLX19A identifies, among others, a well-defined conjugate set II set of fractures. Stress inversion on these fractures leads to a very robust paleo-stress tensor, comparable to the results obtained for conjugate set II in the field and other boreholes.*

interpretation, but the overall impression is that the sinistral fractures of set I are actually locally displaced by the other sets and are therefore older. Set I is interpreted as the oldest, and this is in line with the observation that a few thin magmatic dykes, striking NS, were emplaced by exploiting the same NS-trending sinistral corridor (Figure 3-12 and /Viola and Venvik Ganerød 2007a/). This is indicative of a long-lived sinistral shearing episode (genetically linked to set I) that initiated at high-T conditions and continued during progressive cooling of the bedrock.

It has to be borne in mind that the orientation of dextral fractures of conjugate set II is more or less parallel to that of the sinistral fractures of set I and this spatial superposition caused localised reactivation of set I at the time of set II faulting.

The results discussed so far are consistent with some of the observations reported in the summary edited by /Söderbäck 2008/, which suggests the Palaeozoic reactivation of lineament ZSMNS001 (immediately to the west of outcrop PSM007640 described by /Viola and Venvik Ganerød 2007a/) based on the observation that in the strongly fractured dolerite of KLX20A calcite of inferred Palaeozoic "warm brine" type is sheared by fractures with orientation and kinematics similar to those typical of set II, which would make set II post-dyke intrusion.

In synthesis, whereas conjugate set I can be attributed with confidence to a phase of NNW-SSE-oriented shortening genetically associated with the Svecokarelian bulk crustal shortening direction (although coaxial reactivations at later stages is likely; see below), the attribution of set II to a specific orogenic episode is more controversial. In order to address this issue, it is useful to refer to the "structural marker" of the Ordovician limestones that cover most of the island of Öland, in the hope of distinguishing post-Ordovician deformation episodes.

Figure 3-52. Sinistrally-stepped, granitic dyke-infilled NS-trending fracture. The dyke-infilled fractures in the bridge between the two adjacent fracture segments require a sinistral sense of shear. Outcrop PSM007640 of /Viola and Venvik Ganerød 2007a/.

As summarized in Figure 3-46, out of the three reconstructed post-Ordovician paleo-stress tensors only that computed from the fractures of set b matches vaguely the stress tensor computed for conjugate set II. In fact, the stress tensor of set b is moderately misaligned to that computed from set II and it is therefore not considered genetically linked to the fractures of set II. Therefore, it is suggested that the formation of fractures of set b caused severe reactivation of the fractures of set II, formed during a previous brittle event. The study of /Munier and Talbot 1993/, which constrained two distinct, post-Ordovician paleo-stress tensors, with their greatest compressive stress σ_1 oriented ENE and NNW, respectively (corresponding in orientation to set a and c of the present study; Figure 3-47b, stress states A and B in the bottom row), did not even identify set b and their results also show that set II was developed in response to an earlier deformational episode that predated the deposition of the Ordovician platform limestones.

In this respect, it is worth noting that the bulk shortening direction generally acknowledged for the Gothian orogeny (1.70–1.60 Ga) would be mechanically compatible with the geometry and kinematics of set II. It can therefore be concluded that conjugate set II developed soon after set I (consistent with the similar metamorphic grade of their primary coatings), before the Sveconorwegian orogeny and the Cambro-Ordovician and that it was only reactivated at later stages after the Ordovician. Faulting within the late-Sveconorwegian dolerites dykes in this case would either represent post-Sveconorwegian transtension (very late Sveconorwegian? Permian?) or accommodation of the stress tensor that generated the structural features of set b, or, more likely, a combination of the two.

The NNW-SSE shortening affecting the limestones (formation of set a) is geometrically and kinematically compatible with conjugate set I identified in the bedrock. It implies that set I was also partially reactivated under stress conditions very similar to those that generated it in the first instance and this observation can explain the presence of low-T mineral coating along NS- and NNW-SSE-trending fracture planes, the typical epidote-quartz coating trends. This uniaxial shortening may reasonably be attributed to shortening across the Hercynides or the Alps south of the Baltic shield.

The ENE shortening computed from the conjugate fractures of set c is of great interest, in that it is in good agreement with the computed paleo-stress tensor for conjugate set III. This shortening event affected both the bedrock and its sedimentary cover and can be reasonably associated with the Caledonian orogeny, although the typical shortening direction (though determined in the ductilely deformed hinterland) is more NW-SE to WNW-ESE.

The stress field associated with the Sveconorwegian orogeny was also oriented from ENE-WSW to c. EW and it is reasonable to expect some structural evidence of its effects. It cannot be ruled out, therefore, that fractures and faults of conjugate set III formed initially during the compressional pulse of that orogeny and that they were reactivated at the time of formation of fractures of set c at a later stage during the Caledonian phases.

3.6.3 Extensional tectonics

Figure 3-47a, together with the main mountain building orogenic cycles, suggests a series of loading and unloading cycles in connection with the burial and denudation of sedimentary rocks and proper exhumation phases, presumably linked to denudation in response to crustal extension. It is expected that loading caused reactivation of steeply dipping fractures, whereas unloading resulted in the dilational reactivation of gently-dipping planar anisotropies and in the formation of new, topography-parallel stress-release joints.

Analysis of fault-slip data bearing evidence of extensional kinematics has indeed confirmed the existence of numerous, extremely low-angle normal faults. As pointed out earlier on, these dip too gently to be mechanically possible in a Mohr-Coulomb faulting regime and other possible explanations about their formation were suggested.

The documented kinematics and the computed stress inversion constrained two distinct extensional episodes, with antithetic normal faults accommodating NE-SW and NW-SE-oriented stretching, respectively. Assignment of these extensional regimes to specific tectonic/deformational episodes is unfortunately not straightforward and only speculations can be made here on this aspect of the regional geological evolution.

Based on field investigations, c. top-to-the-north extensional kinematics was suggested by /Viola and Venvik Ganerød 2007a/ for lineament ZSMEW007A, although the absence of slickenlines on striated fault planes and of stretching lineations prevented the exact extension direction to be determined. However, more information on this lineament and its role in the regional deformational history can be gathered from the logging of drill core KLX09A, whose deformation zone DZ13 intercepts the ZSMEW007A. Cataclasites, ultracataclasites and gouge intervals were described by /Viola and Venvik Ganerød 2007b/ and these are accompanied by numerous striated fault planes (Figure 3-53).

The normal faults mapped in DZ13 are shown in Figure 3-53; their kinematics and the spatial distribution of the PBT axes define a paleo-stress tensor leading to NE-SW extension. This information is used to argue that ZSMEW007A accommodated an extensional component during its evolution, with an overall top-to-the-northeast sense of shear.

DZ13 in KLX09A also matches the location of deformation zone ZSMNW928A, a medium-confidence deformation zone, which corresponds to seismic reflector N, a SSW gently dipping reflector identified by /Juhlin et al. 2004/. Figure 3-54 offers a new interpretation for ZSMEW007A and, at the same time, for ZSMNW928A. Given their mutual spatial arrangement (conjugate planes with a dihedral acute angle of 74°) and the kinematics established for ZSMEW007A, it is suggested that they form a pair of conjugate normal faults accommodating vertical shortening, thus in excellent agreement with the computed mean P and T axis of Figure 3-53. Integrated field observations, core logging and geometric/kinematic analysis thus allow assigning ZSMEW007A and its conjugate ZSMNW928A to the paleo-stress tensor of Figure 3-29, that is, to an extensional phase oriented c. NE-SW. As shown by the presence of thrust fault planes in DZ13 /Viola and Venvik Ganerød 2007b, their Figure 5-59/, extension very likely reactivated pre-existing thrust faults.
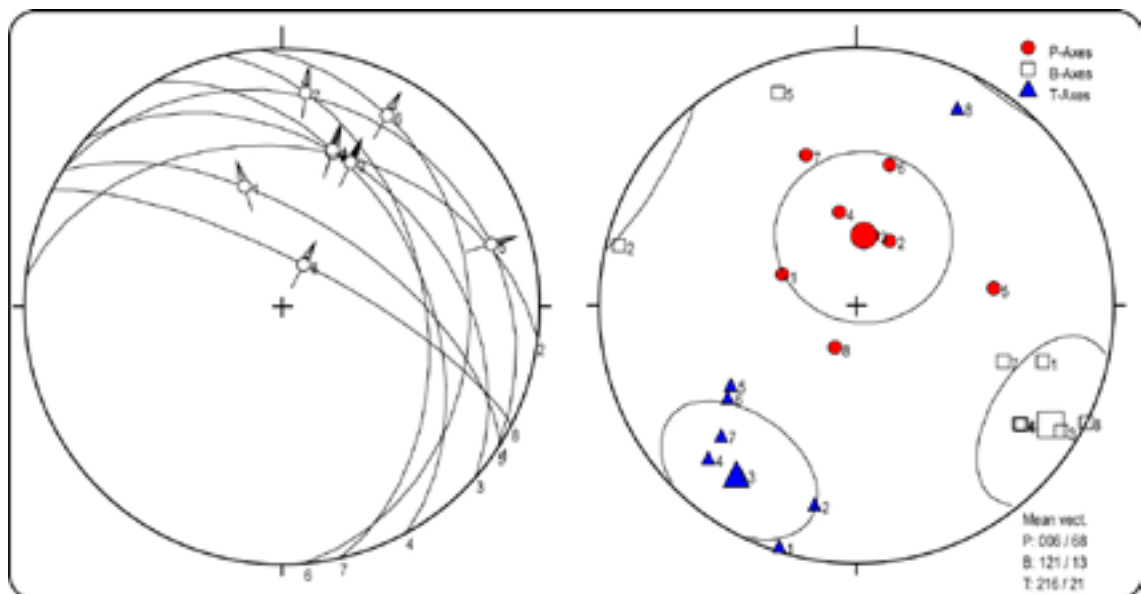
Figure 3-53. Fault-slip data and PBT axes for the extensional faults mapped in DZ13 of KLX09 by /Viola and Venvik Ganerød 2007b/.
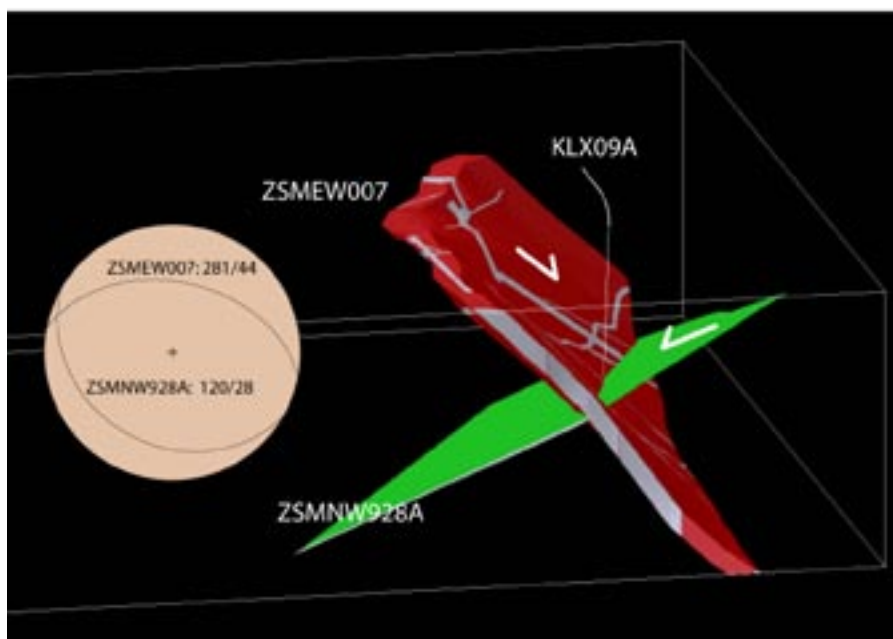
Figure 3-54. *3D model of the local model volume showing zone ZSMEW007A, ZSMNW928A and borehole KLX09A. View to the west. The stereogram plots their orientation (dihedral acute angle of 74°) and the white arrows on the 3D representation suggest they are a pair of conjugate normal faults.*

An extremely important observation is that seismic reflector N is not observed to extend through lineament ZSMEW002A (Mederhult zone; see for example Figure 2-11), which implies a crosscutting relationship and that ZSMNW928A (and therefore ZSMEW007A) is older than ZSMEW002A. As discussed in the first sections of this report, ZSMEW002A belongs to the EW-trending ductile OSZ system, which also contains the Äspö shear zone. The S/C' structural relationships described in section 2.2.2 were used to argue that ZSMEW007A might be older than the Äspö shear zone (possibly 1.4 Ga) and also than ZSMEW002A, a model now supported also by this second part of the study.

It is considered probable that some brittle (also ductile?) extensional features formed very early in the geological evolution of the area, for example at the end of the Svecokarelian orogenic cycle or in connection to the intrusion of the Hallandian granites, but in any case earlier than 1.4 Ga.

At and after 970 and until at least 900 Ma the Sveconorwegian orogenic belt entered a period of relaxation or gravitational collapse /e.g. Bingen et al. 2006, Möller et al. 2007, Bingen et al. 2008/. E-W crustal stretching is documented by a large variety of data and observations in southern Sweden where the phase was characterized by voluminous post-collisional magmatism, gneiss dome and core complex formation and low pressure, high temperature metamorphism. In the Laxemar-Simpevarp area the most obvious effect of such extensional episode was the intrusion of c. NS trending, C. 0.9 Ga doleritic dykes. One of them was intersected during the site investigation studies by several boreholes. Figure 3-50 and Figure 3-51 refer to deformation zones located within the dyke. Extensional faults were documented in the dolerite /Viola and Venvik Ganerød 2007b, 2008/ and these were reported to crosscut steep, conjugate set II fractures. The main implication of these observations is that extension occurred also after the late Sveconorwegian emplacement of the dolerites. The statistics on the normal fault planes deforming the dolerite are unfortunately too poor to constrain a well-defined paleo-stress tensor and it is therefore not possible to establish the exact extension direction. Transtension was suggested as a viable strain model for their emplacement, based on the mutual crosscutting relationships observed between steep strike-slip and low-angle extensional fractures.

Evidence for post-Sveconorwegian extension was already summarised by /Munier and Talbot 1993/, who proposed a phase of NW-SE extension inferred from numerous NE-striking clastic dykes of early Cambrian age and tentatively assigned this episode to the far-field stress effects of the opening of the Iapetus ocean, approximately 600 million years ago. This extension direction is coaxial with the results of stress inversion presented in Figure 3-30 and this model is therefore considered here as possible. /Röshoff and Cosgrove 2002/ studied in detail a number of sedimentary dykes in the Oskarshamn-Västervik area and concluded that dykes are indeed relatively ancient features, possibly linked to the break-up of Pangea in the Permian. Extension and movement along the vertical direction accommodated during this phase may explain some of the normal to transtensional faulting that affected the sub-Cambrian nonconformity.

Useful insights into the post-Cambrian brittle evolution of the region (including extensional episodes) can be derived from the work of /Heeremans et al. 1996/ and /Bergerat et al. 2007/. /Bergerat et al. 2007/ investigated the evolution of paleo-stress fields and brittle deformation of the Tornquist Zone in Scania during the Permo-Mesozoic and Cenozoic times. Figure 3-55 shows the summary evolution proposed by these authors. In their reconstruction, the most prominent tectonic episode of the area is an extensional phase trending c. NE-SW, which is marked by the injection of large amounts of Permo-Carboniferous dykes and mineralised veins, predated but also partly accompanied by normal faulting (Figure 3-55). An overall transtensional behaviour is inferred by /Bergerat et al. 2007/ on the basis of coexisting normal and strike-slip faulting.

A second subordinate extensional field, orthogonal to the NE-SW extension, is also reported as acting probably since the Triassic and until the end of the Cretaceous. A NE-SW compression follows in the Late Cretaceous, before NNE-SSW compression together with ESE-WNW extension, characterized by conjugate strike-slip faults is inferred, probably in conjunction with the Alpine event.

These results are useful to place indirect time constraints on the extensional phases reconstructed from the drill core normal fault dataset, which was used to constrain two orthogonal extensional phases oriented NE-SW and NW-SE, respectively (Figure 3-29 and Figure 3-30), that is, coaxial with the orientation of the Permian extensional phase in Scania reported by /Bergerat et al. 2007/.

Fault planes within the late Sveconorwegian doleritic dikes may be also due to this Permian transtensional episode. On the other hand, the Öland Ordovician limestones do not record any normal faulting, possibly due to the significant distance from the Tornquist Zone in Scania and thus hamper a straightforward reconstruction.

The stress tensors of set a and b can be instead linked to the post-Cretaceous reconstruction of /Bergerat et al. 2007/, with two distinct compressional events tentatively connected to the Laramide or the Late Cimmerian inversion /Norling and Bergström 1987/ and the far-field effects of the Alpine orogeny (set b and a, respectively). These episodes would have caused the partial reactivation of fractures belonging to set I and II. Set c, as postulated above in the case of set III, is likely the effect of an earlier compression oriented NW-SE to E-W and acting in an overall thrusting regime, possibly due to the Caledonian Orogeny. A similar Caledonian shortening direction was also proposed for the Oslo area by /Heeremans et al. 1996/, who computed paleo-stress analysis, mainly based on slickensided fault planes, both within and outside the rift structure.

Figure 3-56 presents a summary of the results obtained by this study. The evolution of the stress field proposed by this study is added to the diagram presented by /Söderbäck 2008/. However, the post-Ordovician stress history is also provided based on the results of the study of brittle deformation accommodated by the Ordovician limestones of Öland and on their comparison with existing studies for other parts of southern Scandinavia.
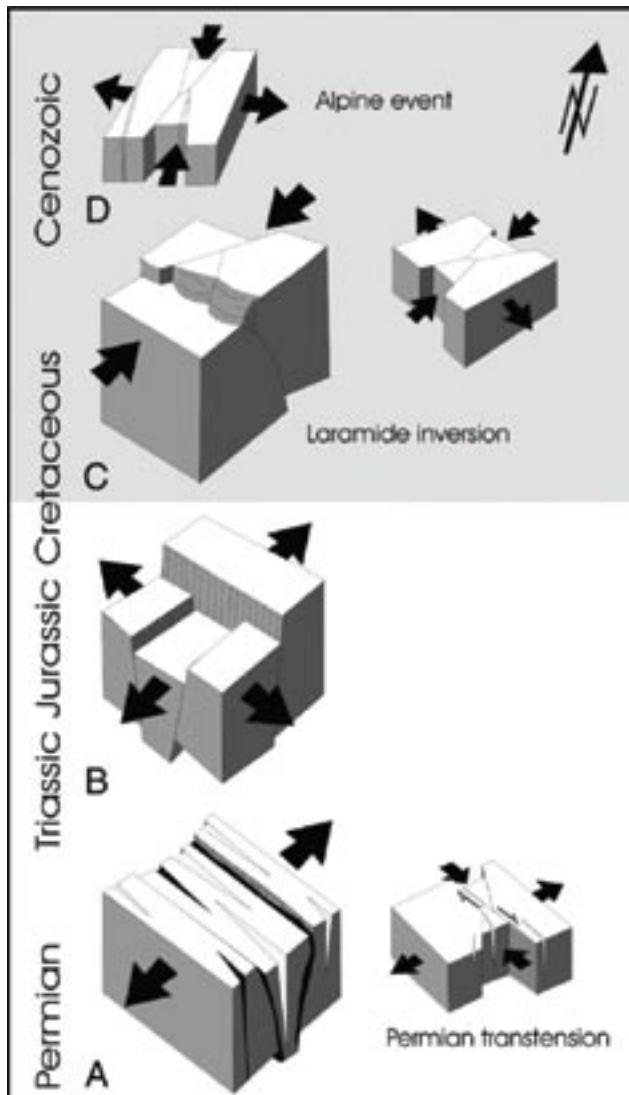
Figure 3-55. *Schematic block-diagrams illustrating the main tectonic phases, mainly extensive (white background) from the Permian to the upper Cretaceous, and mainly compressive (grey background) since the end of the Cretaceous proposed by /Bergerat et al. 2007/ for the Scania region, southwest Sweden (figure taken from /Bergerat et al. 2007/).*
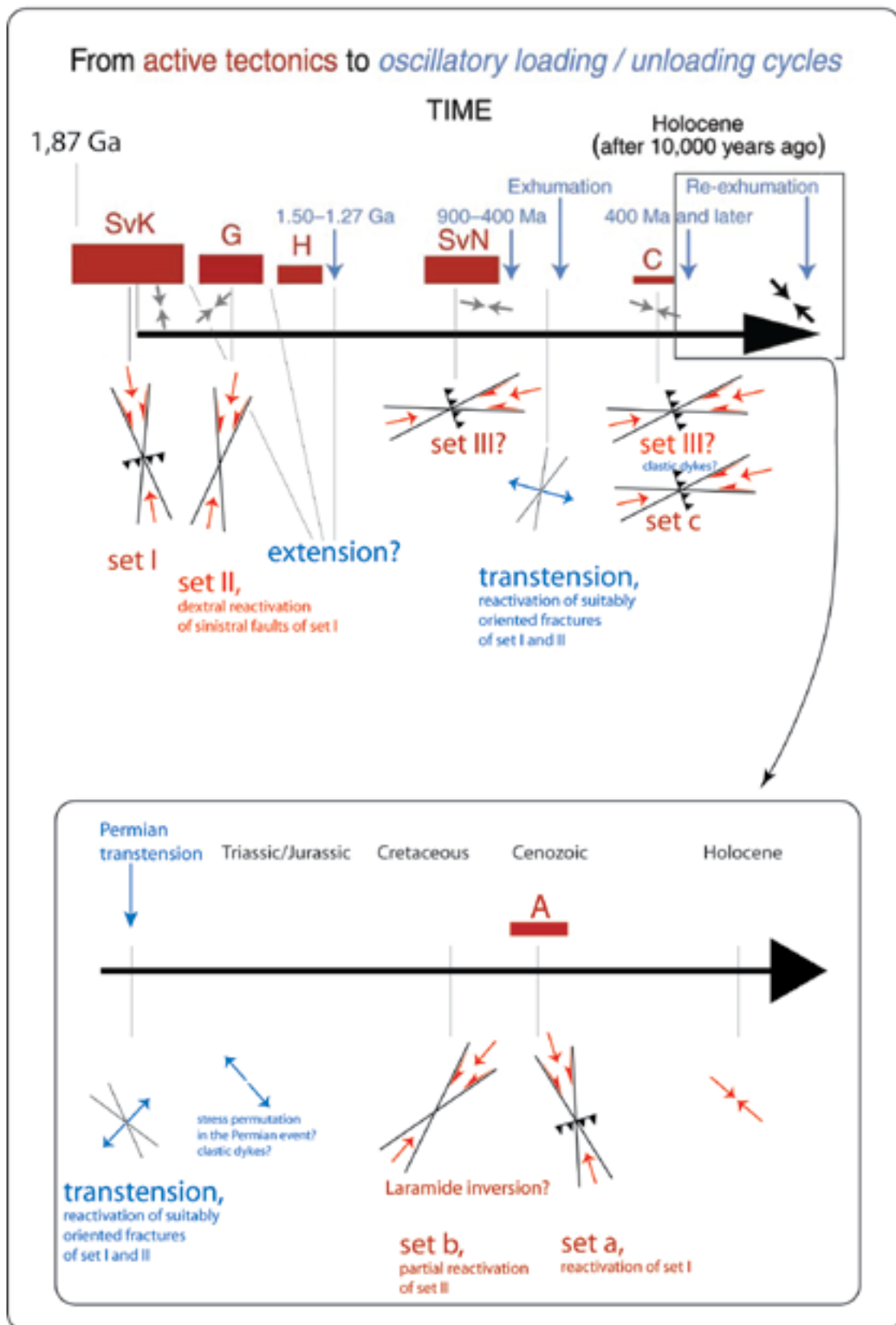
Figure 3-56. *Summary of the stress field evolution proposed in this study integrated in the scheme from /Söderbäck 2008/. Thrust symbols indicate an overall thrusting regime. The figure summarizes active compressive tectonics (red) and overall extensional episodes (blue) during geological time. SvK: Svecokarelian orogeny, G: Gothian orogeny, H: Hallandian orogeny, SvN: Sveconorwegian orogeny, C: Caledonian orogeny, A: Alpine orogeny. The lower part of the figure expands on the model reported in /Söderbäck 2008/ by utilizing the results obtained from the Ordovician limestones of the island of Öland.*

Reference list

Anderson E M, 1951. The Dynamics of Faulting and Dyke Formation with applications to Britain, Oliver and Boyd, Edinburgh, 191 pp.

Angelier J, 1979. Determination of the mean principal direction of stresses for a given fault population. Tectonophysics 56, 17–26.

Angelier J, Tarantola A, Valette B, Manoussis S, 1982. Inversion of field data in fault tectonics to obtain the regional stress; I, Single phase fault populations: a new method of computing the stress tensor. Geophysical Journal of the Royal Adtronomical Society 69, 607–621.

Angelier J, 1984. Tectonic analysis of fault slip datasets, Special section; Fault behavior and the earthquake generation process. American Geophysical Union, Washington DC, USA, pp. 5835–5848.

Åhäll K-I, 2001. Åldersbestämming av svårdaterade bergarter i sydöstra Sverige. SKB R-01-60, Svensk Kärnbränslehantering AB.

Bergerat F, Angelier J, Andreasson P-G, 2007. Evolution of paleostress field and brittle deformation of the Tornquist Zone in Scania (Sweden) during Permo-Mesozoic and Cenozoic times. Tectonophysics 444, 93–110.

Bergman B, Juhlin C, Palm H, 2001. Reflektionsseismika studier inom Laxemarområdet. SKB R-01-07, Svensk Kärnbränslehantering AB.

Berthé D, Choukroune P, Jegouzo P, 1979. Orthogneiss, mylonite and non-coaxial deformation of granites: the example of the South Armorican Shear Zone. Journal of Structural Geology 1, 31–42.

Bingen B, Stetin H J, Bogaerts M, Bolle O, Mansfeld J, 2006. Molybdenite re-Os dating constrains gravitational collapse of the Sveconorwegian orogen, SW Scandinavia. Lithos 87, 328–346.

Bingen B, Nordgulen Ø, Viola G, 2008. A four-phase model for the Sveconorwegian orogeny, SW Scandinavia. Norwegian Journal of Geology, 88, 43–72.

Bott MHP, 1959. The mechanics of oblique slip faulting. Geological Magazine 96, 109–117.

Braathen A, Nordgulen Ø, 2005. Structural investigations of deformation zones (ductile shear zones and faults) around Oskarshamn – a pilot study. SKB P-05-181, Svensk Kärnbränslehantering AB.

Carey E, Brunier B, 1974. Analyse théorique et numérique d'un modèle mécanique élémentaire appliqué à l'étude d'une population de failles. Comptes Rendus de l' Académie des Sciences de Paris 279, 891–894.

Döse C, Stråhle A, Rauséus G, Samuelsson E, 2008. Revision of BIPS-orientations for geological objects in boreholes from Forsmark and Laxemar. SKB P-08-37, Svensk Kärnbränslehantering AB.

Drake H, Page L, Tullborg E-L, 2007. $^{40}Ar/^{39}Ar$ dating of fracture minerals. SKB P-07-27, Svensk Kärnbränslehantering AB.

Etchecopar A, Vasseur G, Daignieres M, 1981. An inverse problem in microtectonics for the determination of stress tensors from fault striation analysis. Journal of Structural Geology 3, 51–65.

Hancock P L, 1985. Brittle microtectonics: principles and practice. Journal of Structural Geology 7, 437– 457.

Heeremans M, Larsen B T, Stel H, 1996. Paleostress reconstruction from kinematic indicators in the Oslo Graben, southern Norway: new constraints on the mode of rifting. Tectonophysics 266, 55–79.

Juhlin C, Bergman B, Palm H, 2004. Reflection seismic studies in the Laxemar area during 2004. SKB P-04-215, Svensk Kärnbränslehantering AB.

Kero L, 2004. Magnetic anomaly map of Southern Sweden. Sveriges Geologiska Undersökning.

Koistinen T, Stephens M B, Bogatchev V, Nordgulen Ø, Wenneström M, Korhonen J, 2001. Geological map of the Fennoscandian Shield, scale 1:2,000000. Geological Surveys of Finland, Norway and Sweden and the North-West Department of Natural resources of Russia.

Lundberg E, Sjöström H, 2006. Kinematic analysis of ductile and brittle/ductile shear zones in Simpevarp and Laxemar subarea. SKB P-06-118, Svensk Kärnbränslehantering AB.

Mansfeld J, 1996. Geological, geochemical and geochronological evidence for a new Paleoproterozoic terrane in southeastern Sweden. Precambrian Research 77, 91–103.

Mattson H, 2006. The magnetic anisotropy of rocks across two major deformation zones in the Laxemar and Simpevarp area. Oskarshamn site investigation. SKB P-06-124, Svensk Kärnbränslehantering AB.

Milnes A G, Gee D G, 1992. Bedrock stability in southeastern Sweden. Evidence from fracturing in the Ordovician limestones of northern Öland. SKB TR 92-23, Svensk Kärnbränslehantering AB.

Möller C, Andersson J, Lundqvist I , Hellström F A, 2007. Linking deformation, migmatite formation and zircon U-Pb geochronology in polymetamorphic gneisses, Sveconorwegian province, Sweden. Journal of Metamorphic Geology, 17, 727–750.

Munier R, Talbot C J, 1993. Segmentation, fragmentation and jostling of cratonic basement in and near Äspö, southeast Sweden. Tectonics, 12, 713–727.

Norling E, Bergström J, 1987. Mesozoic and Cenozoic evolution of Scania, southern Sweden. Tectonophysics 137, 7–19.

Petit J P, 1987. Criteria for the sense of movement on fault surfaces in brittle rocks. Journal of Structural Geology 9, 597–608.

Platt J P, Vissers R L M, 1980. Extensional structures in anisotropic rocks. Journal of Structural Geology 2, 397–410.

Reiter F, Acs P, 1999. TectonicsFP.

Rhén I, Gustafson G, Stanfors R, Wikberg P, 1997. Äspö HRL-Geoscientific evaluation 1997/5. Models based on site characterization 1986-1995. SKB TR97-06, Svensk Kärnbränslehantering AB.

Röshoff K, Cosgrove J, 2002. Sedimentary dykes in the Oskarshamn-Västervik area. A study of the mechanism of formation. SKB R-02-37, Svensk Kärnbränslehantering AB.

Rydström H, Gereben L, 1989. Regional geological study. Seismic refraction survey. SKB PR 25-89-23, Svensk Kärnbränslehantering AB.

Skjernaa L, 1992. Microstructures in the Nyatorp Shear Zone, southeastern Sweden. Geologiska Föreningens i Stockholm Förhandlingar (GFF) 114, 195–208.

Söderbäck B (ed.), 2008. Geological evolution, palaeoclimate and historical development of the Forsmark and Laxemar-Simpevarp areas. Site descriptive modelling, SDM-Site. SKB R-08-19, Svensk Kärnbränslehantering AB.

Söderlund U, Isachsen C, Bylund G, Heaman L, Patchett P J, Vervoort J D, Andersson U B, 2005. U-Pb baddeleyite ages sand Hf-Nd isotope chemistry constraining repeated mafic magmatism in the Fennoscandian Shield from 1.6 to 0.9 Ga. Contributions to Mineralogy and Petrology 150, 174–194.

Söderlund P, Page L M, Söderlund U, 2008. ^{40}Ar–^{39}Ar biotite and hornblende geochronology from the Oskarshamn area, SE Sweden: discerning multiple Proterozoic tectonothermal events. Geological Magazine 145, 790–799.

Stanfors R, Erlström M, 1995. SKB Palaeohydrological programme. Extended geological models of the Äspö area. SKB Arbetsrapport 95-20, Svensk Kärnbränslehantering AB.

Stenberg L, Sehlstedt S, 1989. Geophysical profile measurements on interpreted regional aero-magnetic lineaments in the Simpevarp area. SKB PR25-89-13, Svensk Kärnbränslehantering AB.

Talbot C J, 1990. Some clarification of the tectonics of Äspö and its surroundings. SKB P 25-90-15, Svensk Kärnbränslehantering AB.

Viola G, Venvik Ganerød G, 2007a. Structural analysis of brittle deformation zones in the Simpevarp-Laxemar area, Oskarshamn, southeast Sweden. SKB P-07-41, Svensk Kärnbränslehantering AB.

Viola G, Venvik Ganerød G, 2007b. Structural characterization of deformation zones (faults and ductile shear zones) from selected drill cores and outcrops from the Laxemar area – Results from Phase 2. SKB P-07-227, Svensk Kärnbränslehantering AB.

Viola G, Venvik Ganerød G, 2008. Structural characterisation of deformation zones (faults and ductile shear zones) from selected drill cores from the Laxemar area – Results from Phase 3. SKB P-08-07, Svensk Kärnbränslehantering AB.

Wahlgren C-H, Ahl M, Sandahl K-A, Berglund J, Petersson J, Ekström M, Persson P-O, 2004. Oskarshamn site investigation: Bedrock mapping 2003 – Simpevarp subarea. Outcrop data, fracture data, modal and geochemical classification of rock types, bedrock map, radiometric dating. SKB P-04-102, Svensk Kärnbränslehantering AB.

Wahlgren C-H, Curtis P, Hermanson J, Forssberg O, Öhman J, Drake H, Fox A, La Pointe P, Triumf C-A, Mattsson H, Thunehed H, Juhlin C, 2008. Geology Laxemar. Site descriptive modelling, SDM-Site Laxemar. SKB R-08-54, Svensk Kärnbränslehantering AB.

Wallace R E, 1951. Geometry of shearing stress and relation to faulting. Journal of Geology 59, 118–130.

White S, Burrows S E, Carreras, J, Shaw N D, Humphreys F J, 1980. On mylonites in ductile shear zones. Journal of Structural Geology 2, 175–188.

Yamada Y, Yamaji A, 2002. Determination of paleostresses from mesoscale shear fractures in core samples using the Multi-Inverse method. Journal of Petroleum Geology 25, 203–218.

Yamaji A, 2000a. The multiple inverse method: a new technique to separate stresses from heterogeneous fault-slip data. Journal of Structural Geology 22, 441–452.

Yamaji A, 2000b. Multiple inverse method applied to mesoscale faults in mid Quaternary sediments near the triple trench junction off central Japan. Journal of Structural Geology 22, 429–440.

Yamaji A, 2003. Are the solutions of stress inversion correct? Visualization of their reliability and the separation of stresses from heterogeneous fault-slip data. Journal of Structural Geology 25, 241–252.